

**LONG-RANGE CHARGE TRANSFER IN PLASMID DNA CONDENSATES AND
DNA-DIRECTED ASSEMBLY OF CONDUCTING POLYMERS**

A Dissertation

Presented to

The Academic Faculty

By

Prolay Das

In Partial Fulfillment of the Requirements for the Degree

Doctor of Philosophy in Chemistry

School of Chemistry and Biochemistry

Georgia Institute of Technology, Atlanta 30332

December 2007

LONG-RANGE CHARGE TRANSFER IN DNA CONDENSATES AND DNA-DIRECTED ASSEMBLY OF CONDUCTING POLYMERS

Approved by:

Dr. Gary B. Schuster, Advisor
School of Chemistry and Biochemistry
Georgia Institute of Technology,
Atlanta, GA 30332

Dr. David M. Collard
School of Chemistry and Biochemistry
Georgia Institute of Technology,
Atlanta, GA 30332

Dr. Donald F. Doyle
School of Chemistry and Biochemistry
Georgia Institute of Technology,
Atlanta, GA 30332

Dr. Marcus Weck
School of Chemistry and Biochemistry
Georgia Institute of Technology,
Atlanta, GA 30332

Dr. Uzi Landman
School of physics
Georgia Institute of Technology,
Atlanta, GA 30332

Date approved: 11/09/2007

ACKNOWLEDGEMENTS

This thesis is the result of five years of work whereby I have been accompanied and supported by many people. It is a pleasure to convey my gratitude to all of them in my humble acknowledgement.

I owe my most sincere gratitude to my PhD supervisor, Dr. Gary B. Schuster for giving me the opportunity to work in his laboratory. He has been a constant source of encouragement and support. His invaluable advices and guidance are going to be an asset of lifetime for me. Thanks are due to my Committee members for their encouragement and helpful suggestions.

I am grateful to my present and past lab-mates for their help and co-operation. I want to specially thank Dr. Sriram Kanvah, Dr. Abraham Joy, Dr. Richard Redic, Dr. Joshy Joseph, Dr. Bhaskar Datta, and Dr. Selvi Srinivasan for their priceless help with the laboratory techniques and numerous experiments. I also thank Gozde Guler and Wen Chen for their help and support. I wish to thank Dr. Nicholas Hud and Dr. Andrew Lyon and their graduate students of School of Chemistry & Biochemistry at Georgia Tech for allowing me to perform some important experiments in their laboratory.

I want to extend my special thanks to my wife, Samapti. She has been the most supportive and helpful. Her constant encouragement, love and patience have made this journey possible. I would also thank my brother Prosun and my brother in law, Sudip for their love and affection. Finally, and most importantly, I wish to thank my parents, Hari Pada Das and Arati Das. They raised me, supported me, taught me, loved me and have been the most important to the successful realization of this work. To them I dedicate this thesis.

TABLE OF CONTENTS

ACKNOWLEDGEMENTS	iii
LIST OF TABLES	ix
LIST OF FIGURES	x
LIST OF SYMBOLS AND ABBREVIATIONS	xv
SUMMARY	xviii
PART I: LONG-RANGE CHARGE TRANSFER IN PLASMID DNA CONDENSATES	
CHAPTER 1: INTRODUCTION	1
1.1 Structural Components of DNA	3
1.2 The DNA Double Helix	7
1.3 Conformations of DNA	10
1.4 DNA damage: Causes and Effects	15
1.5 Oxidative damage of DNA	16
1.6 Charge Injection into DNA	19
1.7 Anthraquinone as a Charge Injector	22
1.8 Charge Migration through DNA	25
1.9 Charge Trapping	30
1.10 References	34
CHAPTER 2: RADICAL CATION MIGRATION THROUGH SINGLY LIGATED PLASMID DNA CONDENSATES	39
2.1 Introduction	39
2.2 Plasmid DNA and Restriction Enzyme Recognition	40
2.3 DNA Ligation and Ligases	43

2.4 DNA Condensation	44
2.5 DNA Condensate Morphology	46
2.6 Kinetics and Thermodynamics of Condensation	47
2.7 Forces in DNA Condensation	48
2.8 Research Idea	50
2.8 Design of Synthetic Oligonucleotide Duplex	51
2.9 Experimental	53
2.9.1 Materials and Methods	53
2.9.2 Synthesis of DNA Single Strands	55
2.9.3 Thermal Denaturation Study of DNA Oligomer Duplex	56
2.9.4 Circular Dichroism Study	57
2.9.5 Preparation of Radiolabel DNA	58
2.9.6 Restriction Endonuclease Digestion of Plasmid Puc19	59
2.9.7 Ligation of Plasmid with Radiolabeled Oligonucleotides	60
2.9.8 Purification of Ligated Plasmid	61
2.9.9 Proof of ligation: Autoradiography	62
2.9.10 Preparation of DNA Condensates & Dynamic Light Scattering Study	62
2.9.11 Transmission Electron Microscopy (TEM) Study	63
2.9.12 UV Irradiation and Piperidine Treatment	64
2.9.13 PAGE Analysis	65
2.9.14 Phosphoimagery	66
2. 10 Results	66

2.10.1 Structural Conformation & Thermal Integrity of Oligomer Duplex	66
2.10.2 Ligation of Oligomer with Plasmid	67
2.10.3 DNA Condensation with Spermidine	69
2.10.4 Long-Distance Radical Cation Transfer in DNA Condensates	72
2.11 Discussion	77
2.12 Conclusion	81
2.13 References	82
CHAPTER 3: RADICAL CATION MIGRATION THROUGH DOUBLY LIGATED PLASMID DNA CONDENSATES	86
3.1. Introduction	86
3.2. Anthraquinone Intercalation versus End-Capping	87
3.3 Research Idea	90
3.4. DNA Sequences	91
3.5 Synthesis of Uridine Anthraquinone (UAQ)	93
3.6 Experimental	95
3.6.1 Materials and Methods	95
3.6.2 Uridine Anthraquinone (UAQ) Synthesis	96
3.6.3 Synthesis of DNA Single Strands	98
3.6.4 Characterization of DNA Duplex	100
3.6.5 Preparation of Radiolabeled DNA	100
3.6.6 Restriction Endonuclease Cutting of Plasmid	101
3.6.7 Ligation of Plasmids with Radiolabeled Oligonucleotide	102
3.6.8 Dynamic Light Scattering Study	103

3.6.9 Transmission Electron Microscope Study	104
3.6.10 UV Irradiation	104
3.6.11 Restriction Endonuclease Cutting of Double Ligated Plasmid	105
3.6.12 Piperidine Treatment and PAGE analysis	105
3.7 Results	106
3.7.1 Design, Synthesis and Characterization of UAQ-DNA and its Complementary sequence	106
3.7.2 Thermal Integrity and Structural Confirmation of DNA Oligomer Duplex	107
3.7.3 Ligation of Plasmid DNA with Oligomer Duplex	109
3.7.4 DNA Condensates from SLP and DLP with Spermidine	112
3.7.5 Photochemistry of UAQ-DNA3-DNA 4, SLP and DLP with Spermidine	116
3.7.6 Phosphoimagery	121
3.8 Discussion	122
3.9 Conclusion	126
3.10 References	128

PART II: DNA DIRECTED SELF ASSEMBLY OF CONDUCTING POLYMERS

CHAPTER 4: INTRODUCTION TO DNA DIRECTED SELF ASSEMBLY OF CONDUCTING POLYMERS	131
4.1 The Concept of Nanowire	132
4.2 Conducting Polymers for Nanowire	133
4.3 Conducting Polymers from Polyaniline	135
4.4 Self Assembly of Conducting Polymers	136
4.5 Templated Polymer Synthesis	138

4.6 DNA Templated Polymerization of Conducting Polymers	140
4.7 References	144
CHAPTER 5: SYNTHESIS AND CHARACTERIZATION OF MONOMER UNITS OF CONDUCTING POLYMER ATTACHED TO DNA TEMPLATE 147	
5.1 Introduction	147
5.2 DNA Sequence Programmability Applied to Formation of PANI	148
5.3 Research Idea	150
5.4 Experimental	159
5.4.1 Materials and Methods	159
5.4.2 Synthesis of 3-(2,5-di(biphenyl-4-yl)-1H-pyrrol-1-yl)propan-1-amine (2)	160
5.4.3 Synthesis of 2,5-Bis(biphenyl)-pyrrole linked deoxycytidine-DMT-phosphoramidite (6)	161
5.4.4 Synthesis of tert-butyl4,4'-(1-(3-aminopropyl)-1H-pyrrole-2,5-diyl)bis(4,1phenylene)dicarbamate (12')	164
5.4.5 Synthesis of Tert-butyl 3-(2,5-bis(4-(biphenyl-4-yl(tert-butoxy carbamate)aminophenyl)-1H-pyrrol-1-yl)propylcarbamate (16)	168
5.4.6 Preparation of DNA Conjoined Monomer Units	170
5.5 Results	171
5.5.1 Synthesis of Monomer Units 2, 6, 12 and 16	171
5.5.2 DNA Conjoined Monomer Units	176
5.6 Discussion	178
5.7 Conclusions and Future Scopes	180
5.8 References	181

LIST OF TABLES

Table 1.1: Parameters of Different DNA Helices.	11
Table 1.2: List of Photosensitizers used for Charge Injection in DNA	12
Table 1.3: Oxidation Potentials of the DNA Bases.	13

LIST OF FIGURES

Figure 1.1: Cyclic Furanose Form of Ribose and 2'-Deoxyribose.	4
Figure 1.2: 2'-Deoxyribose Sugar-Puckering.	4
Figure 1.3: Structure of Purine, Pyrimidine and DNA Bases.	5
Figure 1.4: Different Components of DNA.	7
Figure 1.5: DNA Base Pairing by Formation of Hydrogen Bonds.	8
Figure 1.6: Schematic Illustration of the Major and Minor Groove of DNA.	10
Figure 1.7: Hyperchem Generated Picture of a Portion of B-DNA.	12
Figure 1.8: Hyperchem Generated Picture of a Portion of A-DNA.	13
Figure 1.9: Hyperchem Generated Picture of a Portion of Z-DNA.	14
Figure 1.10: Structure of Photosensitizers used for Hydrogen Atom Abstraction in DNA	18
Figure 1.11: Structures of Photosensitizers used for Charge Injection in DNA.	21
Figure 1.12: Structures of different AQ Derivatives.	23
Figure 1.13: Hyperchem Generated image showing AQ "End-Capping" in DNA.	24
Figure 1.14: Charge Injection Mechanism of Anthraquinone by Irradiation.	25
Figure 1.15: Schematic Illustration of Ring Opening of N6-Cyclopropyladenosine by Charge Transfer.	28
Figure 1.16: Schematic of Phonon-assisted Polaron like Hopping Mechanism of Charge Migration in DNA.	29
Figure 1.17: Reaction of Guanine Radical Cation with Water and Oxygen.	31
Figure 1.18: Structure of some Modified Bases Generated from Oxidative DNA Damage.	33
Figure 2.1: Illustration of a Bacterium showing Chromosomal DNA and Plasmids.	41
Figure 2.2: Restriction Map for Puc19 Plasmid.	42

Figure 2.3: Recognition Site for Eco RI and HindIII Restriction Enzyme in Puc19 Plasmid.	43
Figure 2.4: Schematic Representation of Steps Involved in DNA Ligation Reaction.	44
Figure 2.5: Structures of Common DNA Condensation Agents.	46
Figure 2.6: Schematic Diagram of Experimental Design.	51
Figure 2.7: Design of DNA Oligomer Duplex DNA1-DNA2.	52
Figure 2.8: Scheme for Synthesis of Anthraquinone-Phosphoramidite.	53
Figure 2.9.A: Mass Spectra of DNA1.	56
B: Mass Spectra of DNA2.	56
Figure 2.10.A: Thermal Denaturation Curve for DNA1-DNA2.	57
B: Thermal Denaturation Curve for Non-AQ Containing Blunt Ended DNA1-DNA2	57
Figure 2.11: Circular Dichroism Spectra of DNA1-DNA2.	58
Figure 2.12: Nondenaturing Low Melting Agarose Gel.	68
Figure 2.13: Autoradiogram of a Nondenaturing, Low-Melting Agarose Gel, showing Linear Ligated Plasmid and the Duplex Oligomer DNA1-DNA2.	69
Figure 2.14: Dynamic Light Scattering studies: Variation of Intensity of Light Scattered with Spermidine Concentration.	70
Figure 2.15: Dynamic Light Scattering studies: Variation of Average Hydrodynamic Radii with Spermidine Concentration .	71
Figure 2.16: Transmission Electron Microscopy Image of Linear Ligated Plasmid Condensates with 75 μ M .	72
Figure 2.17: Autoradiogram showing Results of Irradiation of DNA1-DNA2, Linear Ligated Plasmid (LLP), and Condensed Plasmid.	75
Figure 2.18: Autoradiogram showing Results of Irradiation of DNA1-DNA2, Condensed and Decondensed Ligated Plasmid	76

Figure 2.19: Histogram showing the Relative Damage at the GG Steps of DNA1-DNA2, Linear Ligated Plasmid and Ligated Condensed Plasmid.	77
Figure 2.20: Semilog Plot of the Relative Amount of Strand Cleavage Detected at GG Steps.	79
Figure 2.21: Pictorial Depiction of the Effect of Condensate Formation on Radical Cation Hopping in DNA	80
Figure 3.1: Molecular Modeling Showing AQ End-Capping the DNA Duplex.	89
Figure 3.2: Assumed Structure of UAQ Intercalated in Duplex DNA.	89
Figure 3.3: Schematic Diagram of Experimental Design.	91
Figure 3.4: Design of Oligomer Sequences DNA3 and DNA4.	92
Figure 3.5: Scheme for Synthesis of Uridine Anthraquinone (UAQ)	94
Figure 3.6.A: Mass Spectra of DNA3.	99
B: Mass Spectra of DNA.	99
Figure 3.7: Thermal Denaturation Curve for DNA3-DNA4 in 10 mM Sodium Phosphate Solution.	108
Figure 3.8. A: Thermal Denaturation Curve for Non-AQ Containing DNA3-DNA4.	108
B: Thermal Denaturation Curve for Blunt Ended DNA3-DNA4.	108
Figure 3.9: Circular Dichroism Spectra of DNA3-DNA4.	109
Figure 3.10: Non-Denaturing Low Melting Agarose Gel Showing Mobility of DNA3-DNA4, SLP and DLP.	111
Figure 3.11: Autoradiography of Agarose Gel Showing DNA3-DNA4, SLP and DLP.	112
Figure 3.12: Plot of Intensity of Scattered Light vs. Concentrations of Spermidine.	113
Figure 3.13: Plot of Average Hydrodynamic Radii vs. Spermidine Concentration.	114
Figure 3.14: Plot of Intensity of Scattered Light vs. Time.	115
Figure 3.15: Plot of Average Hydrodynamic Radii vs. Time.	115

Figure 3.16: Transmission Electron Microscopic Image of DNA Condensate Formed from DLP.	116
Figure 3.17: Autoradiogram Showing Strand Cleavage of DNA3-DNA4, SLP and DLP in Presence of Spermidine	118
Figure 3.18: Autoradiogram showing Results of Irradiation of DNA3-DNA4 with Different Concentrations of Spermidine	120
Figure 3.19: Fuji Phosphoimagery Experiment Histogram Showing the Relative Damage at the GG Steps of DNA3-DNA4, SLP and DLP	122
Figure 3.20: Schematic Diagram of Radical Cation Migration in UAQ Containing SLP and DLP in Presence of Spermidine	126
Figure 4.1: Structures of Common Organic Conducting Polymers.	134
Figure 4.2: Structure of Polyaniline in Three Oxidation States.	135
Figure 4.3: Structures of Different Types of Copolymers of PANI.	136
Figure 4.4: Polyaniline Formation on Sulphonated Polystyrene Template.	140
Figure 4.5: Schematic Representation of DNA Templated Polymerization of PANI in Solution.	141
Figure 4.6: Schematic Representation of Polymerization of PANI on DNA Template Immobilized on Silica Surface.	142
Figure 4.7: Computer Generated Structural Model Showing Six Aniline Groups Bonded head-to-tail Conjoined to a DNA Oligomer.	143
Figure 5.1: Schematic of the Polymerization Scheme of DNA Conjoined PANI and 4-Aminobiphenyl.	150
Figure 5.2: Scheme for Intermolecular Attachment of DNA-Conjoined Monomer Units.	151
Figure 5.3: Scheme for Intramolecular Attachment of DNA-Conjoined Monomer Units.	152
Figure 5.4: Scheme for Attachment of Horizontally Extended Monomer Unit.	153
Figure 5.5: Hyperchem Model of PANI like Monomer Linked Covalently to DNA.	154
Figure 5.6: Scheme for the Synthesis of 2 .	155

Figure 5.7: Scheme for the Synthesis of 6 .	156
Figure 5.8: Scheme for the Synthesis of Boc-Protected 12 .	157
Figure 5.9: Scheme for the Synthesis of Horizontally Extended Monomer Unit 16 .	158
Figure 5.10: ^1H NMR Spectra of Compound 2 .	172
Figure 5.11: ^1H NMR Spectra of Compound 6 .	173
Figure 5.12: ^1H NMR Spectra of Compound 12 .	174
Figure 5.13: ^1H NMR Spectra of Compound 16 .	175
Figure 5.14: DNA Sequences Prepared for Attachment of Monomer 2, 12 and 16.	176
Figure 5.15: ESI Mass Spectra of PSA 1 Attached Covalently to Monomer 2.	177

LIST OF SYMBOLS AND ABBREVIATIONS

DNA	Deoxyribonucleic acid
ssDNA	single-stranded DNA
dsDNA	double-stranded DNA
bp	base pair
M	molar
mM	millimolar
k_B	Boltzmann constant
T	Temperature
A	Adenine
G	Guanine
C	Cytidine
T	Thymine
AQ	Anthraquinone
CD	Circular Dichroism
T _m	melting temperature
TEM	Transmission Electron Spectroscopy
DLS	Dynamic Light Scattering
$\delta A/\delta T$	change in absorbance with respect to the change in temperature
nm	nanometer
$^{\circ}\text{C}$	degree(s) Celsius
Å	Angstrom(s)
G ^{•+}	Guanine radical cation

AQ ^{•-}	Anthraquinone radical anion
k_h	rate of hopping
k_t	rate of trapping
HPLC	High-Performance Liquid Chromatography
UV	Ultraviolet
Vis	Visible
α	alpha
γ	gamma
δ	delta
μ	micro (10^{-6})
ϵ	extinction coefficient
ESI	Electron Spray Ionization
PNK	polynucleotide kinase
TdT	terminal dinucleotide transferase
<i>in vacuo</i>	in a vacuum
cm	centimeter(s)
ATP	5'-Adenosine triphosphate
h	hour
min	minute(s)
cpm	counts(s) per minute
RPM	rotations per minute
SLP	Single Ligated Plasmid
LLP	Linear Ligated Plasmid

DLP	Double Ligated Plasmid
DMT	4,4'-Dimethoxytrityl
CDCl ₃	Deuterated chloroform
Boc	Tertiarybutoxycarbonyl
Fmoc	Fluorenyl-methoxycarbonyl
OSu	Succinimidyl carbonate
PANI	Polyaniline
Pd(OAc) ₂	Paladium(II) acetate
S-BINAP	(S)- (-)-2,2'-Bis(diphenylphosphino)-1'1'-binaphthyl
Na-O ^t Bu	Sodium tertiarybutoxide
DMAP	4-Dimethylamino pyridine
POCl ₃	Phosphorus oxychloride
TLC	thin layer chromatography
^t BuOH	Tertiarybutanol
MeOH	Methanol
EtOAc	Ethyl acetate
CH ₂ Cl ₂	Dichloromethane

SUMMARY

PART I

Long-distance radical cation transport was studied in DNA condensates where linearized pUC19 plasmid was ligated to an oligomer and transformed into DNA condensates with spermidine. DNA condensates were detected by Dynamic Light Scattering and observed by Transmission Electron Microscopy. Introduction of charge into the condensates causes long-distance charge migration, which is detected by reaction at the remote guanines. The efficiency of charge migration in the condensate is significantly less than it is for the corresponding oligomer in solution. This result is attributed to a lower mobility for the migrating radical cation in the condensate, caused by inhibited formation of charge-transfer-effective states. Radical cation transport was also studied in DNA condensates made from an oligomer sandwiched between two linearized plasmids by double ligation. Unlike the single ligated plasmid condensates, the efficiency of charge migration in the double ligated plasmid-condensates is high, indicative of local structural and conformational transformation of the DNA duplexes.

PART II

Organic monomer units having extended π -conjugation as part of a long conducting polymer was synthesized and characterized. The monomer units were covalently attached to particular positions in DNA oligonucleotides by either the convertible nucleotide approach or by phosphoramidite chemistry. Successful attachment of the monomer units to DNA were confirmed by mass spectral analysis. The DNA-conjoined monomer units can self assemble in the presence of complementary sequences which act as templates that can

control polymer formation and structure. By this method the para-direction of the polymer formation can be enforced and may be used to generate materials having nonrecurring, irregular structures.

PART I

LONG-RANGE CHARGE TRANSFER IN PLASMID DNA CONDENSATES

CHAPTER 1

INTRODUCTION

In the 1830's, Theodor Schwann and Mathias Schleiden discovered that the nucleus plays a chief role in the growth and development of living cells, which was the basis of the cell theory, initially founded by Robert Hooke. Further insights into cells with advancement of time and technology established that nuclei of cells contain very long threads of nucleic acids and proteins called chromosomes. In the early 1900's, the hypothesis that chromosomes contain hereditary information was gaining acceptance from the biological community. Once accepted and confirmed that DNA, the main constituent of chromosome was the source of hereditary information it was a race to discover its structure in hopes of better understanding this fascinating molecule. Rosalind Franklin made a significant contribution to the discovery of the structure of DNA with the information she gathered using during X-ray diffraction. At that time scientists knew that DNA consisted of sugars (deoxyribose sugar), phosphates, and four different nitrogen bases: adenine, guanine, cytosine, and thymine. Scientists also established that the number of adenine and thymine molecules was equal, and number of guanine equals that of cytosine molecules in a DNA irrespective of the species of the organism studied. There were many people who contributed to the discovery of the structure of DNA, but it was James Watson and Francis Crick who ultimately developed the first three-dimensional model of a DNA strand in 1953 by stitching together all the information. Watson and Crick's model is still in use today.

After the elucidation of the structure of duplex DNA, it was immediately postulated that the nature of base stacking could facilitate the migration of a charge through the DNA.

The process of charge migration through DNA has been rigorously studied during the last two decades, which is motivated in part by its relevance to two important subjects. First, charges moving through DNA may result in oxidative damage, which is believed to be responsible for aging, apoptosis, and cancer¹⁻⁴. A better understanding of the mechanism of charge migration through DNA may lead to the discovery of tools required for damage prevention and repair⁵. Secondly, the property of charge migration through DNA has led to the hypothesis that DNA could be used as a molecular wire⁶. Although it is acknowledged that charge, in the form of radical cation or electron can migrate into DNA to a limited distance, the mechanism by which this migration process occurs has produced ambiguities among researchers.

There are several proposed mechanisms which explain the migration of radical cation through DNA in the light of tunneling process⁷⁻⁸; however, experimental evidence has restricted this model to special situations only. The second proposed mechanism, which is known as the “Phonon assisted Polaron Hopping Model”, is now the accepted mechanism for the charge migration, which have successfully accounted for the behavior of DNA oligomer duplexes in response to charge migration⁹.

Here we report the radical cation migration in condensed plasmid DNA, which strongly resemble intraphage DNA. Through our studies we tried to gain mechanistic insight of charge transfer in long pieces of plasmid DNA containing end capped or intercalated charge injectors, introduced in the plasmid through ligation with modified oligomer duplex DNA.

1.1 Structural components of DNA

Deoxyribonucleic acid, DNA is chemically a long polymer of simple units called nucleotides, with a backbone made of deoxyribose (furanose) sugar and phosphate groups joined by ester bonds. Attached to each sugar is one of the four types of molecules called nitrogenous bases namely Adenine, Guanine, Thymine and Cytosine.

Sugars

The sugar moiety present in DNA is 2'-deoxyribose, an aldopentose in its cyclic furanose form. The deoxyribose lacks an hydroxyl group in its 2'-position (Figure 1.1). DNA differs from RNA at this point where RNA has the 2'-hydroxyl group. The conformation of deoxyribose sugar ring is very important in determining the overall structure of DNA. The deoxyribose sugar of DNA adopt the β -D-conformation meaning both the substituents at the 1' and the 4' position are facing "up", or above the plane of the ring. For majority of DNA the C2 position is above the plane of the ring and tends to "pucker" out of the plane of the ring (Figure 1.2).

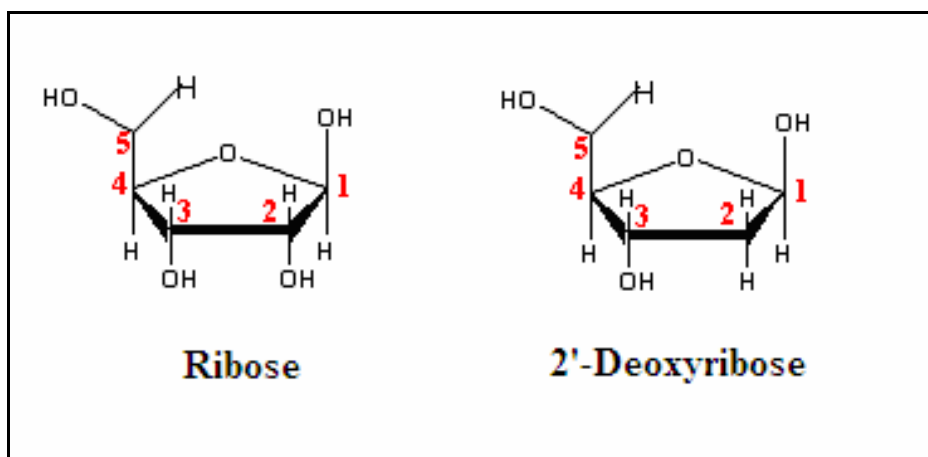


Figure 1.1: Cyclic Furanose Form of Ribose and 2'-Deoxyribose.

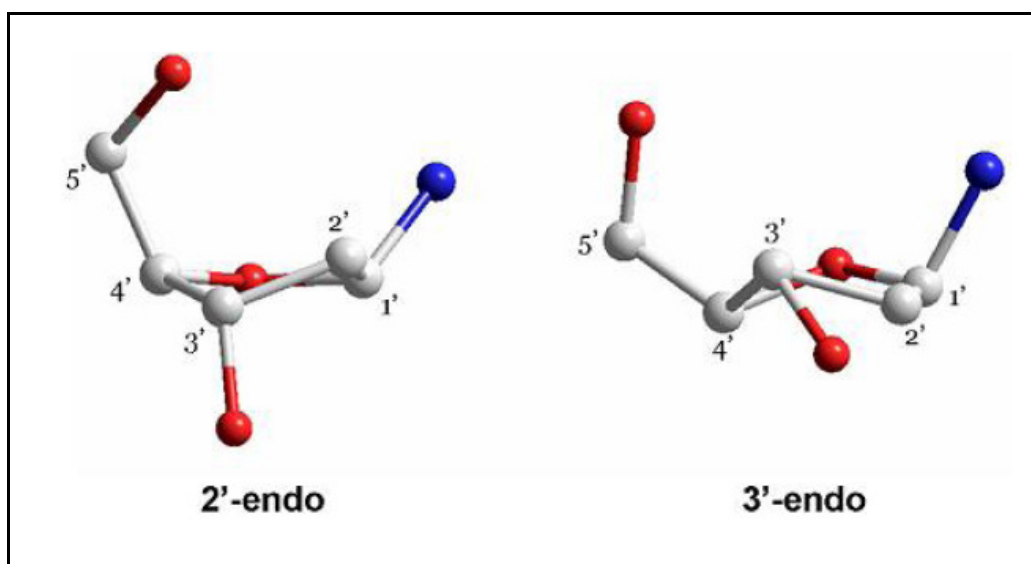


Figure 1.2: 2'-Deoxyribose Sugar-Puckering. White, Red and Blue Balls represent Carbon, Oxygen and Nitrogen Respectively (Hydrogens are not shown).

Bases

There are two types of heterocyclic nitrogenous bases in DNA: purine and pyrimidine. Adenine (A) and Guanine (G) belong to the purine family whereas Thymine (T) and Cytosine (C) are pyrimidines (Figure 1.3). In A, an amine group ($-NH_2$) group is attached to the C6 position of the purine, whereas G has a carbonyl ($-C=O$) group at C6 position and an amine group at C2 position. C has an amine group at C4 position of pyrimidine whereas T has a carbonyl group at C2 and a methyl (CH_3) group at C5 position of pyrimidine. Uracil (U), which is a base normally for RNA has a similar structure as thymine, only difference being the absence of methyl group at C5 of T.

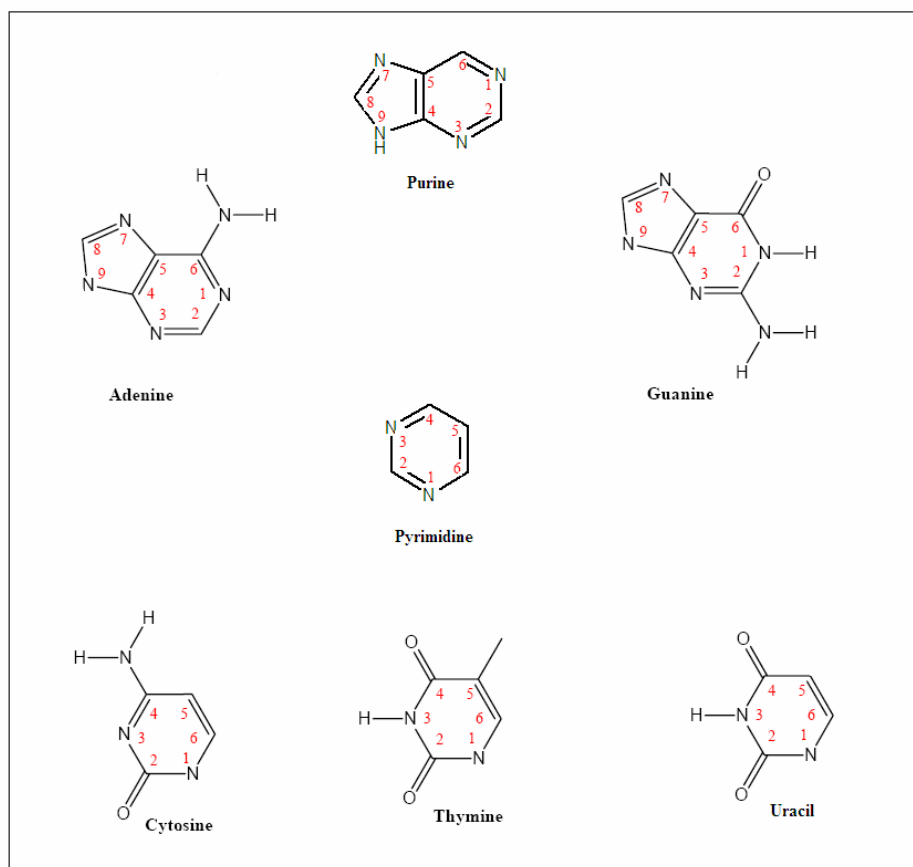


Figure 1.3: Structure of Purine, Pyrimidine and DNA Bases

Glycosidic bond

The carbon-nitrogen bond between the sugar and the base is known as the glycosidic bond (Figure 1.4). In a nucleoside the base is attached to the C1 position of sugar. For adenine and guanine, N9 positions of the bases are attached to the sugar and for thymine and cytosine N1 position of the bases connect to the sugar.

Phosphate backbone and phosphodiester bond

The sugar and phosphates make up the backbone of the DNA with the phosphates attached to the 5'-CH₂OH and 3'-OH of the sugar, giving rise to a 5' and 3' terminus to DNA single strands (Figure 1.4). The O-P bonds between the sugar and phosphates are termed as phosphodiester bonds. The nucleotides are connected to each other through these phosphate groups.

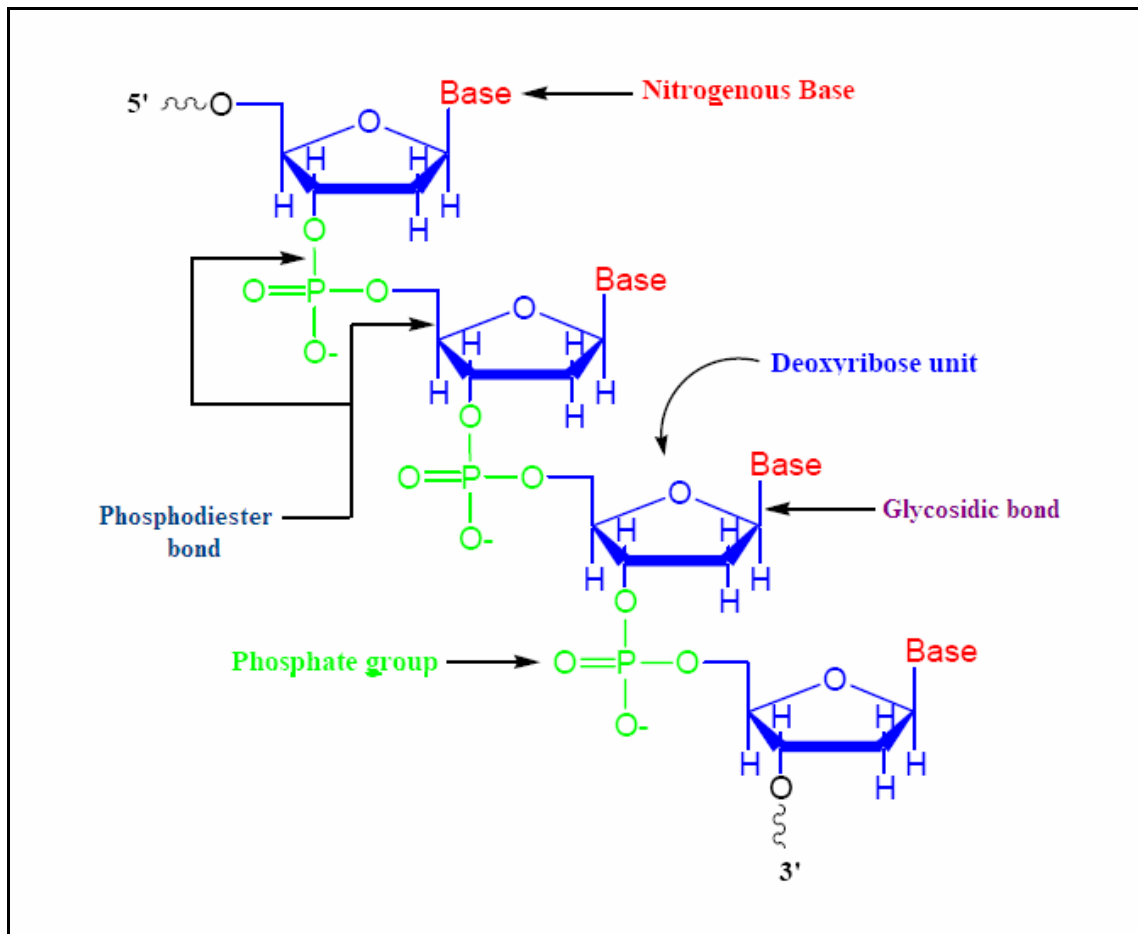


Figure 1.4: Different Components of DNA

1.2 The DNA Double Helix

Wilkins and Franklin obtained X-ray diffraction data and interpreted that DNA was helical in nature¹⁰⁻¹¹. In 1953 Watson and Crick reported that DNA consists of two helical chains each coiled around the same axis. One of the most versatile features of the Watson and Crick model was the base pairing of adenine with thymine and guanine with cytosine, and that these base pairs are held together by hydrogen bonds that are specific for each pair (Figure 1.5). There are two hydrogen bonds between A and T, while G and C are held

together by three hydrogen bonds. In an A-T base pair, the C6-NH₂ of A forms a hydrogen bond with C4=O of T and N1 of A and N3-H of T forms the other one. For G-C base pairs the three hydrogen bonds involve the C6=O of G with C4-NH₂ of C, N1-H of G with N3 of C and lastly C2-NH₂ of G with C2=O of C. The elucidation of the secondary structure of DNA explains how DNA could possibly be the carrier of genetic information with only four base pairs. When both strands are copied, a new duplex is formed which has exactly the same sequence as the parent one. Thus the complementarity of duplex DNA leads to the ability of self-replication, resulting in the creation of identical pairs of DNA¹².

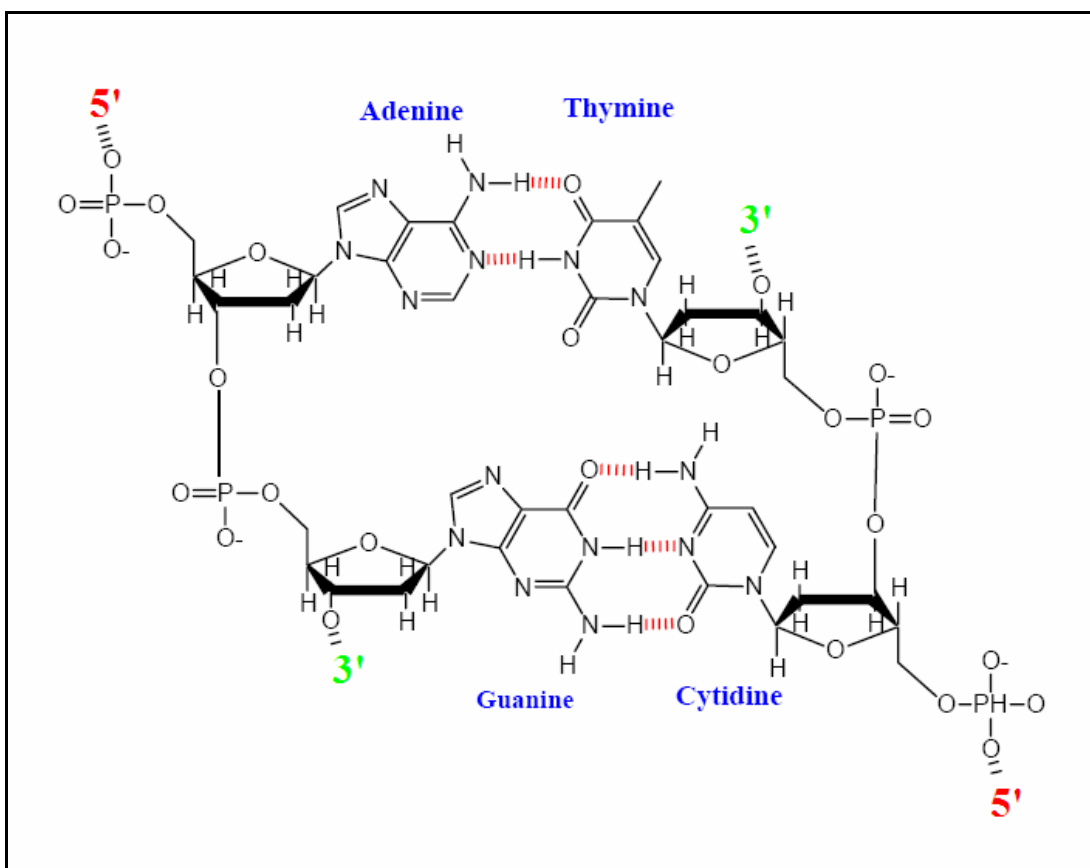


Figure 1.5: DNA Base Pairing by Formation of Hydrogen Bonds.

The characteristic features of the Watson-Crick Double Helical DNA are as follows:

- ❖ The complementary polynucleotide chains wind around a common axis to form the DNA double Helix.
- ❖ The two polynucleotide chains run in opposite direction i.e. antiparallel to each other but individually they form right-handed helix.
- ❖ The heterocyclic bases occupy the core of the helix, and are held together with the complementary bases by hydrogen bonds.
- ❖ The sugar and phosphates make up the backbone of the single strands of DNA with the phosphates attached to the 5'-CH₂OH and 3'-OH of the sugar. The individual sugar phosphate backbone chains run along the periphery, thereby minimizing the repulsions between the charged phosphate groups.
- ❖ As the DNA strands wind around each other, they leave gaps between each set of phosphate backbones, revealing the sides of the bases inside. These give rise to two grooves of different width: The **major groove** occurs where the backbones are far apart, the **minor groove** occurs where they are close together. The grooves twist around the molecule on opposite sides (Figure 1.6).
- ❖ The aromatic heterocyclic bases within the centre of the helix stabilize the duplex through stacking interactions between the aromatic rings in adjacent bases¹³.
- ❖ Metal cations surround the negatively charged phosphate groups in the sugar-phosphate backbone and offer stability to the DNA duplex.
- ❖ Water molecules cooperatively bind along the major and minor groove of the DNA adding further stability¹⁴.

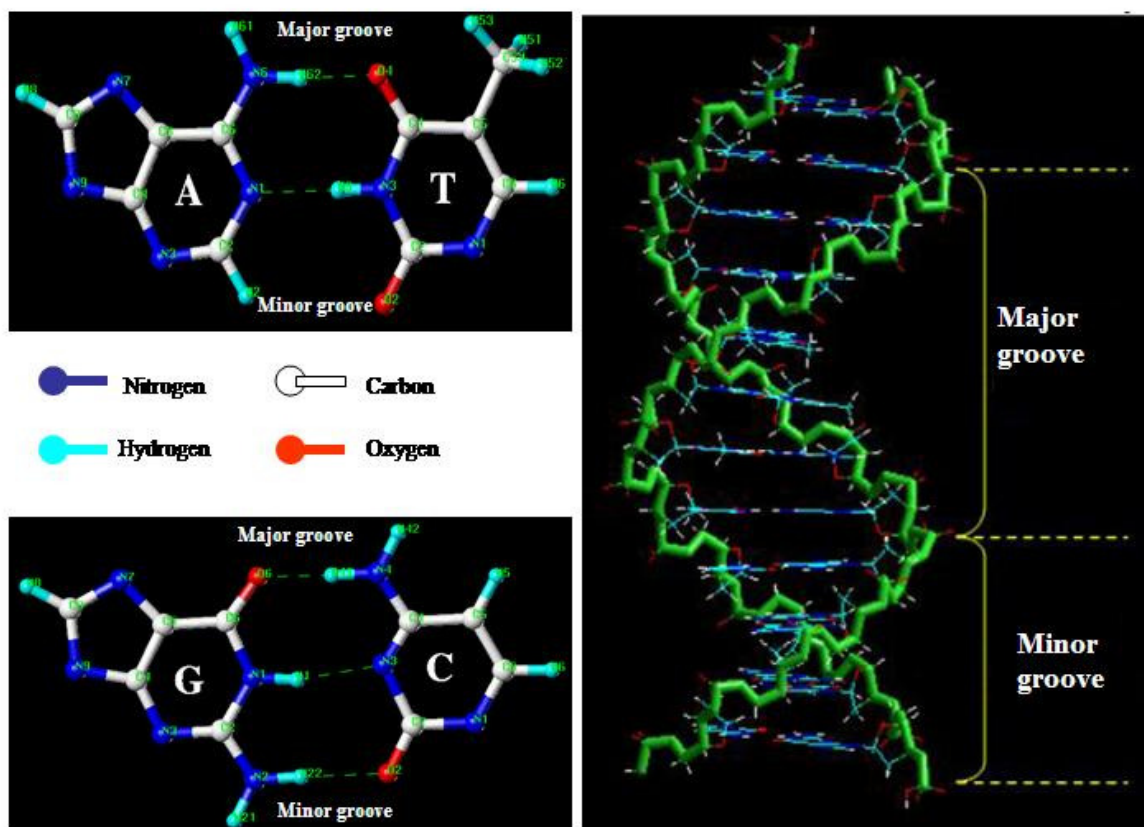


Figure 1.6: Schematic Illustration of the Major and Minor Groove of DNA. Left View: Grooves in Relation to the Functional Groups of the Base Pairs. Right View: Grooves with Respect to the DNA Duplex.

1.3. Conformations of DNA

The secondary structure of DNA can vary depending on the environment. DNA duplex can exist in three different conformations. These are known as A-form, B-form and Z-form of DNA. The conformation and geometry of A-, B-, and Z-DNA vary drastically as a result of the hydration of the phosphate backbone, differing sugar-pucker conformations and stacking interactions between the base pairs²⁶. Characteristics of these DNA conformations are listed in Table 1.1.

Table 1.1:¹⁵ Parameters of Different DNA Helices

Geometry Attribute	A-DNA	B-DNA	Z-DNA
Helix sense	right-handed	Right-handed	left-handed
Repeating unit	1 bp	1 bp	2bp
Rotation/bp	33.6°	35.9°	60°/2
Mean bp/turn	10.7	10.0	12
Inclination of bp to axis	+19°	−1.2°	−9°
Rise/bp along axis	2.3 Å	3.32 Å	3.8 Å
Pitch/turn of helix	24.6 Å	33.2 Å	45.6 Å
Mean propeller twist	+18°	+16°	0°
Glycosyl angle	anti	anti	C: anti, G: syn
Sugar pucker	C3'-endo	C2'-endo	C: C2'-endo, G: C2'-exo
Diameter	26 Å	20 Å	18 Å

B-DNA

B-DNA is a right handed double helix and is the most common DNA conformation (Figure 1.7). The bases of B-DNA are along the axis and the sugar-phosphate backbones are along the periphery. The major groove and minor groove are nearly equivalent in depth, with the major groove being wider than that of the minor groove¹⁶. The N7 and C6 of A and G as well as the C5 of C and T point towards the major groove, while the N3 of A and G as well as the C2-O of C and T point towards the minor groove. Its glycosidic bonds form anti conformations, while its sugar puckers form C2'-endo conformations.

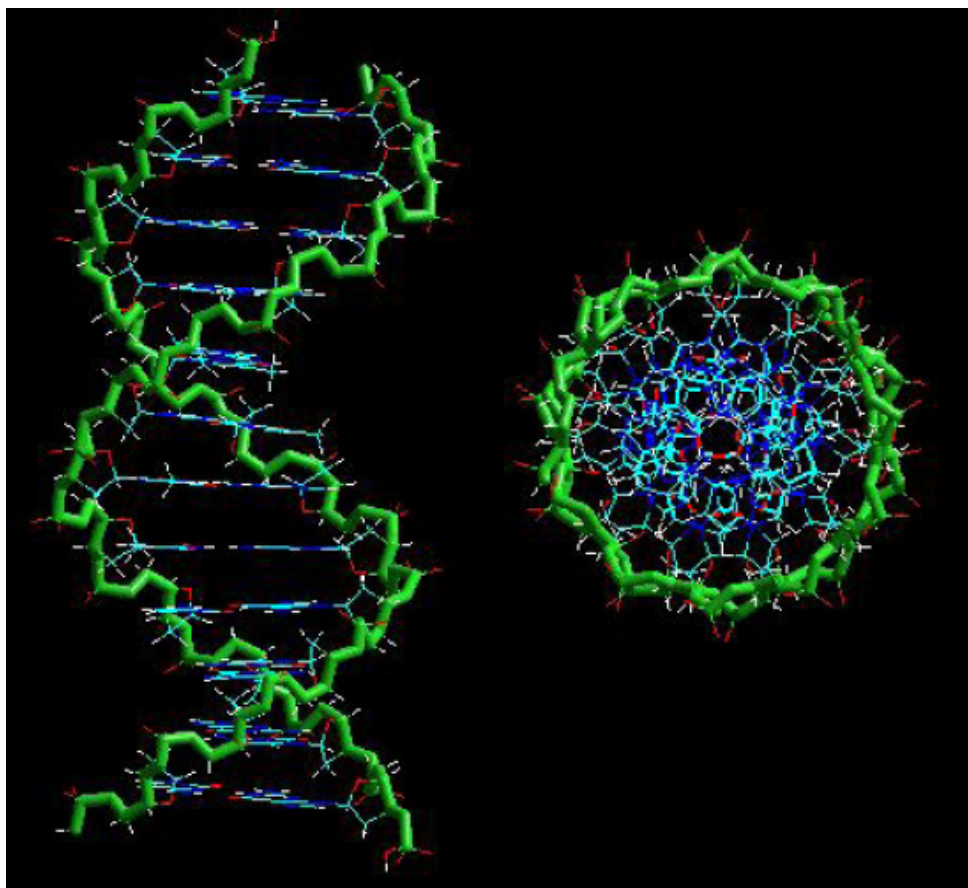


Figure 1.7: Hyperchem Generated Picture of a Portion of B-DNA (side and top view).

A-DNA

A-DNA conformation is preferred when the relative humidity is reduced to less than about 75%. It is also right handed double helix but the helix is wider and shorter than B-DNA. In A-DNA the major groove is very deep and the minor groove is so shallow that it is hardly considered a groove at all. The bases in A-DNA are tilted more sharply with respect to the helix axis and the sugar pucker is C3'-endo.

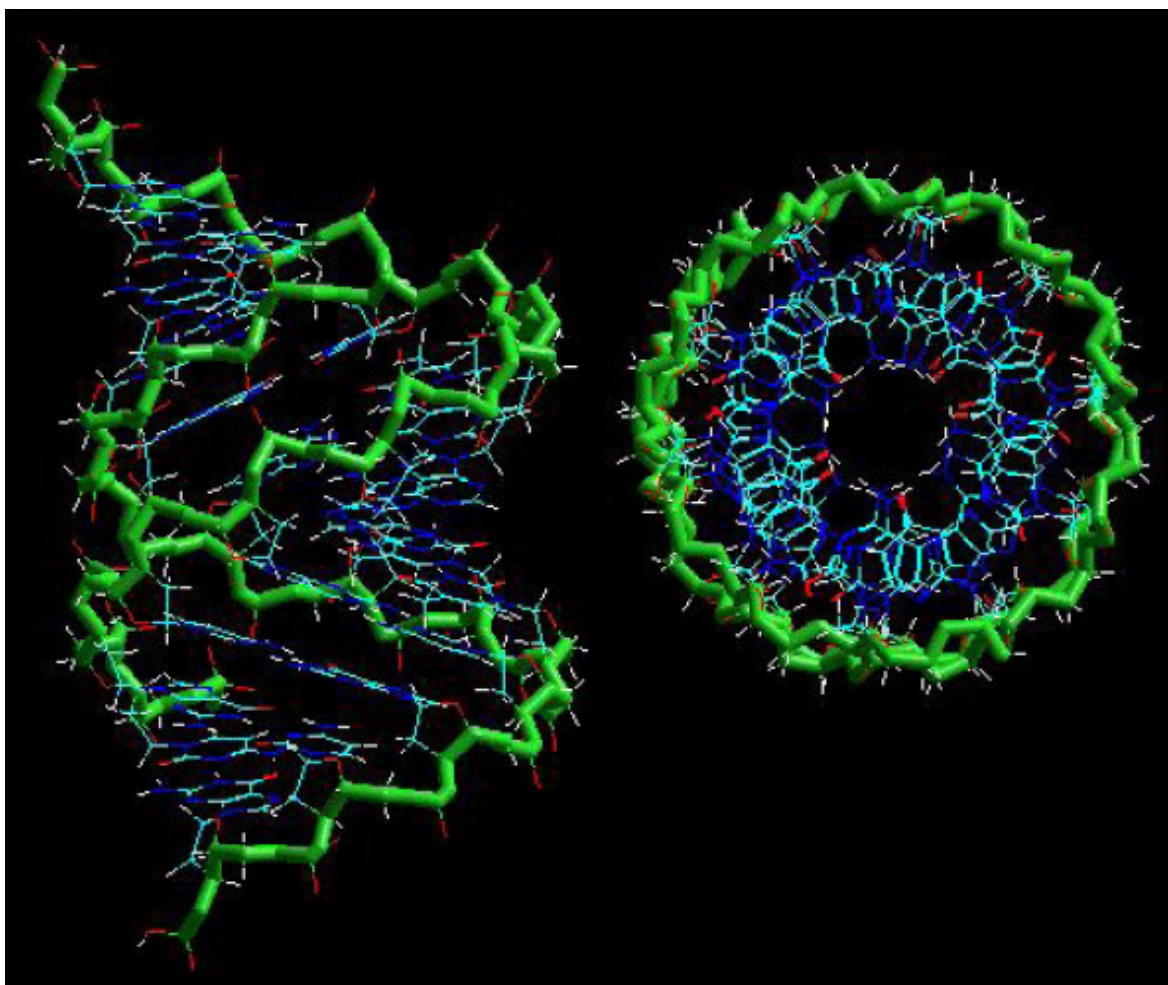


Figure 1.8: Hyperchem Generated Picture of a Portion of A-DNA.

Z-DNA

Z-DNA has a left-handed double helical structure in which the phosphates in the backbone are in zig-zag pattern (Figure 1.9). It uses two consecutive nonequivalent base pairs as the helical repeating unit. Formation of this structure is generally unfavourable, although certain conditions can promote it; such as alternating purine-pyrimidine sequence, DNA supercoiling or high salt and some cations. While no definitive biological significance of Z-DNA has been found, it is commonly believed to provide torsional strain relief (supercoiling) while DNA transcription occurs¹⁷⁻¹⁸.

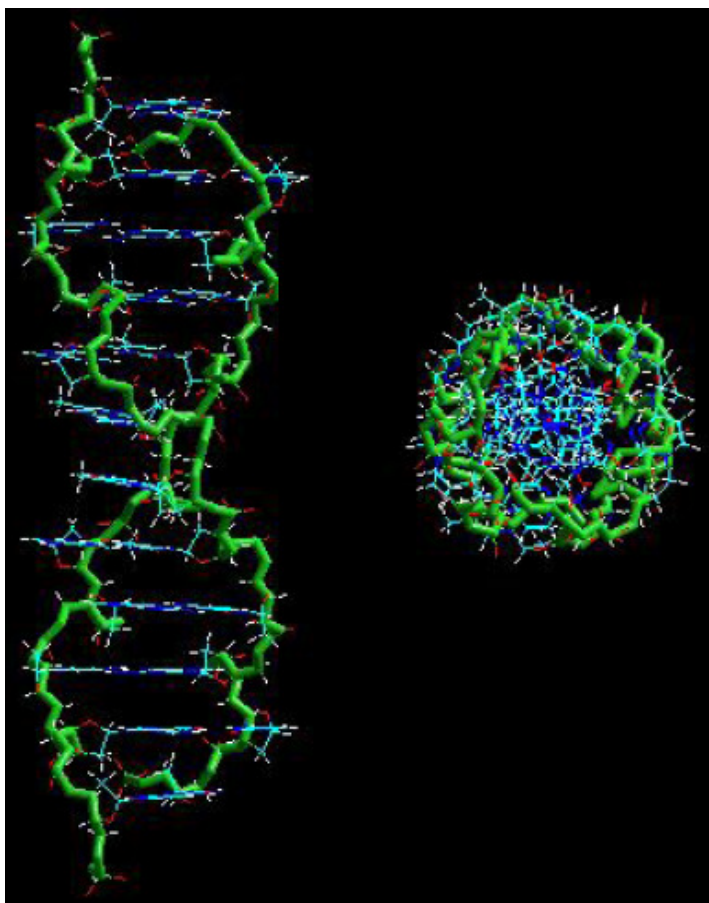


Figure 1.9: Hyperchem Generated Picture of a Portion of Z-DNA

1.4 DNA damage: Causes and Effects

The DNA inside a cell is under constant attack from different sources which are potential threat to the DNA leading to its damage. DNA damage occurs at a rate of 1,000 to 1,000,000 molecular lesions per cell per day¹⁹. While this constitutes only 0.000165% of the human genome's approximately 6 billion bases (3 billion base pairs), unrepaired lesions in critical genes can impede a cell's ability to carry out its function and appreciably increase the likelihood of permanent impairment. The vast majority of DNA damage affects the primary structure of the double helix; that is, the bases themselves are chemically modified. These modifications can in turn disrupt the molecules' regular helical structure by introducing non-native chemical bonds or bulky adducts that do not fit in the standard double helix. DNA is, however, supercoiled and wound around "packaging" proteins called histones, and both superstructures are vulnerable to the effects of DNA damage.

DNA damage can be subdivided into two main types:

1. Endogenous damage such as attack by reactive oxygen species produced from normal metabolic byproducts especially the process of oxidative deamination
2. Exogenous damage caused by external agents such as
 - a) Ultraviolet [UV 200-300nm] radiation from the sun .
 - b) X-rays and gamma rays and also cancer chemotherapy and radiotherapy.
 - c) Hydrolysis or thermal disruption

- d) Plant toxins, human-made mutagenic chemicals, especially aromatic compounds that act as DNA intercalating agents.

The replication of damaged DNA before cell division can lead to the incorporation of wrong bases opposite damaged ones. Daughter cells that inherit these wrong bases carry mutations from which the original DNA sequence is unrecoverable.

There are four main types of damage to DNA due to endogenous cellular processes:

1. Oxidation of bases [e.g. 8-oxo-7,8-dihydroguanine (8-oxoG)] and generation of DNA strand interruptions from reactive oxygen species.
2. Alkylation of bases (methylation), such as formation of 7-methylguanine.
3. Hydrolysis of bases, such as deamination, depurination and depyrimidination.
4. Mismatch of bases, due to errors in DNA replication, in which the wrong DNA base is stitched into place in a newly forming DNA.

1.5 Oxidative damage of DNA

Oxidative damage of DNA is produced in cells by oxygen-derived species resulting from cellular metabolism and from interaction with exogenous sources such as carcinogenic compounds, redox-cycling drugs and ionizing radiations. DNA damage caused by oxygen-derived species including free radicals is the most frequent type encountered by aerobic cells. These agents can cause base and sugar lesions, strand breaks, DNA-protein cross-links and base-free sites²⁰⁻²⁴. Intensive investigations have associated oxidative DNA damage with multiple diseases including aging, arthritis,

neurodegenerative disorders (Alzheimer's disease), cancer, multiple sclerosis and many others²⁵⁻²⁸.

Oxidative damage to DNA is a result of interaction of DNA with reactive oxygen species (ROS). Apart from other ROS, which can result in DNA oxidative damage, there are at least three known chemical sources which can oxidize DNA by photosensitization: hydrogen atom abstraction from an intermediate free radical²⁹, singlet oxygen or hydroxyl radical generated from an excited photonuclease³⁰, and loss of electron from a nucleobase generating a radical cation³¹.

During the hydrogen abstraction process, by irradiation of a photosensitizer in the presence of hydrogen donating substrate, hydrogen is transferred from the donating substrate to the excited photosensitizer³². Presence of multiple hydrogen donating sites in the deoxyribose sugars often make it a hydrogen donor which lead to the formation of sugar radicals. The sugar radicals can ultimately rearrange and bring about strand cleavage. Some examples of photosensitizers that cleave DNA through hydrogen atom abstraction are activated bleomycin³³, photoactive rhodium (III) complexes³⁴, and cationic metal porphyrins³⁵ (Figure 1.10).

Singlet oxygen is formed in the vicinity of DNA when energy transfer takes place from an excited photosensitizer to ground state molecular oxygen, provided the excited photosensitizer has high enough triplet energy to generate singlet oxygen. This particular species is highly reactive and preferentially reacts at the guanine residues in DNA³⁶. Some well known examples of singlet oxygen generating photosensitizers are porphyrins³⁷, ruthenium (III) complexes³⁸ and vanadium (V) complexes³⁹.

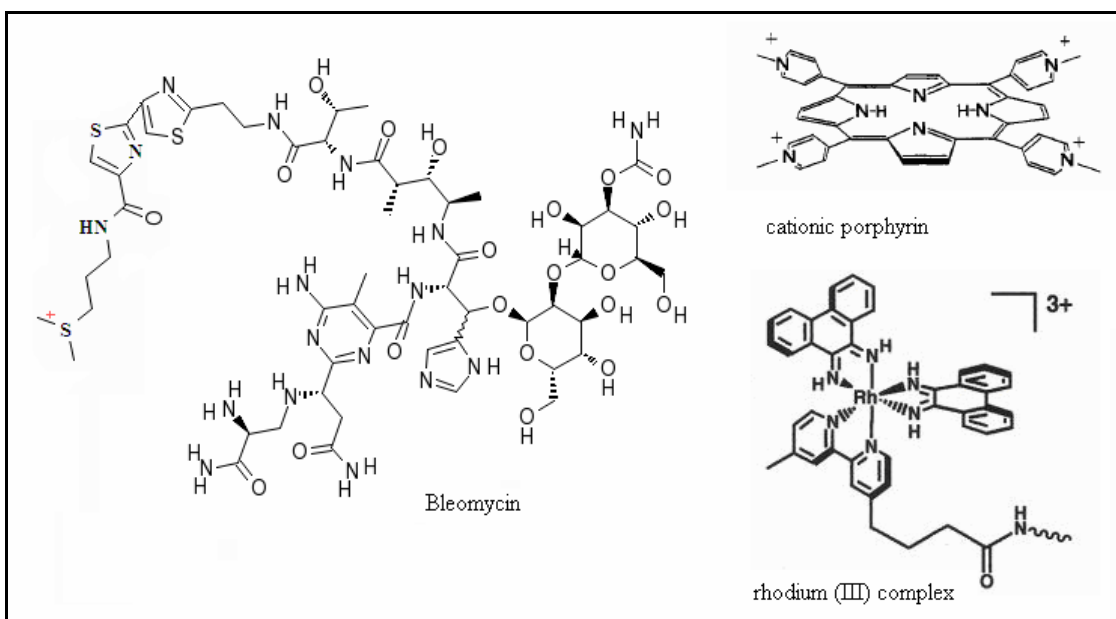


Figure 1.10: Structure of Photosensitizers used for Hydrogen Atom Abstraction in DNA

The electron transfer (E.T.) process in DNA involves the donation of an electron to an excited photosensitizer producing a radical cation on a nucleobase and a radical anion on the photosensitizer. The radical cation thus formed can migrate into the DNA and damage the DNA by reaction with the normal bases to form unwanted mutated products. The migration of the radical cation exhibit a broad range of mechanistic behavior, and its exploration has provided us with detailed understanding of the key components of charge transfer: charge injection into the DNA (removal of an electron from a DNA base), charge transfer mechanism (migration of radical cation to distal sites) and finally reactions of the ionized nucleobase resulting in damaged DNA.

1.6 Charge Injection into DNA

In order to understand the mechanism of charge migration into DNA, a vivid knowledge of the charge injection process is required. Close association of the photosensitizers with the DNA base-pairs is necessary to facilitate the transfer of an electron from the DNA to the sensitizer. Towards this goal, several photosensitizers have been developed that either intercalate between base pairs, bind in the major or minor grooves or covalently attached to one of the terminal base in order to achieve “end capping” of the terminal base pairs. Mechanism of charge injection also varies from one sensitizer to another. A list of important photosensitizers which have been used in charge migration studies, along with their mechanism of action are given in Table 1.2²². The chemical structures of the photosensitizers are shown in Figure 1.11.

Table 1.2:²² List of Photosensitizers used for Charge Injection in DNA

Photosensitizers	Structure (Figure1.11)	DNA target	Mechanism	References
Riboflavin	1	GG	E.T.	168
Anthraquinones	2	GG	E.T.	170
Naphthalimides	3	GG	E.T.	172
	4	T	CH ₃ oxidation	173
Benzophenones	5	GG	E.T.	174
Benzotriazoles	6	GG	E.T.	175
Rh complexes	7	GG	E.T.	177
	8	G	E.T.	179
Ru complexes	9	GG	E.T.	180
	10	G	E.T.	181
	11	G	¹ O ₂	182
	12	G	¹ O ₂	183
	13	G	¹ O ₂	184
methylene blue	14	G	¹ O ₂	185
Porphyrins	15	G	¹ O ₂	186
	16	G	¹ O ₂	187
V complexes	17	G	¹ O ₂	190
Co complexes	18	G	·CH ₃	192
isothioronium salts	19	G	Alkylation	193
Diazomethanes	20	G	Alkylation	88
Monothioacetals	21	A	Alkylation	194

Abbreviation: E.T., electron transfer; ¹O₂, singlet oxygen

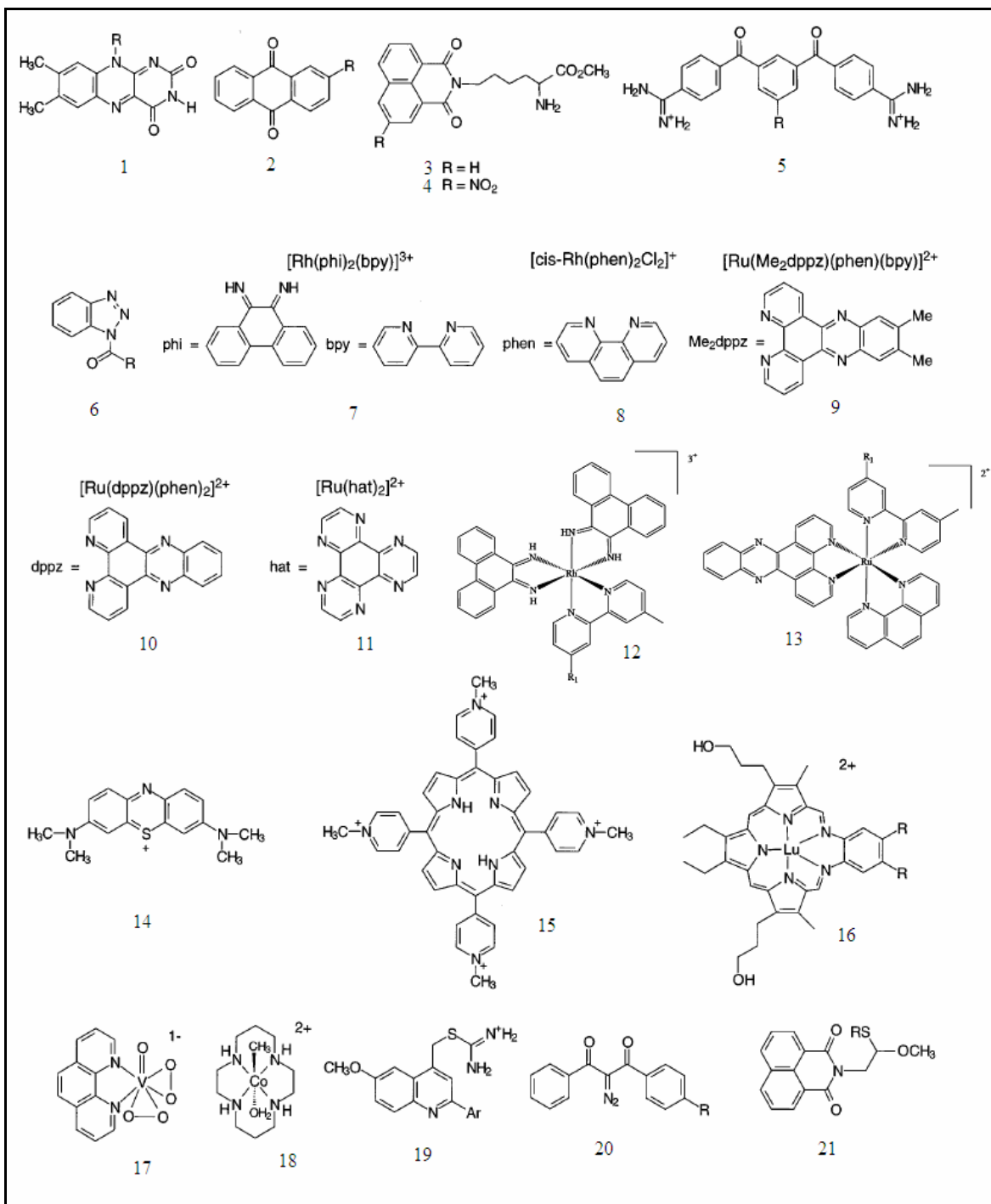


Figure 1.11: Structures of Photosensitizers used for Charge Injection in DNA

1.7 Anthraquinone as a charge injector

The photochemistry of anthraquinone (**2**, Figure 1.11) has been well established⁴⁰ and they are excellent charge injectors for the one-electron oxidation of DNA. They absorb light in the near UV-spectral region around 350 nm where DNA is essentially transparent. This anthraquinone moiety (AQ) can be easily synthesized⁴¹ and can be attached covalently to the DNA by standard phosphoramidite chemistry. The AQ can be tethered to either the 5'-terminus of a DNA or in any other intermediate position in the DNA sequence in the form of Uridine-anthraquinone (UAQ). Figure 1.12 shows the structure of different anthraquinone derivatives used for photosensitization of DNA, including AQ-DNA and UAQ-DNA which are used in this study.

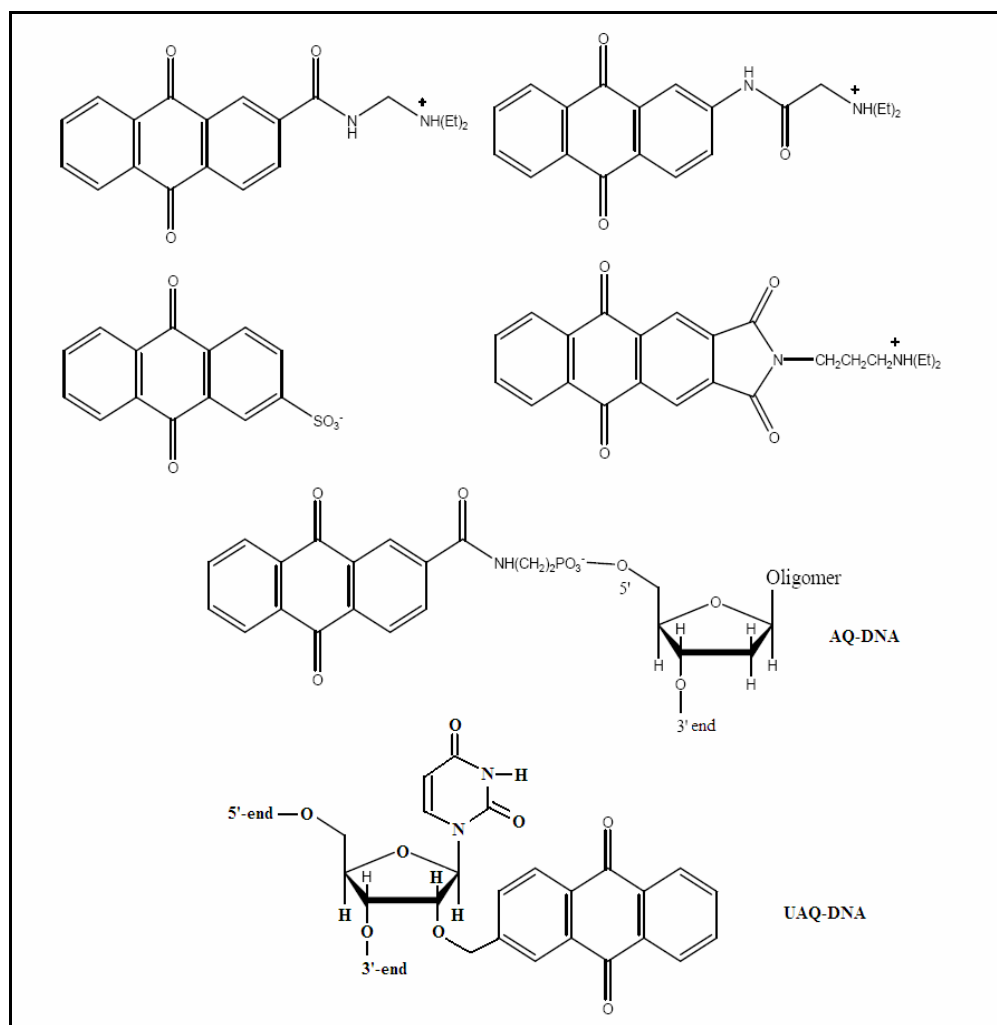


Figure 1.12: Structures of Different AQ Derivatives Including AQ-DNA and UAQ-DNA

Attaching an AQ to the terminus of a DNA single-strand followed by hybridization with its complementary sequence results in “end-capping” of the DNA duplex (Figure 1.13). It has been found that this “end-capping” of the DNA permits π -orbital overlap with the DNA, but doesn’t yield structural distortions to the DNA that can be caused by intercalation⁴².

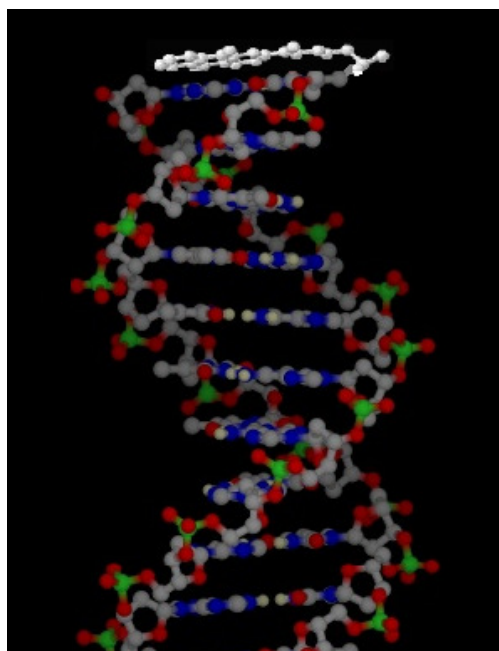


Figure 1.13: Hyperchem Generated Image showing AQ “End-Capping” in DNA (AQ Group is shown in White)

Irradiation of the AQ group at 350 nm promotes it from the ground state to the singlet excited state. The excited singlet state has a very short lifetime and it rapidly intersystem crosses to the excited triplet state. The excited triplet state is capable of abstracting an electron from a neighboring base creating a nucleobase radical cation. Since back electron transfer is forbidden due to spin conservation, this triplet radical ion pair state is relatively long lived. Subsequent reaction of the $AQ^{\cdot-}$ with oxygen gives superoxide and the neutral AQ. The radical cation which has been introduced into the DNA can migrate through the DNA sequence until it is irreversibly trapped by reactions at different bases within the DNA. The efficiency of charge injection by AQ has been found to be sensitive to the bases nearest to the AQ^{43} . Experimental evidences have shown that the

highest charge injection efficiency is obtained in sequences where the AQ group is followed by at least three As (5'-AQ-AAA-3'-oligomer).

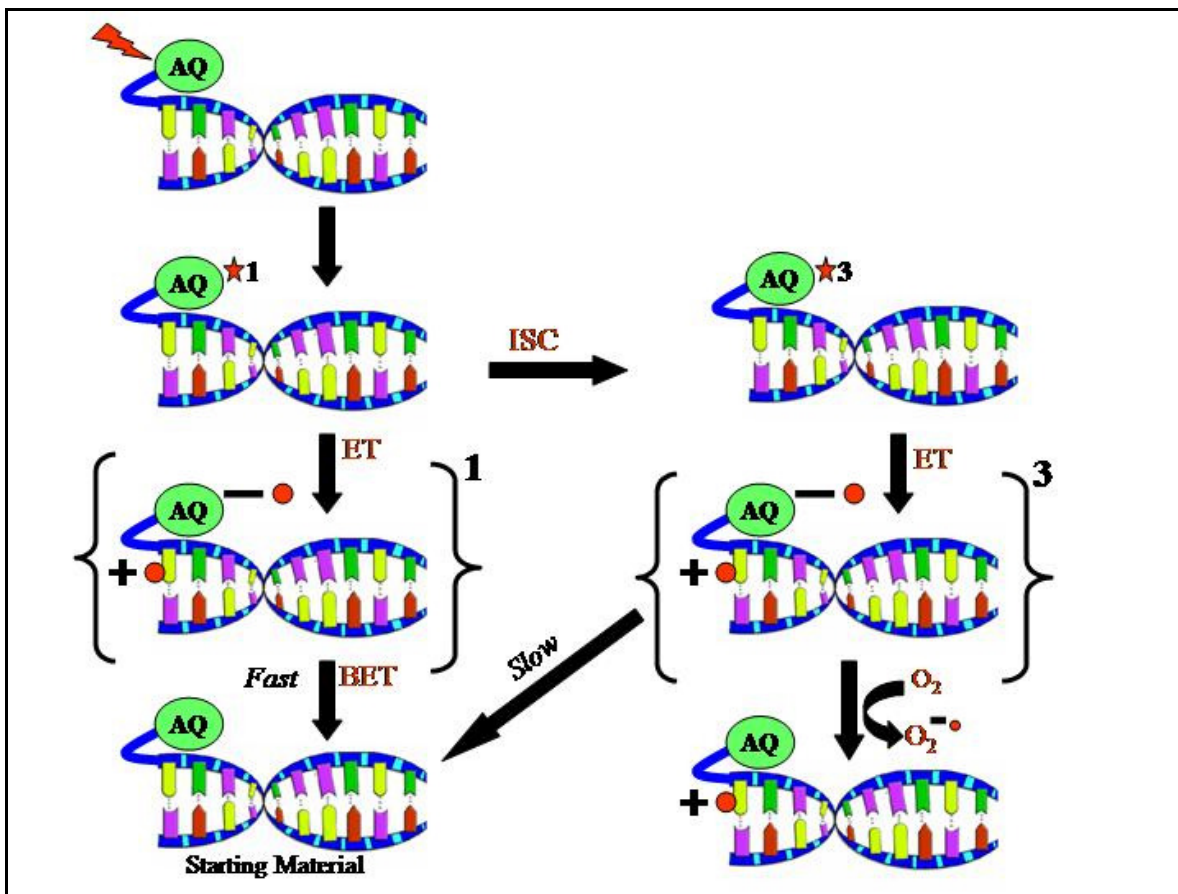


Figure 1.14: Charge Injection Mechanism of Anthraquinone by Irradiation at 350 nm. Abbreviations: ET, Electron Transfer; BET, Back Electron Transfer; ISC, Inter System Crossing.

1.8 Charge Migration through DNA

Introduction of radical cation into a DNA duplex can result in its migration through the DNA up to 200 Å from its site of generation. It has been established that the efficiency of charge migration depends on the DNA base sequence⁴⁴⁻⁴⁸. The challenging task of

understanding the mechanism of long distance radical cation transport in DNA has invited enormous debate for nearly two decades.

Initial reports attributed charge transport over more than 40 Å in less than 1 ns to superexchange through a bridge orbital of well-stacked bases, referred to as “ π -way”⁴⁹. Later, it was suggested that the ability of DNA to transport charge is gated by dynamical disruption of stacking⁵⁰. Subsequent investigations have resulted in contradicting reports that include several possible mechanisms for charge transfer, including superexchange-tunneling and different hopping mechanisms⁵¹⁻⁵⁵. According to the superexchange mechanism, DNA behaves like a wire having a continuous, delocalized molecular orbital. In this orbital, each base pair is in electronic contact with every other, and charge transport occurs by superexchange⁵⁶. In this tunneling mechanism, when the distance between the donor and acceptor is short, the electron tunnels in a single step reaction between the selected bases and the intervening base pairs do not act as charge carriers.

In order to overcome the inability to explain numerous mechanistic aspects of charge migration in different DNA sequences by the superexchange and tunneling mechanism, scientists put forward a completely different model. This model is known as “discrete hopping”, which presumes that the radical cation is localized on one base and has no significant electronic overlap with adjacent bases. The localized radical cation migrates (hops) by a thermally activated process to adjacent bases⁵⁷. This hopping process is treated as a sequential reaction which is characterized by the rates of the electron-transfer steps and trapping steps. This theory recognizes that DNA is not a static molecule and continuous thermal motions of the DNA must influence charge transfer efficiency,

however, it does not offer any explanation as to how these fluctuations are incorporated into the DNA during charge transfer.

The inadequacy of the hopping mechanism to explain some of the observations led to the foundation of a more advanced mechanistic model. This model is known as “Phonon Assisted Polaron like Hopping”^{9, 58-59}. This theory involves delocalization of the radical cation, followed by a hopping mechanism, where the charge does reside on the bridge. After formation of the radical cation, the bases around the radical cation distort themselves to accommodate the charge. This rapid distortion results in a change in the normal inclination angle of the neighboring bases, which bring them closer to the radical cation, thus delocalizing and stabilizing it. A second structural change is a decrease in the twist angle by rotation around the z axis of the DNA. This unwinding will increase the π -electron overlap between bases and will stabilize the radical cation. Another possible distortion is a shift in proton donation of the hydrogen bonds that form the base pairs. The pKa of a localized base radical cation is different from that of the neutral base⁶⁰⁻⁶¹. The pKa of bases carrying delocalized (partial) positive charge also will change, and hydrogen bonds in duplex DNA will shift to accommodate this change. It is the total of these structural changes that are accounted as the polaron-like distortion⁹. The extent of the delocalization is governed by the energy required to distort the DNA and the energy gained by delocalizing the radical cation, which depends on the sequence of the DNA undergoing charge migration. The base radical cation can be considered as a polaron, which is defined as a radical ion self-trapped by structural distortion of its containing medium⁶². Strictly, it is a polaron-like species but not an ideal Polaron, since the detailed properties of the

distortion is sequence dependant. This polaron can extend to that point where the energy required to distort the DNA will just balance the stabilization.

The polaron hopping model requires that the radical cation exist as a detectable entity during its migration through the bridge. Charge transfer studies has been carried out with 2'-deoxy-N6-cyclopropyl-adenosine located between the charge injection site and a distal guanine site. It was found that the radical cation indeed interacts with the bridge as evident from its reaction (ring opening) at the cyclopropyl site⁶² (Figure 1.15). This experiment supports the polaron hopping model as opposed to the superexchange model.

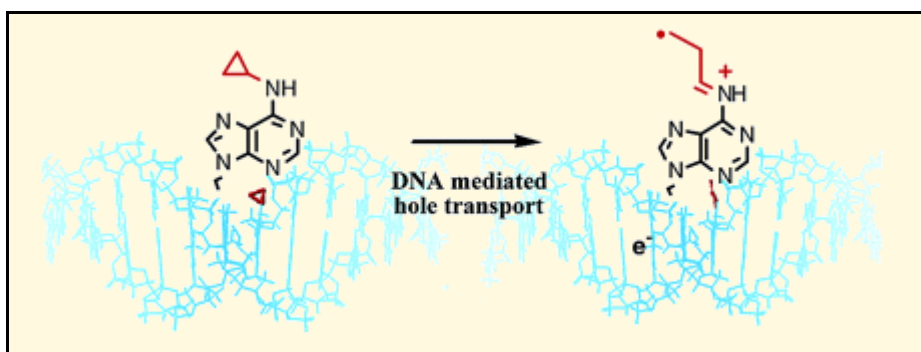


Figure 1.15: Schematic Illustration of Ring Opening of N6-Cyclopropyladenosine by Charge Transfer.⁶²

Thermal motions of the base pairs in and near the structural distortion lead to their leaving or joining the polaron designated as phonon-assisted hopping. The number of base pairs leaving and joining the polaron distortion in a hop depends on the local sequence. The migration of the polaron through DNA occurs as a consequence of normal vibrational fluctuations (phonons). This mechanism bears a close resemblance to classical electron transfer processes described by Marcus theory⁶³.

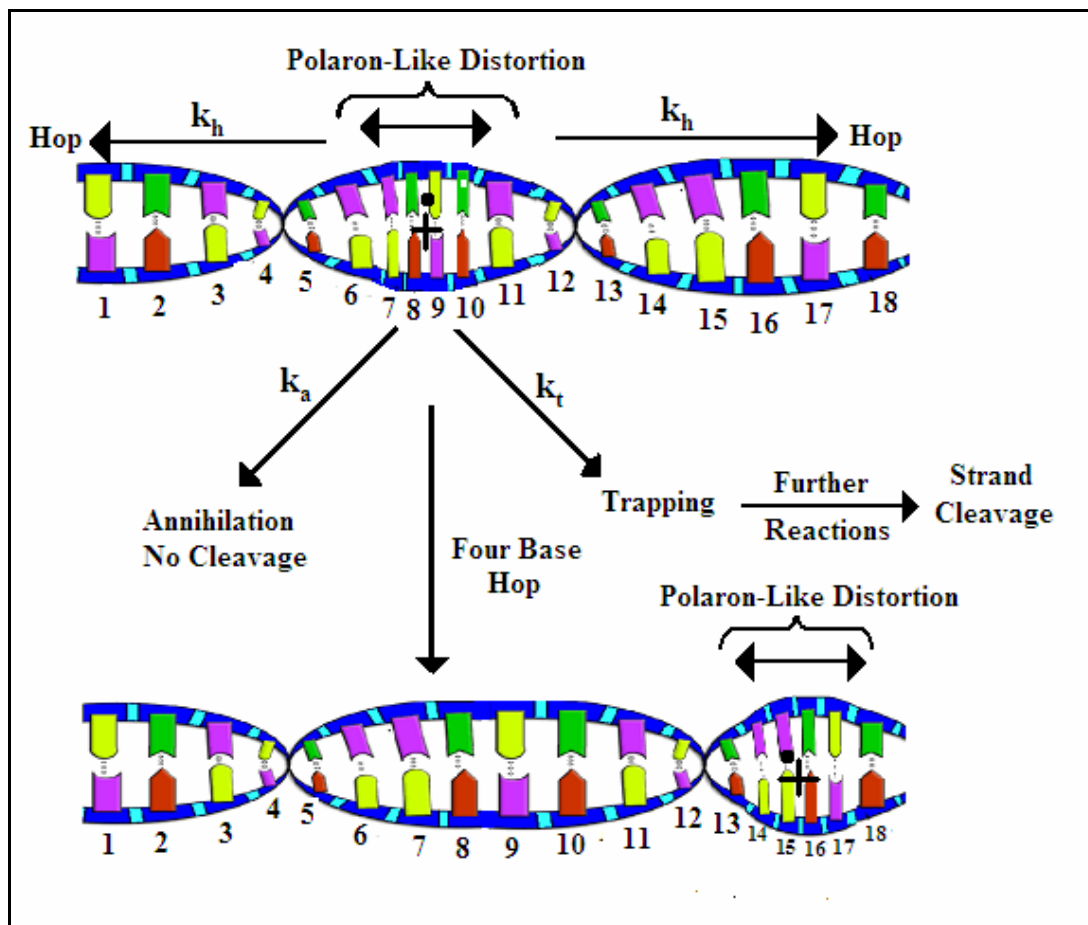


Figure 1.16. Schematic of Phonon-Assisted Polaron like Hopping Mechanism of Charge Migration in DNA.

Schuster and coworkers found that substitution of the phosphate groups by methylphosphonates leads to a significant reduction in radical cation migration, which is predominantly an effect of methylphosphonate substitution in the bridge⁵⁹. This reduction indicates a reduced mobility of the hole across the modified bridge as predicted theoretically. The characteristics of the hole-transport process are expected to be temperature-dependent because of the activated nature of the structural transitions

involved. In addition to that, a strong dependence of the hole-transport efficiency on the identity of the counterions was evident. An appealing feature of this mechanistic proposal of polaron hopping is that it can be generalized to reconcile experimental and theoretical findings that previously seemed contradictory.

1.9 Charge Trapping

A close look at Table 1.2 reveals that the charge injectors target G or GGs to initialize the radical cation migration in the DNA. The radical cation prefers to be predominantly delocalized on guanine bases. The oxidation potential of guanine is lowest among the four bases (Table 1.3) and oxidation potential of repeating Gs such as GG and GGG are even lower. During the hopping through the DNA, the radical cation resides at G_n ($n = 1-3$) and form guanine radical cation. The radical cation then can react with H_2O and/or O_2 to form 8-oxoguanine (8-oxodG) and other products (Figure 1.18). This process is known as charge trapping.

Table 1.3: Oxidation Potentials of the DNA Bases. (n2, 25)

Bases	E_{ox} (V) vs. NHE
Adenine	1.42
Thymine	1.70
Guanine	1.29
Cytosine	1.60

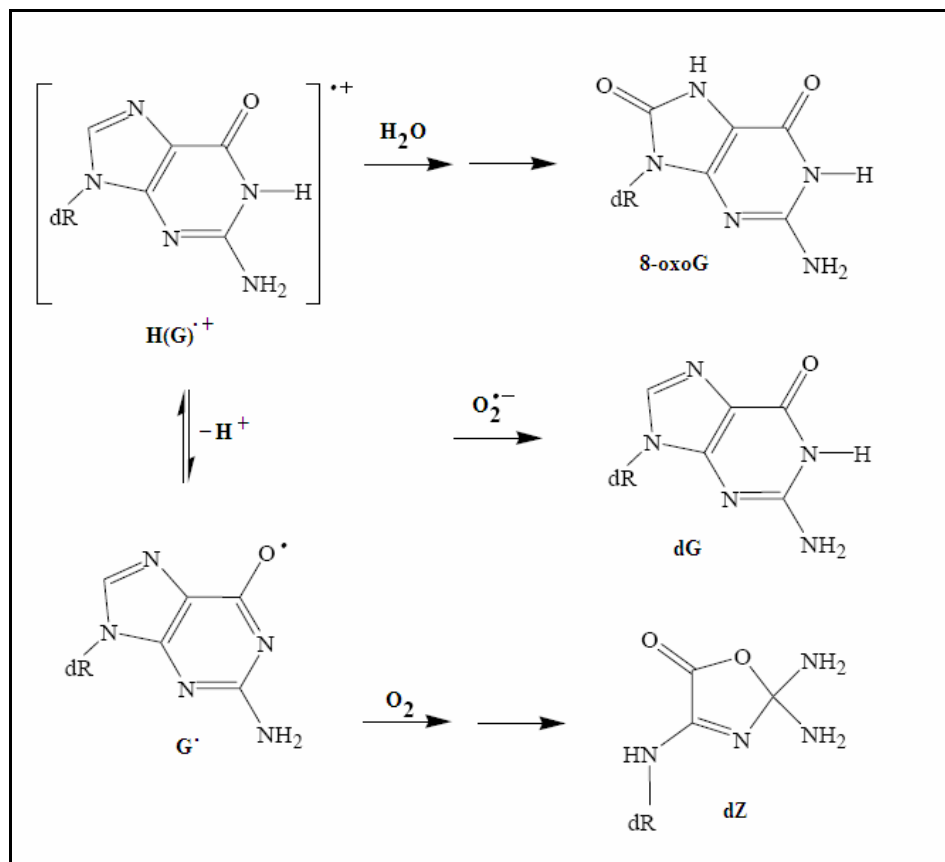


Figure 1.17: Reaction of Guanine Radical Cation with Water and Oxygen.

In order to examine the mechanism of charge migration and oxidation of DNA, development of a method for determining the charge transfer efficiency is important. The property of ease of formation of guanine radical cation, $G^{\bullet+}$, from a GG step, is taken advantage of for monitoring charge transfer processes. Treatment of the oxidized DNA strands with piperidine leads to strand cleavage at sites of guanine oxidation. Gel electrophoresis separates the DNA strands based on their size to charge ratio and the mobility of the cleaved DNA can be visualized by dye staining or autoradiography. The

cleavage and separation technique involving the charge trapping of the migrating radical cation allows for the accurate quantification of charge migration efficiency.

To address the charge transfer efficiency in terms of kinetic terms, two rate constants have been developed following the “Polaron Hopping Model”. They are the rate of hopping of the radical cation (k_{hop}) and the rate of its irreversible trapping (k_{trap}) as shown in Figure 1.16. If the rate of hopping is greater than rate of trapping ($k_{hop} > k_{trap}$), charge transfer will be highly efficient and oxidation at the GG steps will be approximately equivalent throughout the DNA. Dominance of the rate of trapping over the rate of hopping ($k_{hop} < k_{trap}$), suggests that the radical cation migration is highly inefficient and the charge tends to drop down near the site of its generation. If the rate of hopping is approximately equivalent to the rate of trapping, charge transfer will decrease with distance from the AQ.

Besides guanine oxidation, which lead to the formation of 8-oxoguanine, oxidation of other bases are also possible depending on the sequence of the DNA undergoing charge migration. The migrating cation can be trapped by virtually all the bases forming irreversible trapping products, though the rate of formation of them might be low compared to the formation of oxoG lesions. The C4-C5 double bond of pyrimidine is particularly sensitive to attack by hydroxyl radical. Some well known pyrimidine damage products are thymine glycol, uracil glycol, urea residue, 5-hydroxyuracil, 5-hydroxycytosine, hydantoin and others. Even adenine is prone to oxidation and 8-oxoA has been isolated in many charge transfer studies. Formamidopyrimidines (fapy-dG, fapy-dA) and other less characterized purine oxidative products are also formed²².

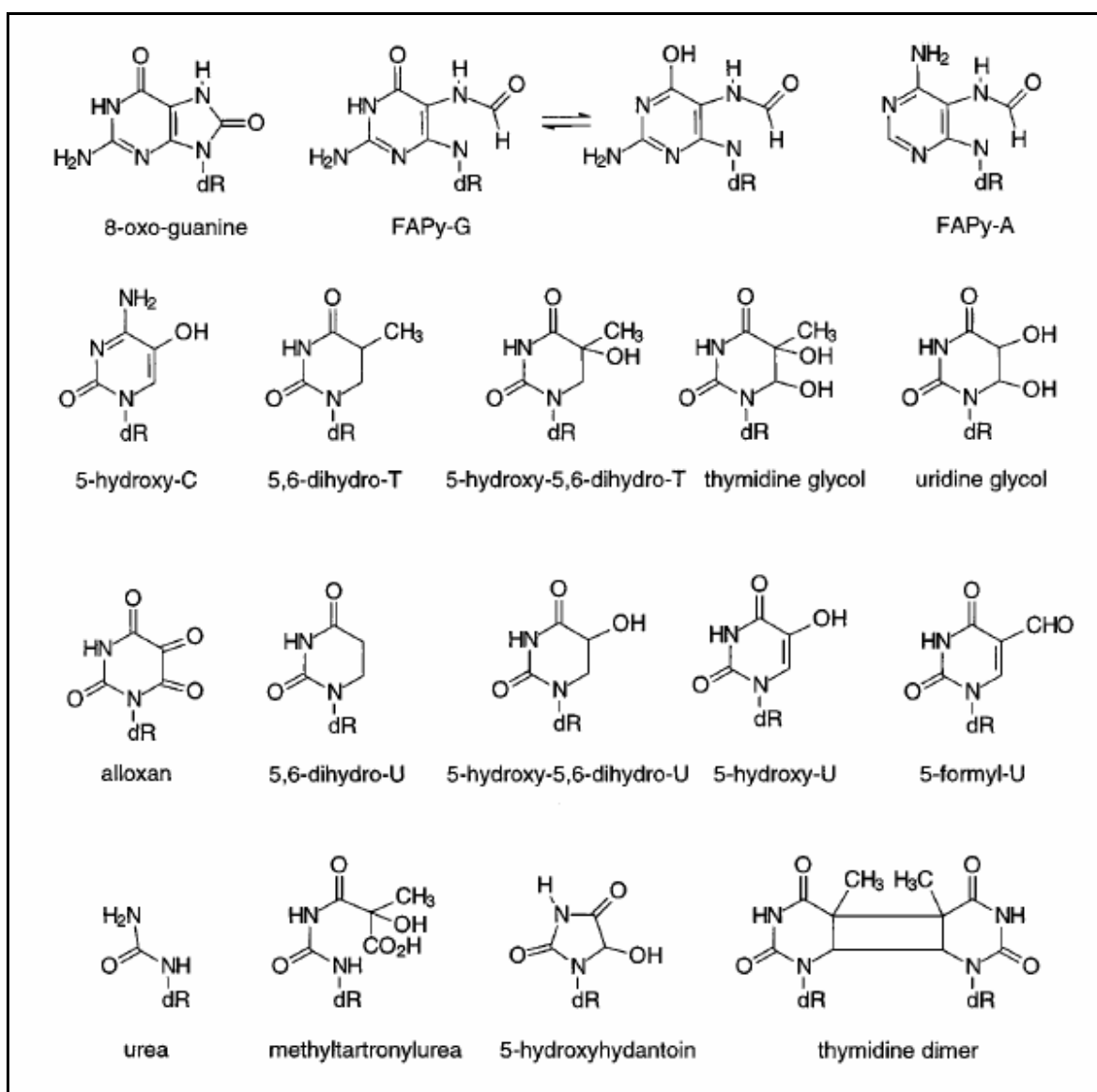


Figure 1.18: Structure of Some Modified Bases Generated from Oxidative DNA Damage

1.10 References

1. Ames, B. N.; Lee, F. D.; Durston, W. E. *Proc. Natl. Acad. Sci. U.S.A.* **1973**, 70, 782-786.
2. Demple, B.; Harrison, L. *Annu. Rev. Biochem.* **1994**, 63, 915-948.
3. Friedman, K. A.; Heller, A. *J. Phys. Chem. B* **2001**, 105, 11859-11865.
4. Norbury, C.J.; Zhivotovsky, B. *Oncogene* **2004**, 23, 2797-2808
5. Boiteux, S.; Gellon, L.; Guibourt, N. *Free Radic. Biol. Med.* **2002**, 32, 1244-1253.
6. DNA Electronics. In *Encyclopedia of Nanoscience and Nanotechnology*, Nalwa, H. S., Ed. American Scientific Publishers, **2004**, 2, 475-493.
7. Topics in Current Chemistry. In *Long-range Charge Transport in DNA I*, Schuster, G. B., Ed. Springer Berlin / Heidelberg: **2004**, 236, 1-204.
8. Topics in Current Chemistry. In *Long-range Charge Transport in DNA II*, Schuster, G. B., Ed. Springer Berlin / Heidelberg, **2004**, 237, 1-228.
9. Henderson, P. T.; Jones, D.; Hampikian, G.; Kan, Y.; Schuster, G. B. *Proc. Natl. Acad. Sci. U.S.A.* **1999**, 96, 8353-8358.
10. Franklin, R. E.; Goslin, R. G. *Nature* **1953**, 172, 156.
11. Franklin, R. E.; Goslin, R. G. *Acta Crystallography* **1953**, 6, 673-685.
12. Watson, J. D.; Crick, F. H. C. *Nature* **1953**, 171, 737-738.
13. Stewart, R. F.; Jensen, L.H. *J. Chem. Phys.* **1964**, 40, 2071-2076.
14. Drew, H. R.; Dickerson, R. E. *Journal of Molecular Biology* **1981**, 151, 535-556.
15. Dickerson, R. E.; Drew, H. R.; Conner, B. N.; Wing, R. M.; Fratini, A. V.; Kopka, M. L. *Science* **1982**, 216, 475-485.

16. Berg, J. M.; Tymoczko, J. L.; Stryer, L. *Biochemistry*, **2002**, 5th ed., W.H. Freeman, New York.
17. Champ, P.C.; Maurice, S.; Vargason, J.M.; Camp, T.; Ho, P.S. *Nucleic Acids Res.* **2004**, 32, 6501-6510.
18. Rich, A.; Zhang, S. *Nature Rev. Genet.* **2003**, 4, 566–572.
19. Lodish, H.; Berk, A.; Matsudaira, P.; Kaiser, C.A.; Krieger, M.; Scott, M.P.; Zipursky, S.L.; Darnell, J. In *Molecular Biology of the Cell*, **2004**, 963-974, 5th ed. W.H. Freeman, New York.
20. Dizdaroglu, M.; Von S. C.; Schulte F. D. *J. Am. Chem. Soc.* **1995**, 97, 2277-2278.
21. Armitage, B. *Chem. Rev.* **1998**, 98, 1171-1200.
22. Burrows, C. J.; Muller, J. G. *Chem. Rev.* **1998**, 98, 1109-1152.
23. Sancar, A. *Annu. Rev. of Biochem.* **1996**, 65, 43-81.
24. Kow, Y. W. *Ann. N.Y. Acad. Sci.* **1994**, 726, 178-180.
25. Kanvah, S.; Schuster, G. B. *J. Am. Chem. Soc.* **2004**, 126, 7341-7344.
26. Demple, B.; Harrison, L. *Annu. Rev. of Biochem.* **1994**, 63, 915-948.
27. Poulsen, H. E.; Prieme, H.; Loft, S. *Eur. J. Cancer Prev.* **1998**, 7, (1), 9-16.
28. Hasty, P.; Vijg, J. *Science* **2002**, 296, 1250-1251.
29. Armitage, B.; Yu, C.; Devadoss, C.; Schuster, G.B. *J. Am. Chem. Soc.* **1994**, 116, 9847-9859.
30. Macgregor, R. B. Jr. *Anal. Biochem.* **1992**, 204, 324-327.
31. Breslin, D. T.; Schuster, G. B. *J. Am. Chem. Soc.* **1996**, 118, 2311-2319.

32. Turro, N. J. *Modern Molecular Photochemistry* **1978**, Benjamin-Cummings Publication Co., Inc., California.
33. Burger, R. M. *Chem. Rev.* **1998**, 98, 1153-1170.
34. Chow, C. S.; Barton, J. K. *Methods Enzymol.* **1992**, 212, 219-242.
35. Pratviel, G.; Pitie, M.; Bernadou, J.; Meunier, B. *Angew. Chem. Int. Ed. Engl.* **1991**, 30, 702-704.
36. Lee, C. C.; Rodgers, M. A. *Photochem. Photobiol.* **1987**, 45, 79-86.
37. Croke, D. T.; Perrouault, L.; Sari, M. A.; Battioni, J. P; Mansuy, D.; Helene, C.; LeDoan, T. J. *Photochem. Photobiol. B.* **1993**, 18, 41-50.
38. Mei, H.; Barton, J. K. *Proc. Natl. Acad. Sci. U.S.A.* **1988**, 85, 1339-1343.
39. Hiort, C.; Goodisman, J.; Dabriowiak, J. C. *Biochemistry* **1996**, 35, 12354-12362.
40. Moore, J. N.; Phillips, D.; Nakashima, N.; Yoshihara, K. *J. Chem. Soc., Faraday Trans. 2* **1987**, 83, 1487-1508.
41. Deshmukh, H.; Joglekar, S. P.; Broom, A. D. *Bioconjugate Chem.* **1995**, 6, 578-586.
42. Gasper, S. M.; Schuster, G. B. *J. Am. Chem. Soc.* **1997**, 119, 12762-12771.
43. Sanii, L.; Schuster, G. B. *J. Am. Chem. Soc.* **2000**, 122, 11545-11546.
44. Giese, B. *Annu. Rev. Biochem.* **2002**, 71, 51-70.
45. Liu, C. S.; Schuster, G. B. *J. Am. Chem. Soc.* **2003**, 125, 6098-6102.
46. Lewis, F. D.; Liu, J.; Weigel, W.; Rettig, W.; Kurnikov, I.V.; Beratan, D. N. *Proc. Natl. Acad. Sci. U.S.A.* **2002**, 99, 12536-12541.

47. Liu, C. S.; Hernandez, R.; Schuster, G. B. *J. Am. Chem. Soc.* **2004**, 126, 2877-2884.
48. Shao, F.; Augustyn, K.; Barton, J. K. *J. Am. Chem. Soc.* **2005**, 127, 17445-17452.
49. Murphy, C. J.; Arkin, M. R.; Jenkins, Y.; Ghatlia, N. D.; Bossmann, S. H.; Turro, N. J.; Barton, J. K. *Science* **1993**, 262, 1025-1029.
50. Kelley, S. O.; Holmlin, E. R.; Stemp, E. D. A.; Barton, J. K. *J. Am. Chem. Soc.* **1997**, 119, 9861-9870.
51. Giese, B. *Acc. Chem. Res.* **2000**, 33, 631-636.
52. Armitage, N. P.; Briman, M.; Grüner, G. *physica status solidi* **2004**, 241, 69-75.
53. Bixon, M.; Giese, B.; Wessely, S.; Langenbacher, T.; Michel-Beyerle, M. E.; Jortner, J. *Proc. Natl. Acad. Sci.* **1999**, 96, 11713-11716.
54. Berlin, Y. A.; Burin, A. L.; Ratner, M. A. *Chem. Phys.* **2002**, 275, 61-74.
55. O'Neill, M. A.; Barton, J. K. *J. Am. Chem. Soc.* **2004**, 126, 11471-11483.
56. Turro, N. J.; Barton, J. K. *J. Biol. Inorg. Chem.* **1998**, 3, 201-209.
57. Ly, D.; Kan, Y.; Armitage, B.; Schuster, G. B. *J. Am. Chem. Soc.* **1996**, 118, 8747-8748.
58. Schuster, G. B. *Acc. Chem. Res.* **2000**, 33, 253-260.
59. Barnett, R. N.; Cleveland, C. L.; Joy, A.; Landman, U.; Schuster, G. B. *Science* **2001**, 294, 567-571.
60. Englander, S. W.; Kallenbach, N. R.; Heeger, A. J.; Krumhansl, J. A.; Litwin, S. *Proc. Natl. Acad. Sci. U.S.A* **1980**, 77, 7222-7226.
61. Steenken, S. *Biol. Chem.* **1997**, 378, 1293-1297.

62. Dohno, C.; Ogawa, A.; Nakatani, K.; Saito, I. *J. Am. Chem. Soc.* **2003**, 125, 10154-10155.
63. Marcus, R. A. *J. Chem. Phys.* **1956**, 24, 966-978.

CHAPTER 2

RADICAL CATION MIGRATION THROUGH SINGLY LIGATED PLASMID DNA CONDENSATES

2.1 Introduction

The DNA double helix is made of two sugar-phosphate backbones wrapped around a central helical axis with heterocyclic base pairs in the middle of the axis. Investigations have showed that the DNA structure can be damaged by different sorts of mutagens resulting in mutation and cancer¹⁻³. These include oxidizing agents, alkylating agents and high-energy electromagnetic radiation such as ultraviolet light and x-rays⁴⁻⁵. It is now known that oxidation of duplex DNA results in the loss of an electron generating a radical cation (“hole”) that migrates by a hopping mechanism until it is trapped irreversibly in a chemical reaction with H₂O or O₂⁶⁻⁹. The irreversible trapping of the radical cation usually occurs at guanines which have the lowest oxidation potential of the four natural bases¹⁰⁻¹¹. Almost all the research on the mechanism of the radical cation migration in DNA have been done with oligonucleotides with restricted length, usually less than hundred base pairs. DNA within cells contains thousands of base pairs and is also tightly packed with Histone proteins and does not closely resemble oligonucleotides in solution¹². Irradiation and DNA damage studies in long pieces of DNA such as plasmid DNA have been restricted to the determination of conformational changes brought about by strand breakage in the plasmid following UV or gamma irradiation¹³⁻¹⁶. The mechanistic study of charge

transfer and DNA damage in plasmid or other long piece of DNA are very limited in number. An examination of the radical-cation hopping through DNA in loosely organized nucleosome core particles showed that Histone binding does not affect the pattern and extent of oxidation¹⁷, which is debatable. Recently Davis and coworkers have found that the charge transport is attenuated in DNA sequences which have been transformed into Nucleosome Core Particles¹⁸ (NCPs). These findings are significantly different to the result of DNA-mediated hole transport in normal oligonucleotide sequences in solution. However, it is not known how the long-distance radical-cation migration that is observed in oligonucleotides is affected by conversion of the DNA to a well ordered structure. We began the systematic investigation of this question by examining the reactions of radical cations that were specifically introduced into DNA condensates.

2.2 Plasmid DNA and restriction enzyme recognition

A Plasmid is a double stranded circular piece of DNA which is separate from the chromosomal DNA but is capable of autonomous replication. It usually occurs in bacteria and contains an antibiotic resistance gene, sometimes more than one. The gene, in the form of DNA, must be transcribed into messenger RNA, and then translated into the protein that is the agent that counteracts the effect of the antibiotic¹⁹. There may be one copy of the plasmid or hundreds of copies of the same plasmid in a single cell and their size can vary from 1 to 400 kilobase pairs (kbp). The PUC class of plasmids is an example of high copy number *E. coli* plasmids containing 2686 bp and contains multiple cloning sites which make them one of the most popular candidates as a cloning vector²⁰.

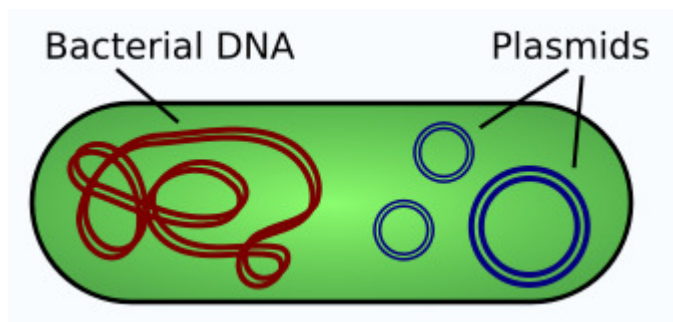


Figure 2.1: Illustration of a Bacterium showing Chromosomal DNA and Plasmids.

Restriction endonuclease is a class of nuclease enzyme that cuts double-stranded DNA. A restriction endonuclease functions by "scanning" the length of a DNA molecule. Once it encounters its particular specific recognition sequence, it will bond to the DNA molecule and makes one cut in each of the two sugar-phosphate backbones of the double helix. The positions of these two cuts, both in relation to each other, and to the recognition sequence itself, are determined by the identity of the restriction endonuclease used to cleave the molecule in the first place. Different endonucleases yield different sets of cuts, but one endonuclease will always cut a particular base sequence the same way, no matter what DNA molecule it is acting on²¹. Not all restriction endonucleases cut symmetrically and leave blunt ends after the restriction digestion. Many endonucleases cleave the DNA backbones in positions that are not directly opposite each other. When the enzyme encounters this kind of sequence, it cleaves each backbone between four to ten base residues apart. Generally, this recognition sequence is a palindromic sequence. Once the cuts have been made, the resulting fragments are held together only by the relatively weak hydrogen bonds that hold the complementary bases to each other. The weakness of these bonds allows the DNA fragments to separate from one each other. Each resulting fragment

has a protruding 5'-end composed of unpaired bases. Other enzymes create cuts in the DNA backbone which result in protruding 3' ends. Protruding ends, both 3'- and 5'-are sometimes called "sticky ends" because they tend to bond with complementary sequences of bases. In other words, if an unpaired length of bases (5'-A A T T-3') encounters another unpaired length with the sequence (3'-T T A A-5') they will bond to each other i.e. they are "sticky" for each other. Ligase enzyme is then used to join the phosphate backbones of the two molecules.

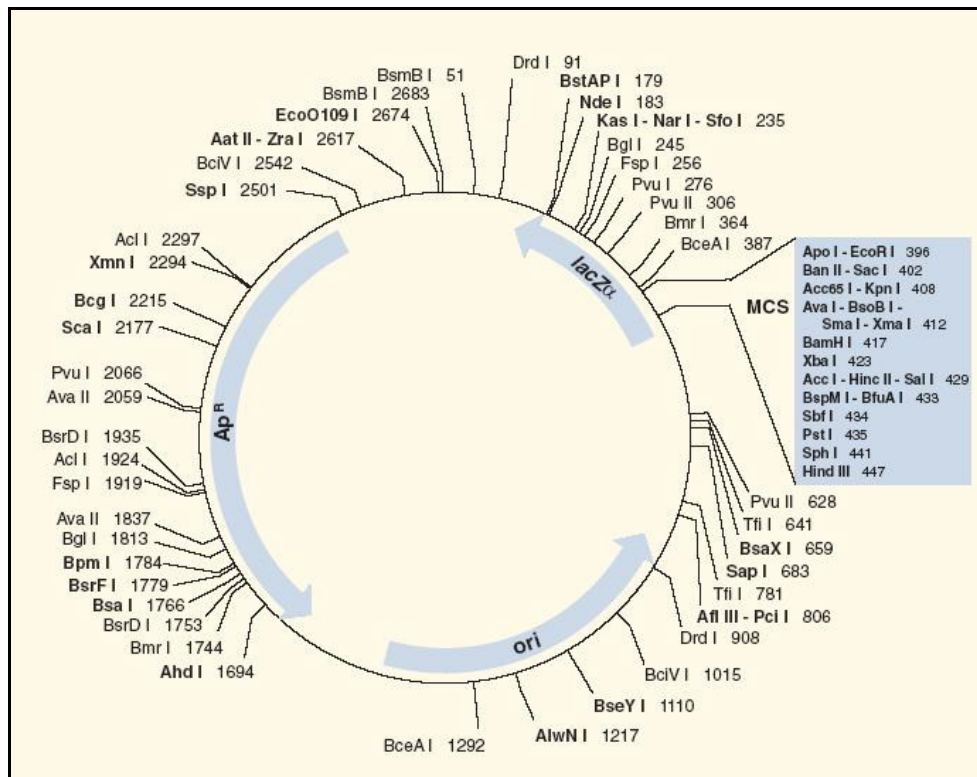


Figure 2.2: Restriction Map for Puc19 Plasmid: Numbers Indicate Exact Location of the Corresponding Enzyme Cut in the Plasmid

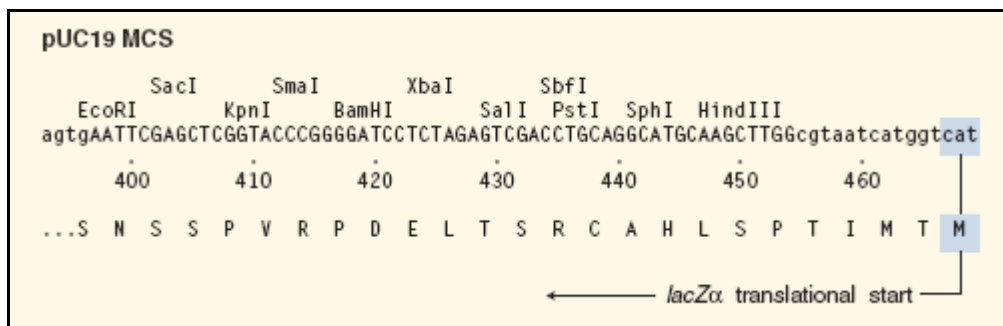


Figure 2.3: Recognition Site for Eco RI and HindIII Restriction Enzyme in Puc19 Plasmid.

2.3 DNA Ligation and Ligases

Ligation is defined as the joining of DNA fragments together with covalent bonds. More specifically, DNA ligation involves creating a phosphodiester bond between the 3' hydroxyl of one nucleotide and the 5' phosphate of another. A typical ligation reaction requires three components in addition to water. First, the two DNA strands that have either both blunt ends or cohesive ("sticky") ends. A buffer is needed which can supply the necessary cofactor and maintain the required salt concentration and a ligase enzyme. The most common commercially available ligase enzyme is T4 DNA ligase which uses ATP as the cofactor and works best at 16°C. This enzyme can join blunt and cohesive end termini as well as repair single stranded nicks in duplex DNA/RNA hybrids²². Enzymes like E. coli DNA ligase use NAD⁺ as a cofactor instead of ATP and are effective only for DNA ligation. Taq DNA ligase is the most robust kind of ligase enzyme that is stable in the temperature range of 45°C -65°C. DNA ligases have become an indispensable tool in modern molecular biology research for generating recombinant DNA sequences. For example, DNA ligases are used with restriction enzymes to insert DNA fragments, often genes, into plasmids.

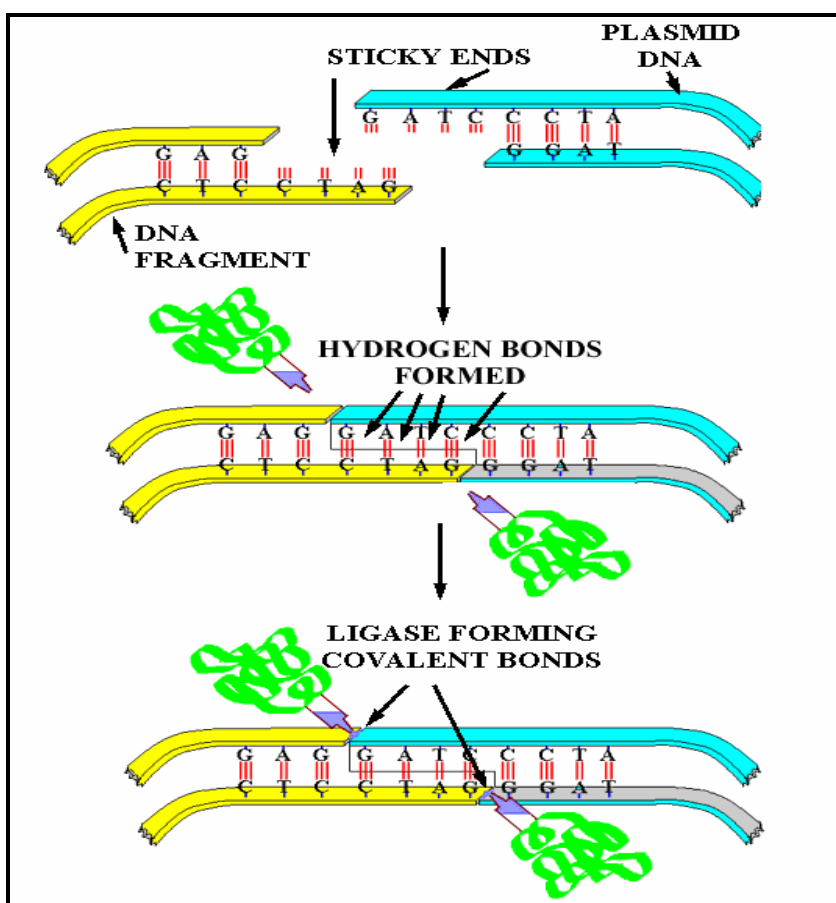


Figure 2.4: Schematic Representation of Steps Involved in DNA Ligation Reaction.

2.4 DNA Condensation

In the presence of multivalent cations, high molecular weight DNA undergoes a dramatic collapse to a highly compact structure known as DNA condensates and the process is known as DNA condensation. Condensation is the decrease in the volume occupied by a DNA molecule from the large domain occupied by a wormlike random coil, to a compact state in which the volume fractions of solvent and DNA are comparable. In the condensed state, DNA helices may be separated by just one or two layers of water. While condensation of single molecules has been observed, it is more common that several

molecules are incorporated into the condensed structure. Thus condensation is difficult to distinguish rigorously from aggregation or precipitation. Use of the term condensation is generally confined to situations in which the aggregate is of finite size and orderly morphology. Widom and Baldwin found that DNA fragments shorter than about 400 base pairs will not condense into orderly, discrete particles²³. This indicates that the net attractive interactions per base pair are very small: at least several hundred base pairs must interact, either intramolecularly or intermolecularly, to form a stably condensed particle²⁴.

Condensing agents usually work either by decreasing repulsions between DNA segments by neutralizing of phosphate charge, and/or reorienting water dipoles near DNA surfaces, or by making DNA-solvent interactions less favorable. Multivalent cations fall in the first category while ethanol, polyethylene glycol which is a poorer solvent than water for DNA, constitutes the second type. Multivalent cations may also cause localized bending or distortion of the DNA, which can also facilitate condensation. In aqueous solutions, condensation normally requires cations of charge +3 or greater. Those most commonly used in condensation studies are the naturally occurring polyamines²⁵⁻²⁶ spermidine³⁺ and spermine⁴⁺ and the inorganic cation $\text{Co}(\text{NH}_3)_6^{3+}$ ²⁷. Others include cationic polypeptides such as polylysine²⁸ and proteins such as histones H1 and H5²⁹⁻³⁰. Alcohols and neutral or anionic polymers can also provoke DNA condensation. High concentrations of ethanol are commonly used to precipitate DNA, but under carefully controlled conditions it can produce particles of well-defined morphology³⁰⁻³¹. Considerably less ethanol is required if $\text{Co}(\text{NH}_3)_6^{3+}$ is added at low ionic strength, since the two agents act synergistically³²⁻³³.

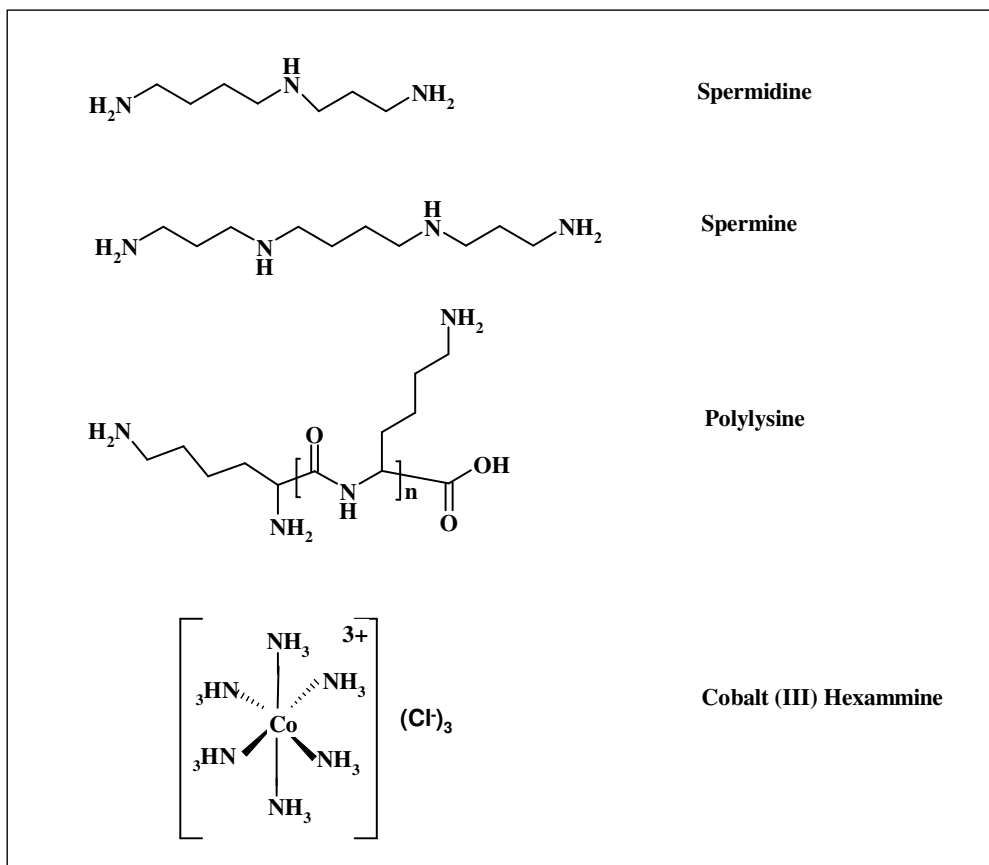


Figure 2.5: Structures of Common DNA Condensation Agents

2.5 DNA Condensate Morphology

Careful addition of polyamines or $\text{Co}(\text{NH}_3)_6^{3+}$ to very dilute aqueous DNA solutions, DNA condensation is achieved where toroids and rods are the structures most commonly observed by electron microscopy. Toroids are the preferred structure of DNA condensates probably because of the stiffness of DNA, the rather weak attractive force between DNA segments, and the very low DNA concentrations at which condensation experiments are generally done. The sizes of the toroids are independent of the DNA

length, indicating that several small DNA molecules, or one large one, are incorporated in a single particle³⁴. Torus-shaped particles of spermidine-condensed DNA exist under the hydrated conditions of freeze fracture electron microscopy, and DNA double helical fibers can be seen circumferentially wrapped around the toroid³⁵. Small numbers of rods are sometimes seen in electron micrographs of mainly toroidal condensates. The diameters and lengths of the rods are similar to the thicknesses and circumferences, respectively, of the toroids. This choice of rodlike over toroidal morphology may rest on the nonpolarity of the solvent or condensing agent³⁶⁻³⁷.

2.6 Kinetics and Thermodynamics of Condensation

Light scattering kinetic studies of DNA condensation show an initial rapid rise in scattering intensity over the first few minutes, followed by a slower rise to a plateau after 30-120 minutes. The increase in intensity is attributable to a collapse of individual DNA molecules resulting in a larger particle structure factor and, in the case of plasmid condensation, to the association of several DNA molecules in the condensing particle. Further moderate rise in intensity after several hours may be due to secondary aggregation of toroids or rods. Experiments on the millisecond time scale³⁸ indicate an induction period during which the condensing agent (spermine in this case) must rearrange on the DNA to reach a critical binding fraction before intramolecular condensation can occur. DNA condensation is a readily reversible process, which depends sensitively on the association of sufficient condensing ligands with the DNA.

DNA molecules smaller than 400 bp do not form ordered, compact particles. Assuming that the total attractive free energy must be at least an order of magnitude greater than thermal energy, to maintain at least a side-by-side bimolecular complex, one may estimate that the attractive free energy per base pair is on the order of $10kBT/400 \text{ bp} = 1/40 \text{ } kBT/\text{bp} = 0.06 \text{ kJ/mole bp} = 0.015 \text{ kcal/mole bp}$. Nevertheless $\Delta G/kBT$ per bp is a very small number, so that DNA condensation must be a delicately poised, highly cooperative process. It has been found that the critical concentration of multivalent cation required to produce DNA condensate increases with increasing salt concentration³⁹. When the amount of binding of multivalent cation and simple salt to the DNA was calculated using Manning's counterion condensation theory⁴⁰, a remarkable regularity was observed which has since been confirmed under a wide variety of circumstances: approximately 90% of the DNA charge must be neutralized for condensation to occur.

2.7 Forces in DNA Condensation

Bending: If a length L of DNA with persistence length a is bent in a path with radius of curvature Rc , the bending free energy is $\Delta G_{\text{bend}} = RTaL/2Rc^2$. Typically, the radius of curvature of the DNA in a toroid is in the order of the persistence length: $Rc \approx a$. If we consider a length of DNA equal to one persistence length, $L = a$, then $\Delta G_{\text{bend}} \approx RT/2$. Since a persistence length of DNA contains about 150 bp, this corresponds to $1/300 \text{ } kBT$ per base pair⁴¹.

Columbic: Although the calculated charge of the DNA is reduced to about 10% of its original value under the ionic conditions required for condensation, it is not reduced to

zero. In fact, the amount of remaining charge is impressively large. If a condensed DNA particle contains 40,000 bp, it has 80,000 negative phosphates or about 8,000 elementary charges after 90% neutralization. These much charge concentrated in a particle a few hundred Å in radius will generate a powerful repulsive force. Substantial reduction of the repulsive electrostatic interaction between DNA helices does not in itself account for the attractive interaction stabilizing the condensed form⁴². One possible source of attraction, suggested by Oosawa⁴³, is induced dipole interactions between the fluctuating ion atmospheres surrounding rod like macro ions such as DNA. Pseudo-two-dimensional character of the counterion distribution very close to the highly charged DNA surface. Columbic repulsion between these surface-adsorbed but mobile ions leads to a two-dimensional ionic lattice. When two DNA molecules with ionic surface lattices approach each other closely, the lattices adjust in complementary fashion, positive charge opposite negative, leading to a net attraction.

Hydration Force: The hydration force is due to reconfiguration of water between macromolecular surfaces. Rather than acting by modifying van der Waals or electrostatic double layer interactions or by directly bridging neighboring molecules, polyvalent ligands bound to DNA double helices appear to act by reconfiguring the water between macromolecular surfaces to create attractive long range hydration forces⁴⁴. There might be similarities between how the ionic hydrogen bonds form in inorganic ammonium phosphate crystals, and how DNA phosphates interact with amines in spermidine and cobalt hexamine. Following this analogy, water may be released from the immediate

hydrational environment of DNA phosphates and multivalent counterions upon DNA condensation⁴⁵.

2.8 Research Idea

It is not known how the long distance radical cation migration in oligonucleotides is affected by conversion of the DNA to a well ordered structure. Also, the study of the mechanism of charge transfer in long pieces of DNA is significant in terms of understanding the cellular situation. We attempted to prepare synthetic oligonucleotide duplexes with desired modification and probes, which were intended to be ligated to linearized plasmid following enzymatic ligation. We decided to transform the ligated plasmids into DNA condensates with the help multivalent cations. The DNA condensates were investigated in the light of charge transfer mechanism and radical cation migration. By doing this we intend to understand the effect of DNA condensation on one electron oxidation. Schematic representation of the experimental design is showed in Figure 2.5.

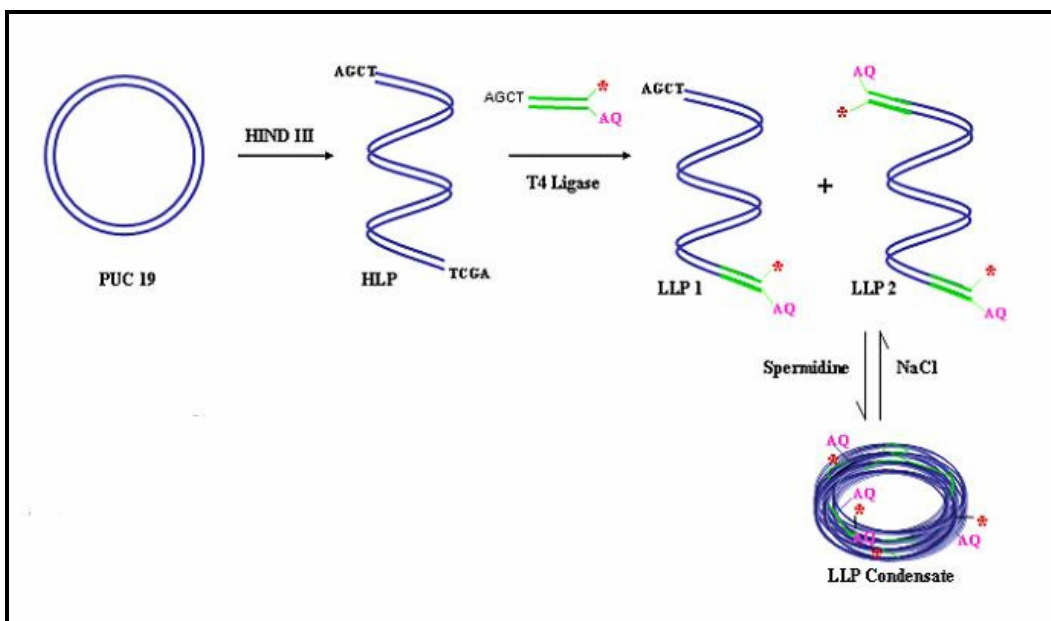


Figure 2.6: Schematic Diagram of Experimental Design

2.8 Design of Synthetic Oligonucleotide Duplex

Charge migration through dsDNA with fully complementary Watson-Crick base pairing is monitored by oxidation at GG steps within the dsDNA. The charge migration properties of $[GG(A)_nGG]_m$ ($n=2$ to 5 , $m=4$ to 6) strands have been studied thoroughly⁴⁶. This would be an ideal strand for our experiment because comparable hopping and trapping will allow us to investigate the differences in charge migration properties in the oligomer duplex and the ligated plasmid containing the duplex as part of the whole strand. DNA1 has six dGdG (for simplicity has been referred as G) opposite to six CC segments and each of the GG steps separated by three consecutive As. These six GG steps are supposed to behave as charge traps for analytical determination of charge transfer efficiency. The 5'-end of DNA1 was phosphorylated with the help of chemical phosphorylating reagent to add PO_4 group for future ligation. The 5'-end also contains the

four base overhangs 5'-AGCT-3' for cohesive end ligation with linearized plasmid DNA. The 3'-end of DNA1 contained radiolabel tag in the form of $^{32}\text{P-PO}_4$. DNA2 contains 5'-Anthraquinone group covalently attached which serve as a charge injector upon UV irradiation. Anthraquinone-phosphoramidite was synthesized following standard procedures in two steps. First anthraquinone carbonyl chloride was reacted with 2-aminoethanol to make the corresponding amide which was further treated with cyanoethylchlorophosphoramidite to give the Anthraquinone-phosphoramidite, ready to go into the expedite DNA synthesizer. The following figure shows the design of DNA1 and DNA2 in details.

DNA1	5- PO_4 -AGCTGATATCA GG_1 AAAG GG_2 AAAG GG_3 AAA GG_4 AAA GG_5 AAA GG_6 TATA-3'- $^{32}\text{PO}_4$
DNA2CTATAGTCC TTTCTTTCC TTTCTTTCC TTTCC ATAT-5'-AQ

Figure 2.7: Design of DNA Oligomer Duplex DNA1-DNA2

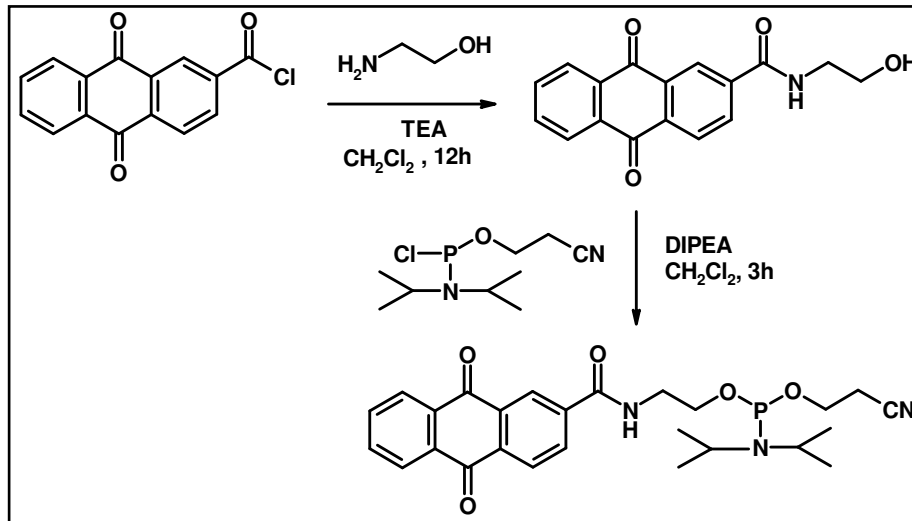


Figure 2.8: Scheme for Synthesis of Anthraquinone-Phosphoramidite.

2.9 Experimental

2.9.1 Materials and Methods

All the chemicals and solvents for synthesis of AQ-phosphoramidite were purchased from Sigma Aldrich and Fisher Scientific and used as obtained. All synthetic DNA oligonucleotides were synthesized in our laboratory by Dr. Sriram Kanvah on an Applied Biosystems Inc. Expedite DNA synthesizer. Nucleotide phosphoramidites, reagents for synthesis and chemical phosphorylating reagent (CPR II) were purchased from Glen Research. The DNA samples were treated with ammonia at 60⁰C overnight to detach the DNA from the CPG (Calcium Pectinate Gel) solid support and also to remove the protecting groups. These synthetic DNA oligonucleotides were then purified by reverse phase HPLC on a Hitachi 7000 HPLC system equipped with Varian Dynamax 25 x 21.4

mm C-18 column using 5-20% Acetonitrile in 0.5 M Triethylammonium Acetate buffer at pH = 7. The purified DNA single strands were then desalted using sep-pak column. UV/Vis studies on DNA oligonucleotides were conducted at 260 nm on a Hewlett Packard Spectrophotometer, and the extinction coefficients using nearest neighbor values (AQ replaced with A for calculation purposes) using a biopolymer calculator. The mass of each oligonucleotide was determined by a Micromass Quattro Electrospray Ionization (ESI) mass spectrometer at the mass spectra facility at Georgia Tech. Radioactively labeled isotope (α - ^{32}P) Adenosine triphosphate (ATP) and the enzyme Terminal Dinucleotide Transferase (TDT) and its buffer were purchased from GE Healthcare, formerly Amersham Biosciences. Plasmid Puc19, T4 DNA Ligase and HindIII restriction enzymes were purchased from New England Biolabs. All DNA samples and enzymes were stored at -20°C. UV melting and cooling curves were performed on a Cary 1E Spectrophotometer equipped with a multi-cell block temperature controller and sample transport accessory. Circular Dichroism (CD) measurements were conducted on a Jasco-720 instrument equipped with a temperature controller. Dynamic light scattering experiments were done using a Dynapro MS_X dynamic light-scattering instrument (Proterion, Piscataway, New Jersey). Transmission Electron Microscopy images were recorded on a JEOL-100 C Transmission Electron Microscope at 100,000 magnification. Autoradiography was performed on a Fuji 2340 BAS-Image system. Kodak films were purchased from Aldrich. Gel-extraction kits were purchased from Qiagen, and spermidine hydrochloride was obtained from Aldrich. Tris-Acetate-EDTA (TAE) buffer, Boric acid, Trizma and urea were purchased from Fisher. Spin columns and centrifugal filters were obtained from

Millipore. Carbon coated copper grids for Transmission Electron Microscopy were purchased from Ted Pella Inc., Redding, California.

2.9.2 Synthesis of DNA single strands

Anthraquinone phosphoramidite was incorporated into the DNA along with other commercially available protected normal nucleoside phosphoramidites in an Expedite DNA synthesizer. After synthesis of DNA, the samples were treated with ammonia at 60⁰C overnight to cleave off the DNA from the CPG (Calcium Pectinate Gel) solid support and also to remove protecting groups. These single strand DNA strands were purified using reverse phase HPLC system using an appropriate mixture of water, Acetonitrile and TEAA (Triethylamine-Acetic Acid) buffer as solvent. The salts from the HPLC eluted DNA samples were removed by desalting with sep-pak columns and then the concentration of the DNA single strands were calculated by using the Lambert-Beer Law.

$$A_{\text{abs}} = \epsilon \cdot \text{conc.} \cdot l \quad \dots\dots\dots \text{Equation 2.1}$$

Where A_{abs} is the absorbance value at 260nm, l is the path length of 1 cm, conc. is the concentration of the DNA single strands and ϵ is the extinction coefficient calculated using the nearest-neighbor values with the help of a biopolymer calculator. The individual DNA strands were characterized by ESI mass spectrometry (Figure 2.9. A & B) to determine the accuracy of the purification as well as verification of the oligomer purity.

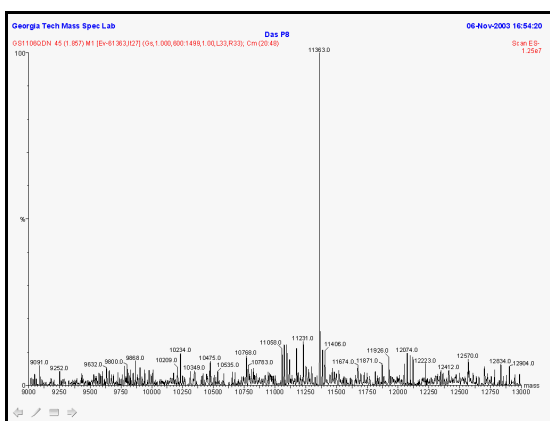


Figure 2.9.A: Mass Spectra of DNA1

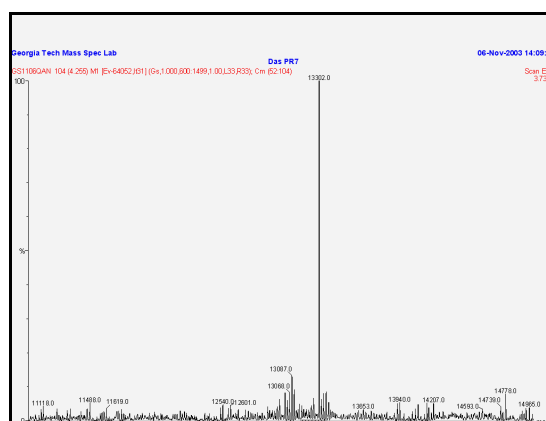


Figure 2.9.B: Mass Spectra of DNA2

2.9.3 Thermal Denaturation study of DNA oligomer duplex

The thermal denaturation properties of DNA duplexes (DNA1 and DNA2) were characterized by UV absorption at 260 nm. The first derivative of the absorbance vs. temperature curve gives the melting temperature of the DNA duplex. 25 μ L of 100 μ M solution of each of DNA1 and DNA2 were mixed to make a 1000 μ L solution with sodium phosphate buffer with overall buffer strength at 10mM and pH = 7. The solutions were taken in a UV transparent quartz cell with a 1cm path length and placed inside the Cary 1E Spectrophotometer. To verify the reversibility of the thermal transitions several temperature ramps starting from 15 $^{\circ}$ C to 90 $^{\circ}$ C at a rate of 1 $^{\circ}$ C/min, were investigated.

The results (figure 2.10. A) show that the modified DNA duplexes made out of DNA1 and DNA2 show sharp melting behavior at 59 $^{\circ}$ C. Absence of Anthraquinone in the unmodified blunt ended DNA duplex increases the melting temperature by 5 $^{\circ}$ C. Addition of magnesium chloride in small amounts (overall concentration 2.5 μ M) to these duplexes

raises the melting temperature by several degrees delivering additional stability to the DNA duplex.

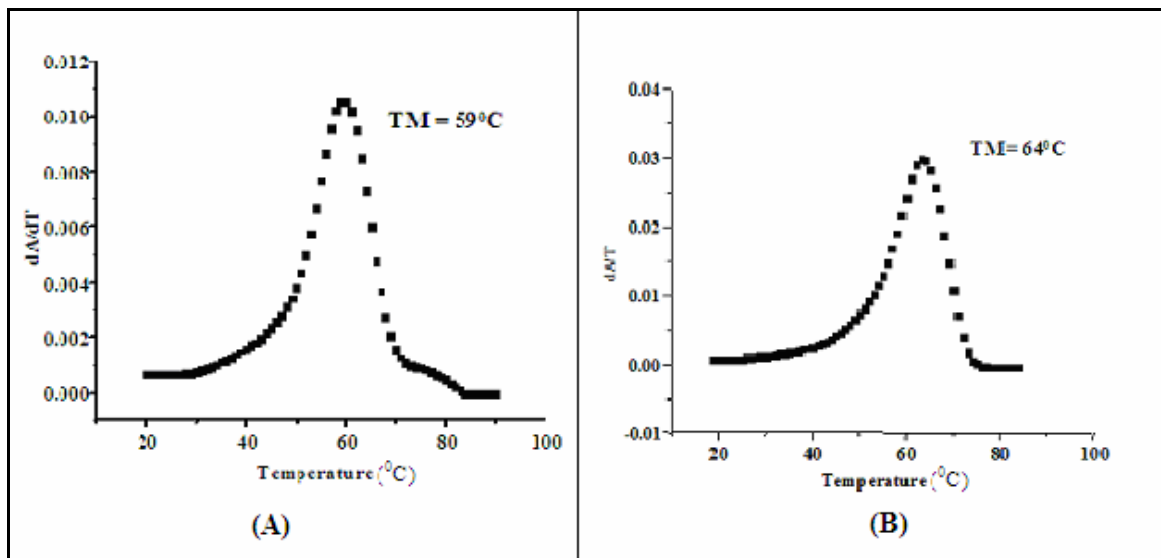


Figure 2.10.A: Thermal Denaturation Curve for DNA1-DNA2; **B:** Thermal Denaturation Curve for Non-AQ Containing Blunt Ended DNA1-DNA2

2.9.4 Circular Dichroism study

The secondary structure of DNA1-DNA2 was determined by CD experiments at room temperature with a scan rate of 200 nm 400 nm. A total of 5 scans per sample were completed, and the scans were averaged to the result in the CD spectrum for each DNA duplex (Figure 2.11). The spectral resolution and the bandwidth were 0.2 nm and 1 nm, respectively. The samples were taken directly from the T_m (DNA melting experiments) to the CD instrument, and therefore have the same DNA and the salt concentration as described above in the melting temperature studies. The CD spectrum shows formation of B-form double helix DNA with the oligomer DNA1 and DNA2.

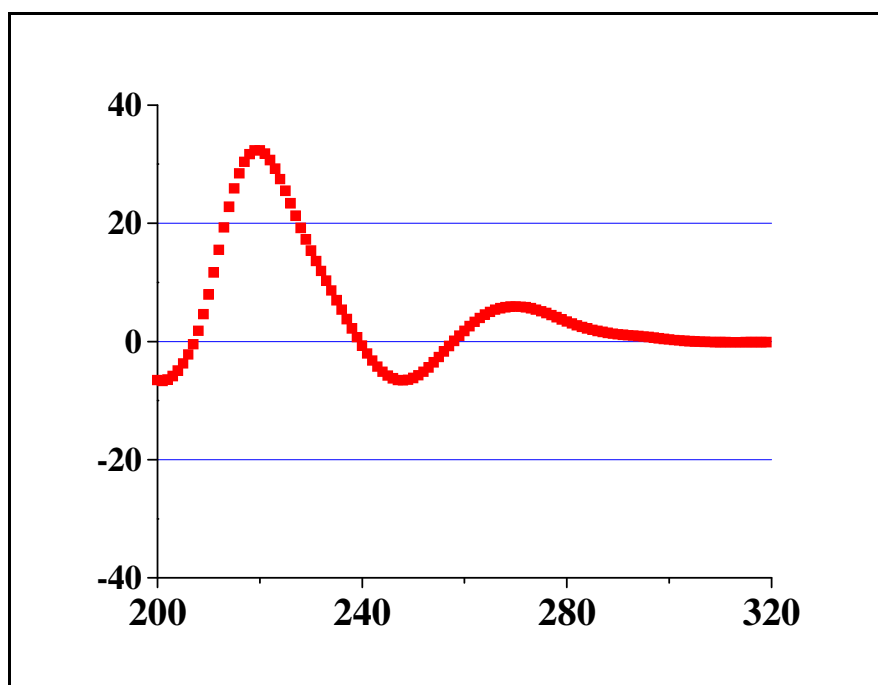


Figure 2.11: Circular Dichroism Spectra of DNA1-DNA2

2.9.5 Preparation of radiolabel DNA

Visualization of the amount of damage at GG steps in the DNA is essential for determining the efficiency of charge migration. End-labeling the ssDNA oligomer containing the GG steps with α or γ - ^{32}P -radiolabeled phosphate (α is placed at the 3'-end of the ssDNA, whereas γ is placed on the 5'-end) allows for quantitative measurement of the ratio of damage occurring at the GG steps within the dsDNA.

The DNA oligomer DNA1 was radiolabeled at the 3'-end using [α - ^{32}P] ATP and TDT enzyme. A 5 μL , 100 μM solution of desired DNA strand was incubated with 2 μL of [α - ^{32}P] ATP, 2 μL of TDT enzyme and 2 μL of 10X TDT buffer in a total volume of 20 μL at 37 $^{\circ}\text{C}$ for 1 hour. After incubation, the DNA sample was suspended in a denaturing loading dye containing tetrabromophenolsulfonphthalein (bromophenol blue) in 4:1 water-

formamide. This DNA mixture was loaded onto a 20% 19:1 acrylamide/ bisacrylamide denaturing gel to separate the radiolabel DNA from enzyme, unreacted radiolabel and truncated pieces of DNA. The radiolabeled DNA bands were identified by autoradiography and the desired DNA band was excised from the gel. The gel pieces were cut into very small pieces with a razor and eluted with 800 μL of elution buffer (0.5 M NH_4OAc , 10 mM $\text{Mg}(\text{OAc})_2$, 1.0 mM EDTA and 0.1% SDS) at 37°C for 12 hours. The DNA was precipitated in presence of 100% ethanol at -78°C for 1 hour. The supernatant was removed after 45 minits of centrifugation and the DNA precipitate was washed twice with 80% ethanol to remove the salts. The DNA samples were then dried *in vacuo* and stored in appropriate storage area for future use.

2.9.6 Restriction endonuclease digestion of plasmid Puc19

1 μL of pUC19 plasmid (1 $\mu\text{g}/\mu\text{L}$ solution as obtained from NEB) was treated with 2 μL HIND III restriction endonuclease (40 units) in presence of 1X Hind III buffer in a total volume of 50 μL in a micro centrifuge tube and incubated overnight at 37°C . The plasmid sample was precipitated by 100% ethanol at -78°C and washed twice with 80% ethanol and air dried. 7.5 μL water and 7.5 μL non-denaturing dye (bromophenol blue in 3:1 water and glycerol). The DNA sample was subjected to electrophoresis using an analytical, 1% non-denaturing, low melting agarose gel. The gel was prepared by dissolving 1 g of low melting agarose in 100 ml of 1:1 water and 1X TAE (Tris-Acetate-EDTA) buffer and heating the solution in microwave for 2/3 minits with occasional whirling until clear solution is obtained. The gel solution was then poured into gel cast and

left undisturbed for 1 hour. The electrophoresis experiment was carried out at 120 volts for 1 h in TAE buffer containing 1000 µg/L Ethidium bromide solution which enables the visualization of DNA bands under UV light in a UV illuminator. The agarose gels were photographed by using a canon digital camera for record purposes. The restriction cut plasmid was identified by comparison with the uncut supercoiled and relaxed forms of the plasmid (Figure 2.12). The mobility of the supercoiled uncut puc19 is the highest, while the mobility of the relaxed uncut plasmid is the lowest. The mobility of the Hind III enzyme cut puc19 plasmid is in between the supercoiled and relaxed form of the uncut plasmid. The plasmids which were cut with restriction enzyme for the purpose of ligation were washed with ethanol and air dried. Calculated amount of nanopure water was added to solubilize the plasmid and the UV absorption of was measured to determine the concentration. The linearized plasmid solution thus obtained was used as such without further gel purification.

2.9.7 Ligation of plasmid with radiolabeled oligonucleotides

Prior to ligation, the radiolabeled DNA1 and AQ containing DNA2 were annealed. To the air dried radiolabeled DNA1 sample, 5 µL, 100 µM solution of DNA2 was added and hybridization was achieved in 10 mM sodium phosphate buffer solution at pH 7.0 with a total volume of 50 µL. The samples was heated at 90⁰C for 5 min and slowly cooled to room temperature overnight. The oligomer duplex was ligated to the linearized pUC19 plasmid (10:1 molar ratio) with T4 DNA ligase, 1 mM ATP and 1 µL PEG 8000 in 1X T4 DNA Ligase buffer in 10 separate microcentrifuge tubes with a total volume of 20

μL in each tube. The samples were incubated at 16⁰C overnight in a thermo NESLAB RTE7 incubator. After ligation, all the samples were mixed together and 1000 μL cold ethanol were added and kept at -78⁰C for 1 hour. The samples were centrifuged and the supernatant discarded appropriately and washed twice with 80% ethanol and air dried.

2.9.8 Purification of ligated plasmid

The ligated plasmid samples were mixed with water and dye and put into preparative non-denaturing agarose gel in multiple wells (2 μg of puc19 per well) of the gel. After one hour of running the gel electrophoresis at 120 volts, the ethidium bromide stained plasmid bands were excised with a razor and put into a microcentrifuge tubes and freezed immediately at -78⁰C for 30 minits. The centrifuge tube containing the gel pieces was then heated at 50⁰C for 10 minits and a clear solution was obtained. To this solution 500 μL Qiaex buffer A (Qiagen, chaotopic reagent) solution was added until the pH is alkaline as indicated by the yellow color of the buffer. To this solution, 30 μL Qiaex suspensions (Qiagen, silica beads for adsorption of DNA) was added and kept at 50⁰C for 15 minits with frequent vortexing. The suspension was then centrifuged and the supernatant liquid was discarded. The precipitate was washed again with Qiaex buffer A to eliminate the last traces of agarose gel particles and then washed twice with Qiaex buffer B (ethanol and NH₄OAc salt solution) to precipitate the DNA and to eliminate the buffer A. The suspension was air dried and 20 μL of Qiaex elution buffer (50 mM Tris-acetate-EDTA buffer) was added. After 15 minits at 50⁰C, the sample was centrifuged and the supernatant was collected as this supernatant now contains the plasmid DNA. This process

of elution was repeated to make sure the entire DNA have been separated from the silica bead suspension. The linearized plasmid DNA solution was introduced into a buffer exchanger spin column (molecular weight cut off 30,000) and washed 5 times with 10 mM sodium phosphate buffer (pH=7.0) at low centrifuge speed to exchange the existing salts for the phosphate buffer. These samples were then stored at -20°C for future use in condensation and charge transfer studies.

2.9.9 Proof of ligation: Autoradiography

Freshly ligated plasmid solutions were washed with ethanol and made into a suspension in bromophenol dye solution and water. The suspension was loaded into a 0.8% non-denaturing low melting agarose gel and run at 120 volts for one hour. After completion of the electrophoresis, the gel was allowed to cool and carefully transferred to a clean blotting paper. The gel was covered with cellophane paper and glycerol was added to fill in the air gaps. The gel was then dried in a gel drier for 4 hours at 45°C . Photographic film was placed on the dried gel in dark and kept in a cascade at -78°C for 10 hours. After exposing the gel to the photographic film, the film was taken out of the cascade and developed with appropriate developer and fixer solution in dark. The photographic plate was then finally washed with water and air dried revealing spots corresponding to radiolabeled DNA.

2.9.10 Preparation of DNA condensates and dynamic light scattering study

Condensations were performed in 10 mM sodium phosphate buffer (pH 7.8) by bringing the DNA to appropriate buffer concentration by the use of Microcon YM-30

buffer exchange spin column (Millipore). All solutions were filtered through Amicon Ultrafree-MC centrifugal filters with 0.22- μ m diameter (Millipore) prior to use in condensation reactions. An aliquot of 7.5 μ L solution of gel purified linearized ligated pUC19 plasmid (25 μ g/mL) in sodium phosphate buffer was added to an equal volume of spermidine solutions (50 μ M to 400 μ M at intervals of 50 μ M). Following 5 min of gentle agitation, the samples were analyzed by dynamic light scattering using a Dynapro MS/X dynamic light scattering instrument (Proterion, Piscataway, NJ). The intensity of scattered light increased with increase in concentration of spermidine. Upon addition of 1 M NaCl solution to the condensate solution, decrease in the intensity of scattered light was observed but increase in noise similar to data collected for ligated plasmid that does not contain spermidine was obtained. For each dynamic light scattering experiment, 30 data points were collected over a period of 5 min and the intensity of scattered light and hydrodynamic radii were obtained as average of these data points.

2.9.11 Transmission Electron Microscopy (TEM) study

Condensates were prepared according to the standard procedure, deposited on a carbon-coated copper grid (Ted Pella, Redding, CA) and allowed to settle for 10 min. The grids were stained by the direct addition of 5 μ L of 2% uranyl acetate, rinsed in 95% ethanol and air-dried. Images of the DNA condensates at room temperature were collected on film using a JEOL-100C Transmission Electron Microscope at 100 000 X magnification.

2.9.12 UV irradiation and piperidine treatment

Prior to inducing the charge injection into the oligomer duplex control strands DNA1 and DNA2, they were annealed together by heating at 90⁰C for 5 minits followed by slow overnight cooling. A total volume of 20 μ L per sample were constructed with each of the radiolabeled duplex oligomer, linear ligated plasmid, or freshly prepared condensates in 10 mM sodium phosphate buffer at pH= 7.0 . These samples were irradiated in microcentrifuge tubes at ca. 30 ⁰C in a Rayonet Photoreactor (Southern New England Ultraviolet Co., Barnsford, CT) equipped with eight 350 nm lamps for varying amounts of time. There was always one sample corresponding to one particular kind of sample that was not irradiated because it was used as the control, often known as dark controlled lane. In these experiments, the extent of reaction was controlled so that the DNA samples were reacted only once or not at all. This was demonstrated by showing that the results of irradiation were independent of the irradiation time at the relevant extent of reaction. Varying irradiation time and showing that the ratio of damage at the GG steps for the desired irradiation time was equivalent for all times of irradiation was an indication that the DNA samples were reacted only once or not at all. After irradiation, the samples were precipitated with cold ethanol and glycogen, at kept at -78⁰C for 1 hour and resulting supernatant solution after centrifugation were discarded. The samples were further washed twice with 80% ethanol, dried and treated with piperidine at 90⁰C for 30 min. The hot piperidine cleaved the alkaline-labile lesions in the double stranded DNA samples and that were caused by charge transfer to the GG steps followed by oxidation with water or

oxygen. After removal of the piperidine *in vacuo*, the samples were suspended 20 μ L nanopure water and again dried *in vacuo* to ensure complete removal of piperidine.

2.9.13 PAGE Analysis

In order to accurately quantify the efficiency of charge migration, the DNA samples after piperidine treatment were introduced in a polyacrylamide gel containing urea which denatures the DNA. The smaller fragments of DNA will migrate at a faster rate affording adequate separation of all DNA fragments.

The piperidine treated and air dried DNA samples were suspended in appropriate amount denaturing loading dye (bromophenol blue in formamide-water mixture), and radioactive counts are adjusted to 1000 cpm per 1 μ L of solution. The samples were then loaded in the polyacrylamide gel, with ca. 5000 cpm per lane (5 μ L solution). The electrophoresis experiments were run at 70 watts for 2-2.5 hours with TBE (Trizma-Boric Acid-EDTA) buffer. After completion of the electrophoresis, the gel were separated from the glass plates and placed on sheets of blotting paper and covered with cellophane. The gels were then placed in closed caskets with a sheet of Kodak film for 14-18 hours depending on the age of the radioactive ^{32}P -ATP used. The Kodak film were removed from the casket after the exposure time and developed to give the image of the gel. The gel images for DNA samples are shown in Figure 2.17 and Figure 2.18.

2.9.14 Phosphoimager

To determine the relative amount of DNA at each GG step, the gels were “counted” on a FUJI 2340 BAS-Image system. The gels are placed within a FUJI casket for 4 to 6 hours then removed. The imaging plate is then removed from the casket and recorded by the FUJI image system. The image looks essentially the same as the image on the Kodak film, however, this image could be counted using Image Gauge Software. Each of the dark spots in the image represents the ^{32}P -radiolabel attached to the 5'-end of a DNA fragment. Assuming the rate of reaction at each GG step is equivalent to the efficiency of charge transfer through the DNA.

2. 10 Results

2.10.1 Structural Conformation and Thermal Integrity of Oligomer Duplex

Radical Cation migration in plasmid DNA ligated to oligomer duplex containing 6 repeating GG steps has been studied. Figure 2.7 shows the sequences of the DNA1 and DNA2 which were used to form the oligomer duplex to be ligated to the plasmid Puc19. Examination of the overall secondary structure of normal Watson-Crick base paired oligomer duplex DNA by Circular Dichroism (CD) spectra showed a CD curve with a positive peak at ~ 275 nm and a negative peak at ~ 245 nm, which is characteristic of B-DNA. The customary curve of B-DNA is a result of the bases of the DNA absorbing right- and left-handed polarized UV light to varying degrees depending on their overall secondary structure. However, the CD is roughly an average of the molecules' overall

secondary structure and minor local distortions are difficult to analyze under these experimental conditions.

Thermal stability of Oligomer duplex DNA1-DNA2 was measured in 10 mM sodium phosphate buffer. DNA1-DNA2 containing Anthraquinone (AQ) group at one 5'-end and four bases overhang at another 5'-end which is complementary to HindIII cut linearized plasmid Puc19, has a melting temperature of 59⁰C. This is 5⁰C less than the non-AQ containing, both side blunt ended oligomer duplex synthesized for comparison purposes (see Figure 2.10.A & B). However, the sharp thermal melting temperature of DNA1-DNA2 suggests stable duplex formation and also provided a platform for further experimental studies to be carried out safely at room temperature.

2.10.2 Ligation of oligomer with plasmid

A single cut with HindIII restriction endonuclease linearized the circular plasmid Puc19 leaving cohesive ends with 5'-AGCT-3' overhangs. The radiolabeled AQ-containing DNA1-DNA2 duplex had a phosphorylated 5' overhang of four bases designed for cohesive ligation with the HindIII-cut linearized plasmid. The formation of linearized plasmid was confirmed by agarose gel electrophoresis, where it's mobility in the gel was in between the relaxed and the supercoiled form of the circular plasmid (Figure 2.12). The reaction of the linearized plasmid with the duplex oligomer in presence of T4 DNA ligase linked the duplex oligomer once or twice (at opposite ends, Fig. 2.6) to the plasmid to form the ligated linearized plasmid (LLP; LLP1 and LLP2). Confirmation that ligation occurred successfully is based on the appearance of radioactivity from the oligomer in the linearized

plasmid band on an agarose gel (Fig. 2.12). This synthesis provided a DNA sample of sufficient length to form condensates that contained an AQ group positioned for introduction of a radical cation, a series of guanines in the oligomer, and plasmid components that can act as traps for the radical cation, and a ^{32}P label placed for analysis of reaction at these guanines by high resolution PAGE.

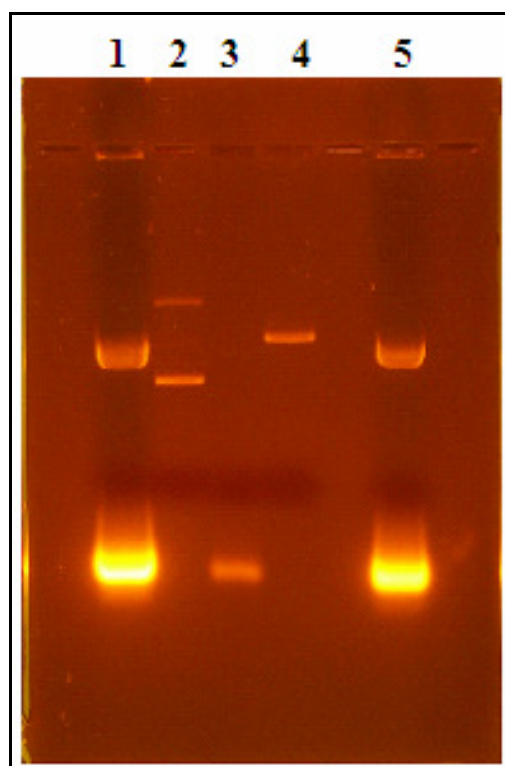


Figure 2.12: Nondenaturing Low Melting Agarose Gel

Lane 1: Linear Puc19 plasmid + DNA1-DNA2; Lane 2: Circular Puc19 plasmid

Lane 3: DNA1-DNA2 control; Lane 4: Linear Puc19 plasmid

Lane 5: Linear Puc19 plasmid + DNA1-DNA2 + T4 DNA Ligase

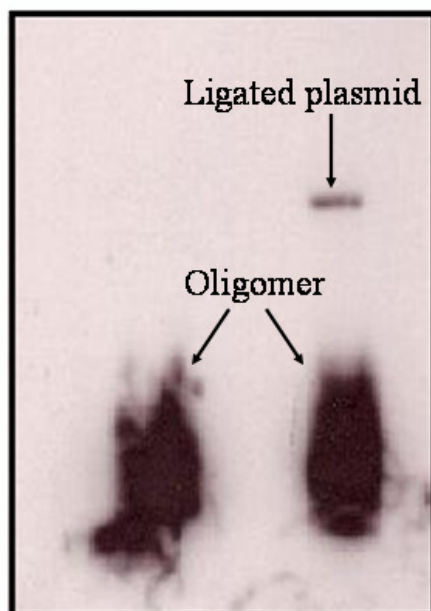


Figure 2.13: Autoradiogram of a Nondenaturing, Low-Melting Agarose Gel, showing Linear Ligated Plasmid and the Duplex Oligomer DNA1-DNA2. Left lane: DNA1-DNA2, Right lane: Product mixture from reaction of DNA1-DNA2 and linear Plasmid with T4 DNA ligase.

2.10.3 DNA condensation with spermidine

DNA condensates were formed from linear ligated plasmid with the help of spermidine as a condensing agent. In the absence of spermidine, experimental light-scattering autocorrelation curves for linear plasmid and linear ligated Plasmid in phosphate buffer solutions (12.5 $\mu\text{g/ml}$) were noisy and of low intensity, confirming the expected absence of significant numbers of light-scattering particles under these conditions⁴⁷. The addition of spermidine to these solutions resulted in the significant increase in light-scattering intensity, as shown in Figure 2.14. The amount of light scattering increased slowly when the spermidine concentration is raised in steps to 50 μM and then increased dramatically and reaches a plateau when the concentration of spermidine is 75–130 μM .

This increase in intensity indicates the formation of stable, light-scattering particles over this concentration range. Further increase in spermidine concentration to $>150\ \mu\text{M}$ caused an additional increase in the light-scattering intensity, which signals the formation of aggregates. A summary of these experimental results is shown in Fig. 2.14. Analysis of these data indicates that the phosphate buffer solutions of Linear Ligated Plasmid that contained spermidine in the concentration range of $50\text{--}130\ \mu\text{M}$ form particles with an average radius of $100 \pm 25\ \text{nm}$ (Figure 2.15), which is consistent with the formation of a condensate composed of $>90\%$ of the DNA in solution. In support of this conclusion, we observe that these particles were disrupted when $1\ \text{M}\ \text{NaCl}$ is added to the mixture, as indicated by the drop in intensity values and absence of autocorrelation.

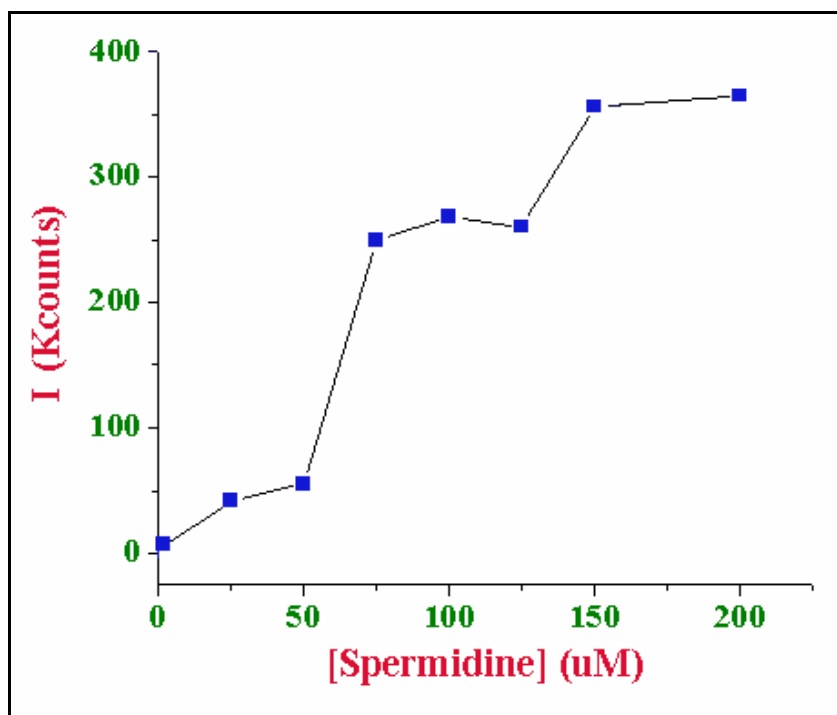


Figure 2.14: Dynamic Light Scattering Studies: Variation of Intensity of Light Scattered with Spermidine Concentration

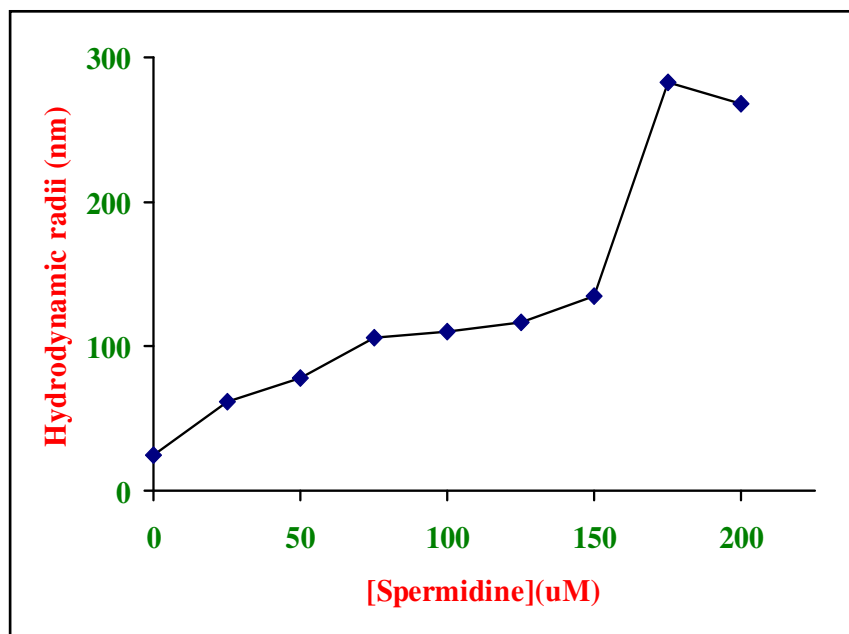


Figure 2.15: Dynamic Light Scattering Studies: Variation of Average Hydrodynamic Radii with Spermidine Concentration

Confirmation of condensate formation under the mentioned conditions was obtained by TEM, in which toroids and rod-shaped objects were visible (Fig. 2.16) at x 100,000 magnification. The outer diameter of the toroid is ~150 nm, which indicates that it was composed of 10–12 molecules of Linear Ligated Plasmid. Particles that were formed in this way were used to study long-distance radical cation transfer in B-form DNA condensates.

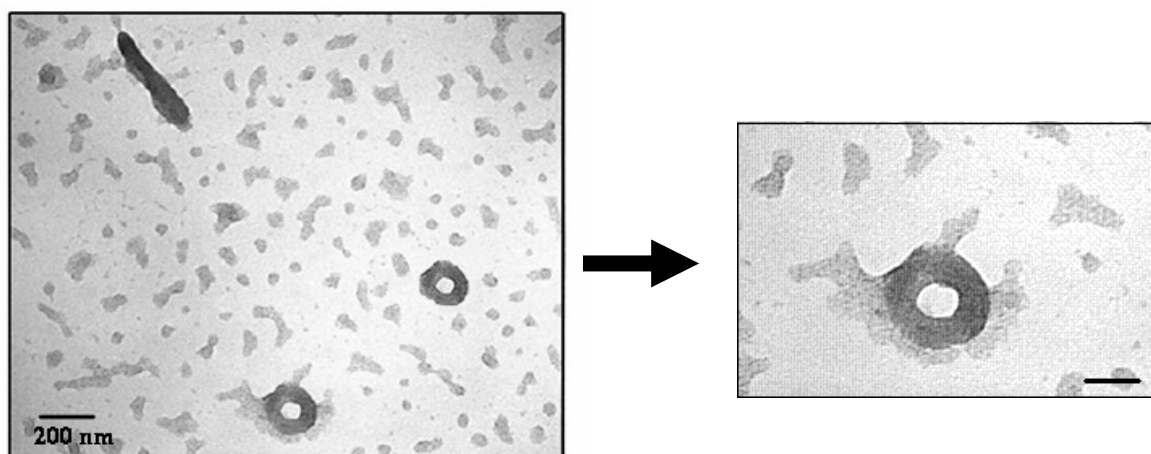


Figure 2.16: Transmission Electron Microscopy Image of Linear Ligated Plasmid Condensates with 75 μM

2.10.4 Long-Distance Radical Cation Transfer in DNA Condensates

Intensive investigation has shown that irradiation of a DNA sample that contains a covalently linked AQ group at 350 nm, at which only the AQ absorbs, forms the excited singlet state of the AQ, which rapidly intersystem crosses to form its triplet state⁴⁸⁻⁴⁹. The triplet is a powerful one-electron oxidant that initiates electron transfer from an adjacent nucleobase to form the AQ radical anion and a base radical cation⁵⁰⁻⁵². The AQ radical anion is consumed by reaction with O_2 to form superoxide, and the base radical cation can migrate through the DNA by hopping until it is trapped (usually at a guanine) by reaction with H_2O and/or O_2 ⁵³⁻⁵⁴. This process forms lesions at guanines that yield strand breaks when the sample is treated with piperidine. These strand breaks are characterized by high-resolution PAGE in samples radiolabeled with ^{32}P , and their relative yields are quantified by autoradiography. At low conversion (single-hit conditions, in which on average each DNA molecule reacts once or not at all), the distribution of strand breaks mirrors the

distribution of the radical cation in the DNA oligomer. Numerous experiments of this sort that have been carried out on oligonucleotides in solution have revealed the mechanism of long-distance radical cation transfer and how the nucleobase sequence determines the efficiency of radical-cation migration. We applied these techniques to the study of long-distance radical cation transfer in the AQ-containing condensates formed from Linear Ligated Plasmid. A sample containing condensates formed from AQ-linked Linear Ligated Plasmid (5 μ M, pH 7.0) by addition of spermidine was irradiated and subsequently treated with piperidine. Analysis by light scattering showed that the condensates were stable during and after the irradiation. The results of irradiation and charge transfer experiment are shown in Figure 2.17 as the autoradiogram of a high-resolution PAGE and in Figure 2.20 as a semilog plot of strand cleavage efficiency with distance from the AQ. It is clear from these data that a radical cation injected into the DNA condensate leads to the formation of lesions at nearby guanines that are detected as strand cleavage. Moreover, the GG steps that are closer to the AQ react more frequently than those located farther away, which is characteristic of those cases where hopping of the radical cation from one GG step to the next (k_{hop}) is slower than its trapping at a GG step by reaction with H_2O or O_2 (k_{trap})⁵⁵⁻⁵⁶. For the condensates, this distance dependence is rather steep, falling ~ 10 -fold over a distance of 70 Å. The effect of condensate formation on radical cation transfer in DNA is revealed by comparison with similar reactions carried out on the linear-linked plasmid and on the oligomeric duplex DNA1-DNA2 in the presence of spermidine. These results are also shown in Figs. 2.17, in which it is clear that both of these samples behave similarly but give results significantly different from that observed for the condensate. In

particular, the semilog plots of reactivity with distance for Linear Ligated Plasmid and DNA1-DNA2 falls off much more slowly than for the condensate. In a control experiment, we showed that piperidine-induced strand cleavage of DNA samples that had been condensed and then decondensed (by the addition of NaCl) is identical with DNA that had never been condensed (Figure 2.18). These findings indicate that long distance radical cation transfer in the organized structure of the condensate is appreciably less efficient than it is for oligonucleotides in solution.

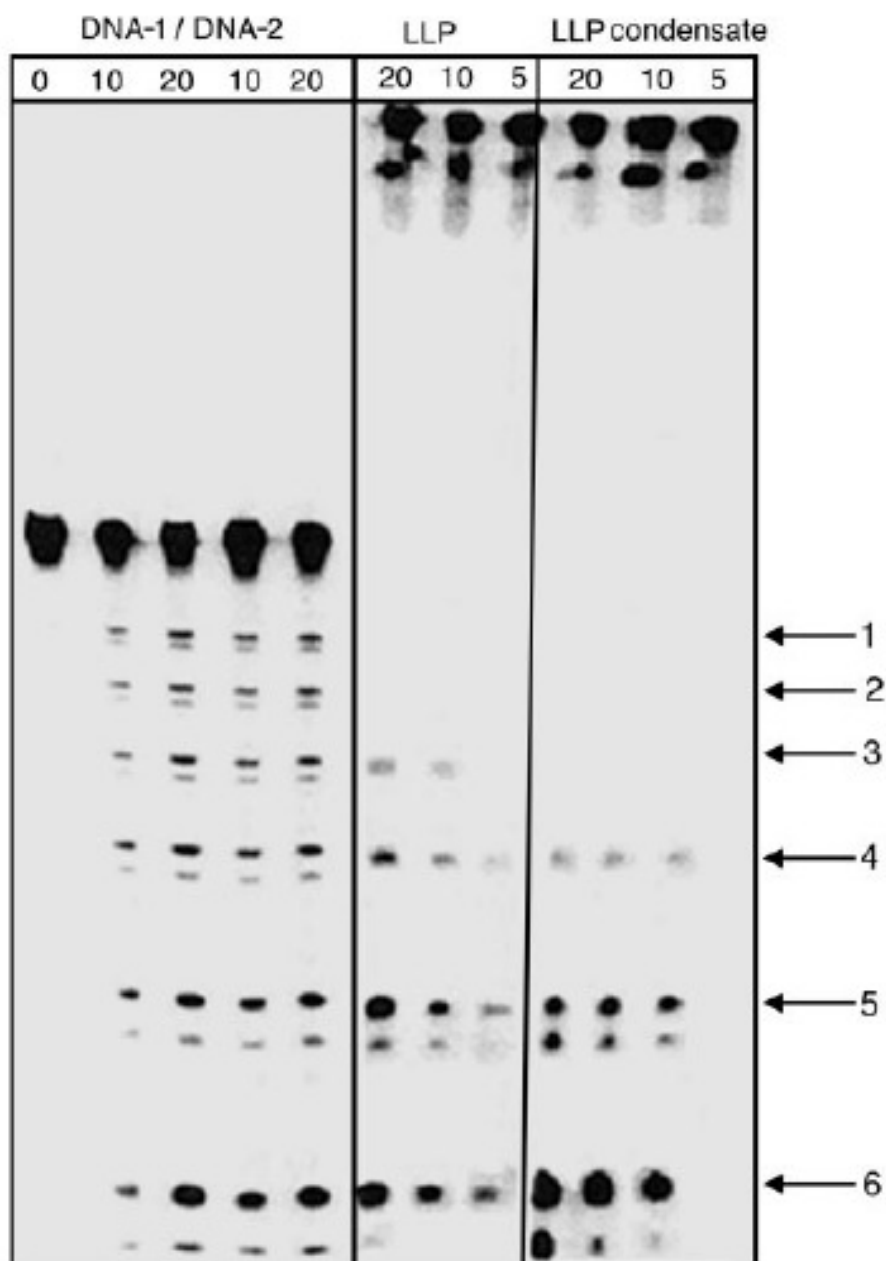


Figure 2.17: Autoradiogram Showing Results of Irradiation of DNA1-DNA2, Linear Ligated Plasmid (LLP), and Condensed Plasmid.

Numbered arrows on the right indicate the six GG steps of these DNA oligomers. The first five lanes correspond to the dark control, 10 and 20 min of irradiation of the oligomer duplex DNA1-DNA2, mixed with 75 μ M spermidine and DNA1-DNA2, respectively. The next three lanes correspond to 20, 10, and 5 min of irradiation of the LLP, and the last three lanes to that of 20, 10, and 5 min of irradiation of the ligated condensed plasmid, respectively.

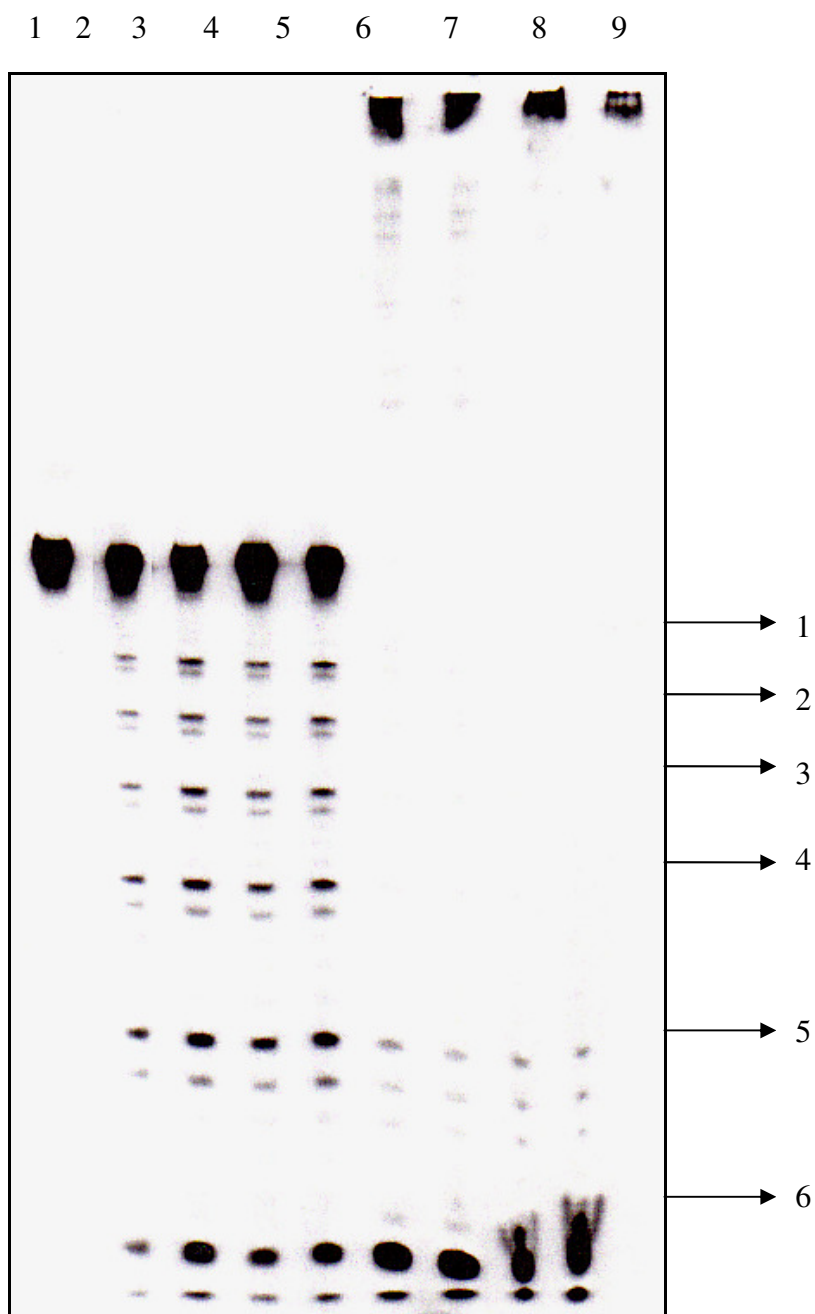


Figure 2.18: Autoradiogram Showing Results of Irradiation of DNA1-DNA2, Condensed and Decondensed Ligated Plasmid.

Numbered arrows on the right indicate the six GG steps. Lane 1-5: dark control, 10 and 20 min of irradiation of the oligomer duplex DNA1-DNA2, mixed with 75 μ M spermidine and DNA1-DNA2, respectively. Lane 6,7: 10 and 20 min of irradiation of the Condensed Ligated Plasmid; Lane 8,9: 10 and 20 min of irradiation of the ligated condensed plasmid, decondensed with 2 M NaCl after irradiation.

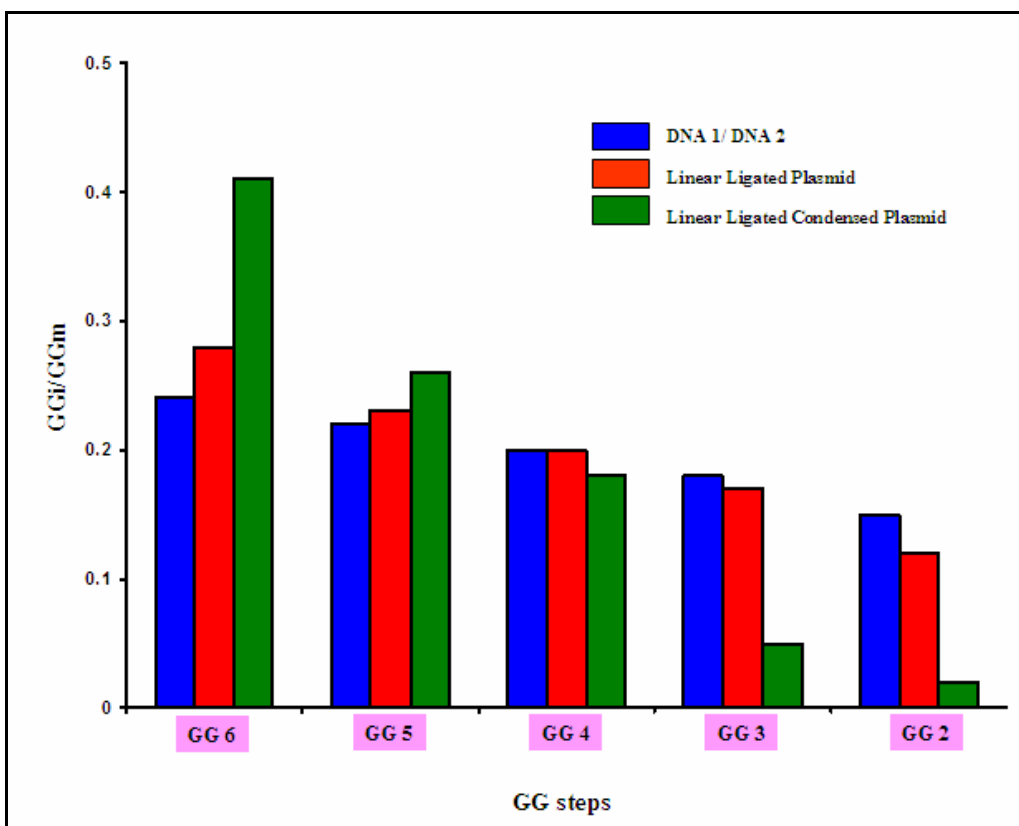


Figure 2.19: Histogram showing the Relative Damage at the GG Steps of DNA1-DNA2, Linear Ligated Plasmid and Ligated Condensed Plasmid.

2.11 Discussion

The accepted mechanism for long-distance radical-cation migration in duplex DNA is phonon assisted polaron like hoping⁵⁷⁻⁵⁸. In this model, the radical cation is stabilized by local distortions of the DNA structure and its environment, particularly tightly bound water molecules and associated counter ions. This self-trapped radical cation (the polaron) is usually located predominantly on guanines, but in appropriate sequences, it can also be delocalized onto adjacent adenines. Barriers to migration of the polaron from one site to another are overcome by thermal fluctuations (phonons) of the DNA and its environment that form charge-transfer effective states⁵⁹. For example, the duplex oligomer

DNA1-DNA2 contain consecutive AGGA segments (identified as the polaronic site) separated by a single adenine (the barrier)⁴⁶. If the rate of hopping from one polaronic site to an adjacent site is much faster than the rate of its irreversible trapping in a chemical reaction, then the radical cation will be distributed approximately equally over all equivalent sites and there will be no apparent distance dependence for radical-cation migration. However, if the rate of irreversible trapping is much faster than hopping, then reaction will be detected only at those sites closest to the point of radical cation injection (the AQ, in this case). The results from the investigation of DNA1-DNA2 reveal intermediate behavior. Strand cleavage is observed at all six of the reactive GG sites in this duplex oligomer when the irradiated sample is treated with piperidine, but the amount of cleavage at a particular site decreases as the distance from the AQ increases. Quantitatively, the slope of the semilog plot of cleavage efficiency against distance has a value of -0.007 \AA^{-1} (Fig. 2.20). A kinetic analysis has been developed that permits characterization of the distance dependence of radical-cation migration with the dimensionless parameter *kratio*, which is equal to $k_{\text{hop}}/k_{\text{trap}}$. The slope of the semilog plot for DNA1-DNA2 reveals that, in this case, *kratio* = 15, which indicates that hopping of the radical cation from site-to-site is 15 times faster than its irreversible consumption. The value of *kratio* for DNA1-DNA2 is unaffected by the addition of spermidine, and it does not change meaningfully when the oligomer is ligated to the linearized plasmid, but the value *kratio* decreases to 5 for the condensate, which shows that the efficiency of long-distance charge transfer decreases in this highly ordered structure.

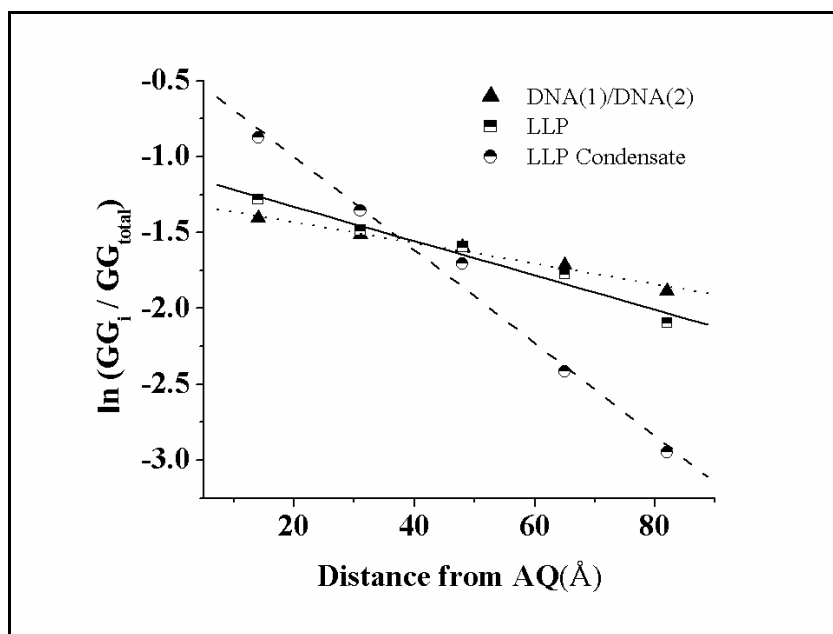


Figure 2.20: Semilog Plot of the Relative Amount of Strand Cleavage Detected at GG Steps of DNA1-DNA2, Linear Ligated Plasmid (LLP) and Ligated Condensed Plasmid (LLP Condensate) with Distance from the AQ Group.

Condensation of DNA may affect both the rate of hopping and the rate of trapping. One explanation for the observed decrease in charge transfer efficiency in the condensates is a reduction in k_{hop} . Ionization of the phosphate groups makes DNA a polyanion at normal physiological pH at which the negative charges are compensated by mobile counter ions (typically sodium). Detailed quantum mechanical calculations have shown that motions of the sodium ions modulate the energy of a radical cation polaron in DNA⁶⁰. In some configurations, the sodium ions (and associated water molecules) form charge transfer effective orientations in which the energy of the polaron matches that of the barrier separating it from an adjacent site, which allows the polaron to hop⁶¹⁻⁶².

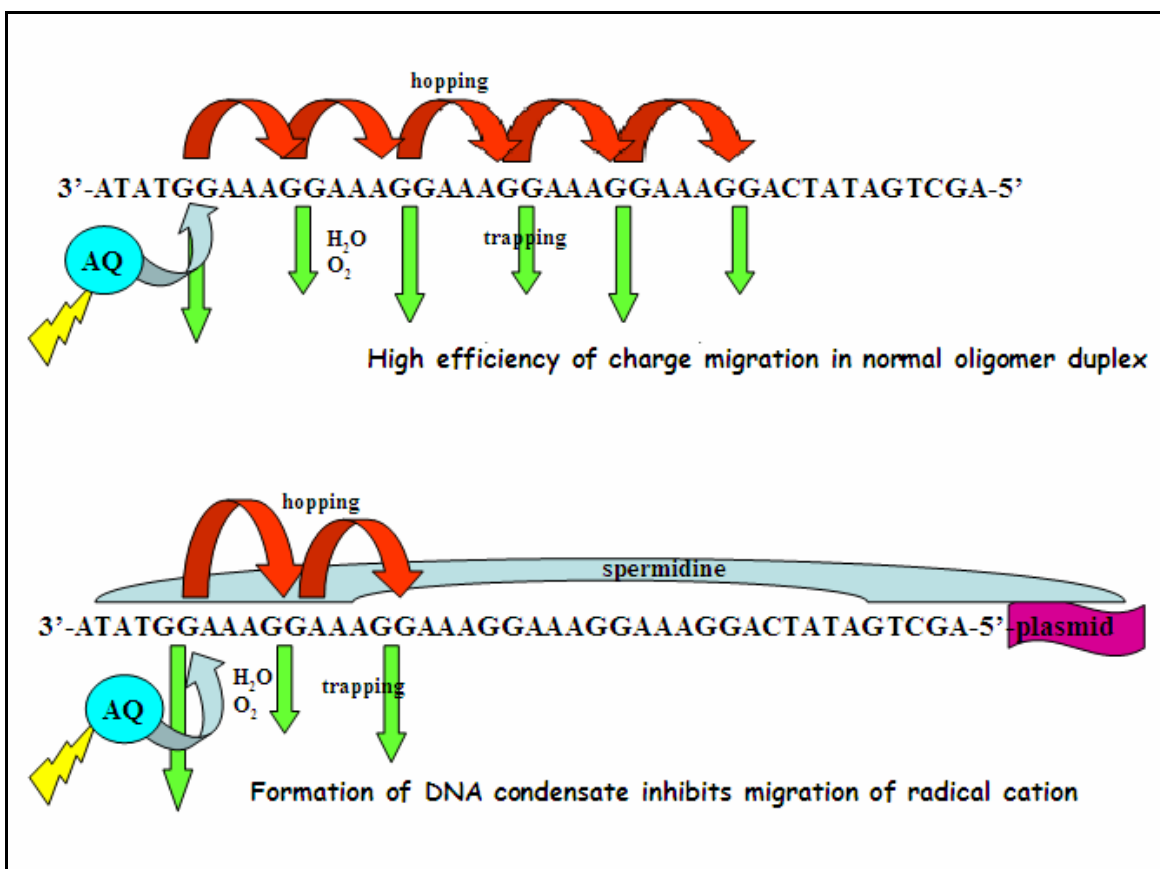


Figure 2.21: Pictorial Depiction of the Effect of Condensate Formation on Radical Cation Hopping in DNA

In condensates, >90% of the mobile sodium ions are replaced by spermidine trications that will be far less mobile than a monovalent ion. In this circumstance, it will be more difficult to attain a charge transfer effective configuration, and hopping will be slower. It is unlikely that condensate formation will increase the magnitude of k_{trap} , which would be required if condensation were the primary cause of the reduced charge efficiency. Spermidine wraps the DNA into a compact core having high peripheral positive charge that is resistant to hydrolytic cleavage by DNase I enzyme⁶³. This structure hinders access of oxygen and water molecules to the interior of the condensate, where reaction with the

radical cation occurs. Consequently, the rate of trapping will be retarded, and if hindered access were the major consequence of condensate formation, then an increase in the efficiency of long-distance charge transfer is expected and not the decrease that is actually observed.

2.12 Conclusion

It is widely accepted that the one-electron oxidation of DNA is a major source of genetic damage leading to mutations. In particular, the conversion of a guanine to an 8-OxoG results in G-to-T transversion because the stable base pair that 8-OxoG forms with adenine causes failure of mismatch repair⁶⁴. Numerous experiments have shown that the nucleobase radical cations formed by electron loss from DNA oligomers in solution can migrate long distances before being trapped at a guanine. We have shown that this process also occurs in DNA condensates, which mimic genomic DNA in significant ways. However, the efficiency of radical cation transport in condensates is considerably less than that for an oligomer having an identical nucleobase sequence. The formation of DNA condensates with the multivalent cation spermidine inhibits the migration of radical cations and, consequently, DNA damage is more localized at the site of initial electron loss. This inhibition is attributed to the decreased probability for forming the charge-transfer effective states that are required for radical-cation hopping when sodium counter ions of high mobility are replaced with the low-mobility polycationic agents used to form the condensate.

2.13 References

1. Hasty, P.; Vijg, J. *Science* **2002**, 296, 1250-1251.
2. Kanvah, S.; Schuster, G. B. *J. Am. Chem. Soc.* **2004**, 126, 7341-7344.
3. Demple, B.; Harrison, L. *Annu. Rev. Biochem* **1994**, 63, 915-948.
4. Armitage, B. *Chem. Rev.* **1998**, 98, 3, 1171-1200.
5. Akpa, T. C.; Weber, K. J.; Schneider, E.; Kiefer, J.; Frankenberg-Schwager, M.; Harbich, R.; Frankenberg, D. *Int. J. Radiat. Biol.* **1992**, 62, 279-87.
6. Breslin, D. T.; Schuster, G. B. *J. Am. Chem. Soc.* **1996**, 118, 2311-2319.
7. Gasper, S. M.; Schuster, G. B. *J. Am. Chem. Soc.* **1997**, 119, 12762–12771.
8. Nunez, M.; Hall, D. B.; Barton, J. K. *Chem. Biol.* **1999**, 6, 85–97.
9. Schuster, G. B.; Landman, U. *Topics. Curr. Chem.* **2004**, 236, 139–162.
10. Burrows, C. J.; Muller, J. G. *Chem. Rev.* **1998**, 98, 3, 1109-1152.
11. Steenken, S.; Jovanovic, S. V. *J. Am. Chem. Soc.* **1997**, 119, 617–618.
12. Van Holde, K. E.; Allen, J R.; Tatchell, K.; Weischet, W. O.; Lohr, D. *Biophys. J.* **1980**, 32, 271–282.
13. Schmid, S. E.; Daune, M. P.; Fuchs R. P. *Proc. Natl. Acad. Sci. U. S. A.* **1982**, 79, 4133– 4137.
14. Pang, D.; Rodgers, J. E.; Berman, B. L.; Chasovskikh, S.; Dritschilo, A. *Radiat. Res.* **2005**, 164, 755-765.
15. Nevins, S. A.; Siles, B. A.; Nackerdien, J. E. *J. Chromatogr. B.* **2000**, 741, 243-255.
16. Gulston, M.; Fulford, J.; Jenner, T.; DeLara, C.; O'Neill, P. *Nucleic. Acids Res.*

- 2002**, 30, 3464-3472.
17. Nunez, M. E.; Noyes, K. T.; Barton, J. K. *Chem. Biol.* **2002**, **9**, 403–415.
 18. Bjorklund, C. C.; Davis, W. B. *Nucleic Acids Res.* **2006**, 34, 1836–1846.
 19. White, C. I.; Sedgwick, S. G. *Mol. Gen. Genet.* **1985**, 201, 99-106.
 20. Yanisch-Perron, C.; Vieira, J.; Messing, J. *Gene* **1985**, 33, 103-119.
 21. Linn, S.; Arber, W. *Proc. Natl. Acad. Sci. U.S.A.* **1968**, 59, 1300-1306.
 22. Remaut, E.; Tsao, H.; Fiers, W. *Gene* **1983**, 22, 103-113.
 23. Widom, J.; Baldwin, R. L. *J. Mol. Biol.* **1980**, 144, 431-453.
 24. Bloomfield, V. A. *Biopolymers* **1991**, 31, 1471-1481.
 25. Chattoraj, D. K.; Gosule, L. C.; Schellman, J. A. *J. Mol. Biol.* **1978**, 121, 327-337.
 26. Gosule, L. C.; Schellman, J. A. *Nature* **1976**, 259, 333-335.
 27. Widom, J.; Baldwin, R. L. *Biopolymers* **1983**, 22, 1595-1620.
 28. Laemmli, U. K. *Proc. Natl. Acad. Sci. U.S.A.* **1975**, 72, 4288-4292.
 29. Garcia-Ramirez, M.; Subirana, J. *Biopolymers* **1994**, 34, 285-292.
 30. Hsiang, M. W.; Cole, R. D. *Proc. Natl. Acad. Sci. U.S.A.* **1977**, 74, 4852-4856.
 31. Eickbush, T. H.; Moudrianakis, E. N. *Cell* **1976**, 13, 295-306.
 32. Lang, D. *J. Mol. Biol.* **1973**, 78, 247-254.
 33. Arscott, P. G.; Ma, C.; Wenner, J.; Bloomfield, V. A. *Biopolymers* **1995**, 36, 345-365.
 34. Arscott, P. G.; Li, A. Z.; Bloomfield, V. A. *Biopolymers*. **1990**, 30, 619-630.
 35. Marx, K. A.; Ruben, G. C. *Nucleic Acids Res.* **1983**, 11, 1839-1854
 36. Lang, D.; Taylor, T. N.; Dobyan, D. C.; Gray, D. M. *J. Mol. Biol.* **1976**, 106, 97-

107.

37. Plum, G. E.; Arscott, P. G.; Bloomfield, V. A. *Biopolymers*. **1990**, 30, 631-643.
38. Porschke, D. *Biochemistry*. **1984**, 23, 4821-4828.
39. Wilson, R. W.; Bloomfield, V. A. *Biochemistry*. **1979**, 18, 2192-2196.
40. Manning, G. S. *Q. Rev. Biophys.* **1978**, 11, 179-246.
41. Marquet, R.; Hossier, C. J. *Biomol. Struct. Dynam.* **1991**, 9, 159-167.
42. Bloomfield, V. A.; Wilson, R. W.; Rau, D. C. *Biophys. Chem.* **1980**, 11, 339-343.
43. Oosawa, F. *Biopolymers*. **1968**, 6, 1633-1647.
44. Rau, D. C.; Parsegian, V. A. *Biophys. J.* **1992**, 61, 246-259.
45. Matulis, D.; Rouzina, I; Bloomfield, V. A. *J. Mol. Biol.* **2000**, 296, 1053-1063.
46. Liu, C.-S.; Hernandez, R.; Schuster, G. B. *J. Am. Chem. Soc.* **2004**, 126, 2877-2884.
47. Allison, A. S.; Herr, C. J.; Schurr, M. J. *Biopolymers* **1981**, 20, 469-488.
48. Navas, A. D. *J. Photochem. Photobiol. A* **1990**, 53, 141-167.
49. Giese, B.; Biland, A. *Chem. Commun.* **2002**, 667-672.
50. Ly, D.; Kan, Y.; Armitage, B.; Schuster, G. B. *J. Am. Chem. Soc.* **1996**, 118, 8747-8748.
51. Armitage, B.; Yu, C.; Devadoss, C. *J. Am. Chem. Soc.* **1994**, 116, 9847-9859.
52. Breslin, D. T.; Schuster, G. B. *J. Am. Chem. Soc.* **1996**, 118, 2311-2319.
53. Kasai, H.; Yamaizumi, Z.; Berger, M.; Cadet, J. *J. Am. Chem. Soc.* **1992**, 114, 9692-9694.
54. Schuster, G. B. *Acc. Chem. Res.* **2000**, 33, 253-260.

55. Giese, B.; Amaudrut, J.; Kohler, A.; Sporman, M.; Wessely, S. *Nature* **2000**, 412, 318–320.
56. Henderson, P. T.; Jones, D.; Hampikian, G.; Kan, Y.; Schuster, G. B. *Proc. Natl. Acad. Sci. USA* **1999**, 96, 8353–8358.
57. Giese, B. *Acc. Chem. Res.* **2000**, 33, 631–636.
58. O'Neill, M. A.; Barton, J. K. *J. Am. Chem. Soc.* **2004**, 126, 11471–11483.
59. Barnett, R. N.; Cleveland, C. L.; Joy, A.; Landman, U.; Schuster, G. B. *Science* **2001**, 294, 567–571.
60. Barnett, N. R.; Cleveland, L. C.; Landman, U.; Boone, E.; Kanvah, S.; Schuster, G. B. *J. Phys. Chem. A* **2003**, 107, 3525–3537.
61. Liu, C.-S.; Schuster, G. B. *J. Am. Chem. Soc.* **2003**, 125, 6098–6102.
62. Leone, A. M.; Tibodeau, J. D.; Bull, S. H.; W., F. S.; Thorp, H. H.; Murray, R. W. *J. Am. Chem. Soc.* **2003**, 125, 6784–6790.
63. Adami, R. C.; Collard, W. T.; Gupta, S. A.; Kwok, K. Y.; Bonadio, J.; Rice, K. G. *J. Pharm. Sci.* **2000**, 87, 678–683.
64. Hsu, G. W.; Ober, M.; Carell, T.; Beese, L. *Nature* **2004**, 431, 217–221.

CHAPTER 3

RADICAL CATION MIGRATION THROUGH DOUBLY LIGATED PLASMID DNA CONDENSATES

3.1. Introduction

Polycationic polyamines like spermine and spermidine plays an important role in eukaryotic organisms by influencing many molecular functions. They are found to be essential to the normal physiology and development of virtually all cells¹ and its presence can result in the formation of mutagenic DNA adducts². In fact, the production of cellular polyamines is found to be frequently and markedly increased in association with cancer³. Moreover, elevated polyamine concentrations have been found in hyperproliferative tissues and depletion of cellular polyamines has been associated with growth inhibition and programmed cell death⁴⁻⁶. Ongoing research has shown that polyamines have the ability to prevent endonuclease mediated DNA fragmentation⁷ and inhibit DNA damage⁸⁻¹⁰ by acting as a scavenger for reactive oxygen species (ROS) and play a direct role in protecting DNA from free radical attack¹¹⁻¹², but the mechanisms by which these polycations function are still unidentified.

A clear understanding of DNA damage mechanism is necessary because these processes are being responsible for mutations, aging and diseases¹³. One electron oxidation and electron transfer experiments in DNA have shown that a radical cation (“hole”) introduced into a duplex DNA oligomer in solution, will migrate long distances before being irreversibly trapped by reaction with water or molecular oxygen by the “Phonon

assisted Polaron like Hopping mechanism”¹⁴⁻¹⁷. In this process, the radical cation is self-stabilized in a distortion of the DNA and its nearby environment (water molecules and counterions to the phosphate backbone) that spreads the charge over several bases (the polaron). Thermal activation (phonons) causes the polaron to hop from one site to a neighboring site. The number of hops required is determined by the extent of charge delocalization, whereas the activation barrier determines the time scale of hops.

An initial investigation of charge transfer in DNA in presence of polycationic spermidine showed that in plasmid DNA having an anthraquinone charge injector (AQ) at a 5' terminal position of a condensate, the charge migration efficiency decreased, which was attributed to the lack of formation of charge transfer effective states¹⁸. In the current study, the anthraquinone is placed in an interior position of a DNA condensate formed from by ligation of two linearized puc19 plasmids to an AQ-containing oligomer duplex. Here we report the pattern of oxidative damage of DNA in the double ligated systems containing an intercalated Anthraquinone moiety, in presence of spermidine.

3.2. Anthraquinone intercalation versus end capping

To adequately study the properties of charge migration through DNA, a sufficient method has to be determined for one electron oxidation of at least one of the DNA bases. Close association of the photosensitizers with the DNA base-pairs is required to facilitate the transfer of an electron from the DNA to the sensitizer. To obtain this critical association with DNA, several photosensitizers have been developed that either intercalate between the base-pairs, bind in the major groove or minor grooves, or “end- cap” the

terminal base-pairs. Since the photochemistry of anthraquinone has been well established²², we have focused our research on using this photosensitizer. This anthraquinone moiety (AQ) is easily synthesized and can be tethered to terminal position as well as any other intermediate position via standard phosphoramidite chemistry. Molecular modeling and spectroscopic experiments have shown this “end-capping” of the DNA permits π -overlap with the DNA, but doesn’t yield structural distortions to the DNA that can be caused by intercalation²³. The phosphorescence of the quinones is almost completely quenched by electron transfer from an adjacent base when the AQ is intercalated into duplex DNA. In contrast, when the associated quinone is not intercalated, less phosphorescence quenching is observed. These findings suggest that the intercalated anthraquinone is much more efficient electron acceptor than end-capped anthraquinone group. Internally linked anthraquinone which are associated with the duplex by intercalation are stabilized by hydrophobic interaction with adjacent bases²⁴. One added advantage of using intercalating anthraquinone is that the radical cation can travel to both sides from the site of generation and this could give additional information regarding side selection and influence of the charge injector’s geometry on hopping or trapping of the radical cation inside the condensates.

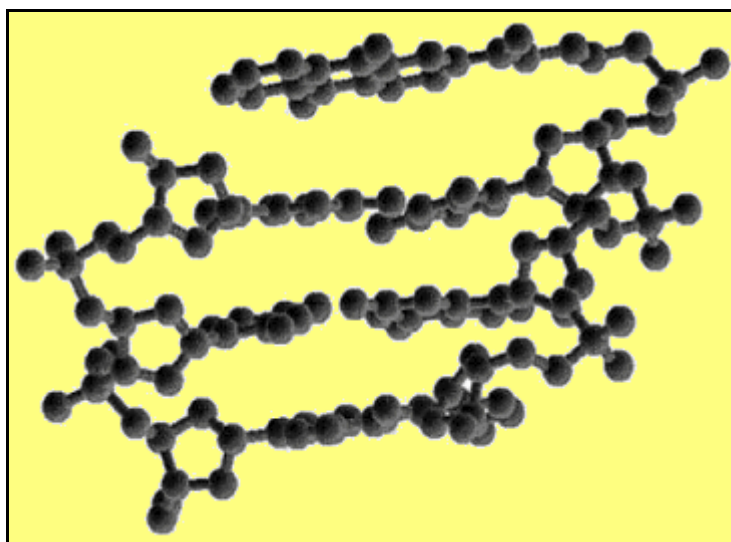


Figure 3.1: Molecular Modeling Showing AQ End-Capping the DNA Duplex¹⁹.

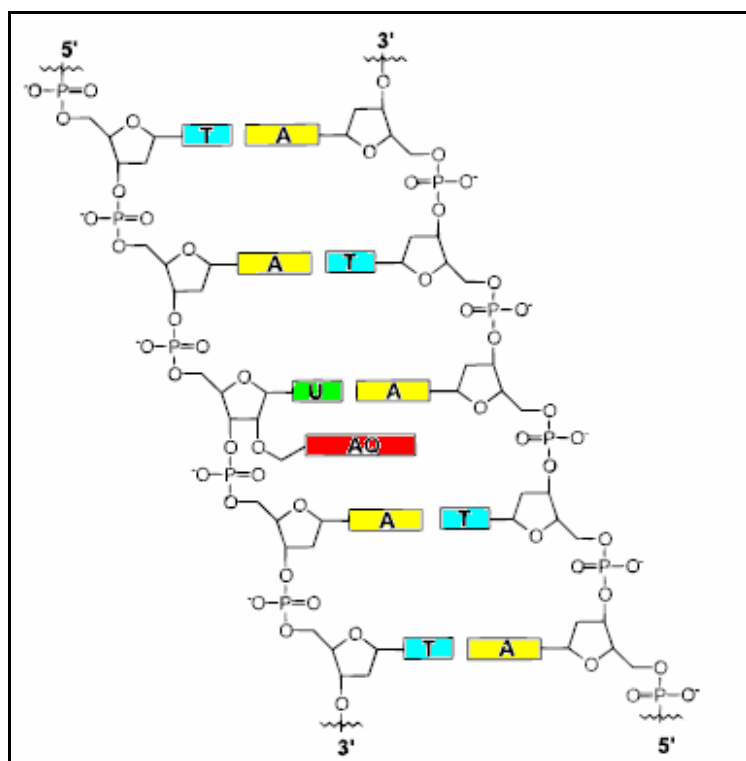


Figure 3.2: Assumed Structure of UAQ Intercalated in Duplex DNA. (Based upon the NMR Spectroscopic Data of Broom and co-workers²⁰⁻²¹).

3.3 Research Idea

Our experimental strategy is based on the idea of sandwiching a DNA oligomer duplex between two very long linear plasmids. The DNA oligomer duplex would be tailor made to have all the components necessary to perform charge transfer studies. Ligating this oligomer duplex twice, with two linearized plasmid can give a long enough piece of DNA suitable for charge migration studies in condensate form. In this work we attached the electron acceptor, the anthraquinone group (AQ) to the central position of the DNA duplex which has been designed so that it has the same base sequence extending from this central point in both the 5'- and 3'-directions. This arrangement allows us to modify the geometry of the charge acceptor on one hand, and also increase the total length of the DNA molecule on the other. The anthraquinone moiety is now intercalated in the DNA instead of being end-capped at the 5-terminus. This arrangement also gives us opportunity to study the geometrical dependence of the anthraquinone group in radical cation transfer through the DNA and preferential side selection of charge hopping if any.

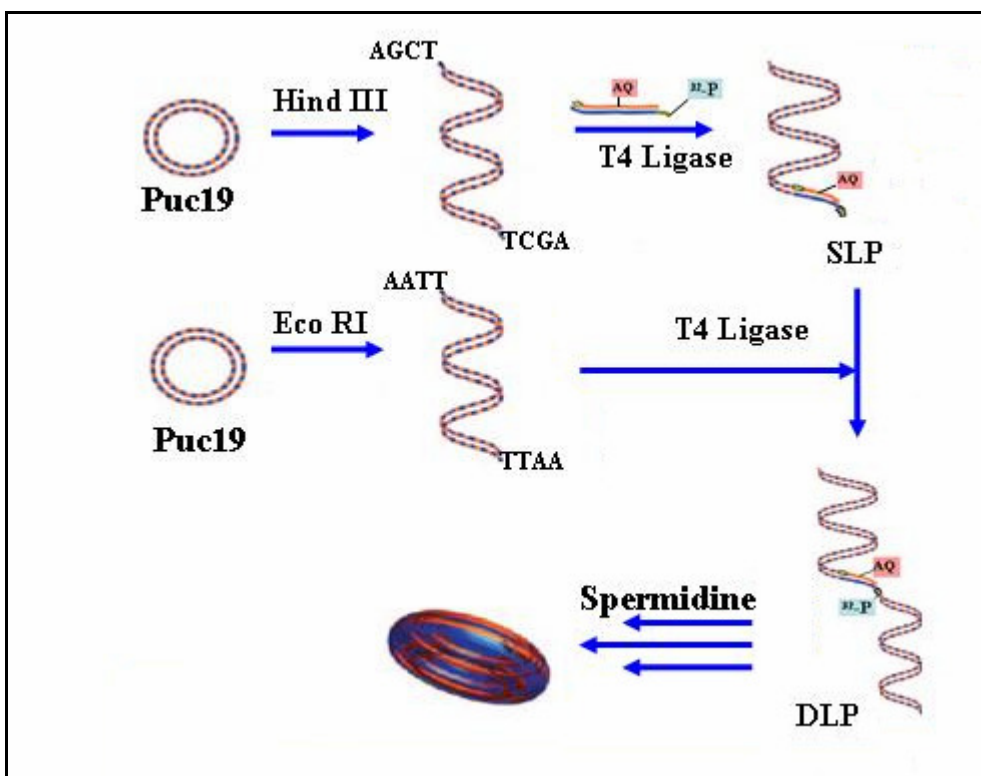


Figure 3.3: Schematic Diagram of Experimental Design

3.4. DNA sequences

The DNA oligomers DNA3 and DNA4 used in this study are listed in Figure 3.4. The sequences are similar to the ones used in the previous work, but with some significant differences. DNA3 is 50 bases long and contains Uridine anthraquinone (UAQ) in the middle of the sequence. There are a total of six GG steps in DNA3, but unlike the previous sequence DNA1, they are now placed on two sides of the UAQ, three on each side. The 5'-end of this strand is radiolabeled with 32 -P ATP, which serves dual purpose. It works as radioactive probe for autoradiography analysis, and also acts as the 5' phosphate end for ligation. The 5'-end of DNA3 has the four base overhangs 5'-AATT-3' compatible for

cohesive end ligation with linear plasmid, which has been cut with EcoRI restriction enzyme. DNA4 is the complementary sequence for DNA3 which is 5'-phosphorylated by chemical phosphorylating reagent (CPR II) for the ligation reaction. It has a 5'-cohesive end containing four base overhangs 5'-AGCT-3' which is compatible with HindIII cut linear plasmid. Upon annealing of DNA3 and DNA4, the DNA oligomer duplex generates a new restriction endonuclease site. This site can be cut with the restriction enzyme PaeR7I. The plasmid Puc19 lacks this restriction site, which leave this site as unique in the whole double ligated system. This site is generated to cut the doubly ligated system into approximately two halves to facilitate the analysis of the DNA damage by gel electrophoresis where loading big pieces of DNA can complicate the experiments.

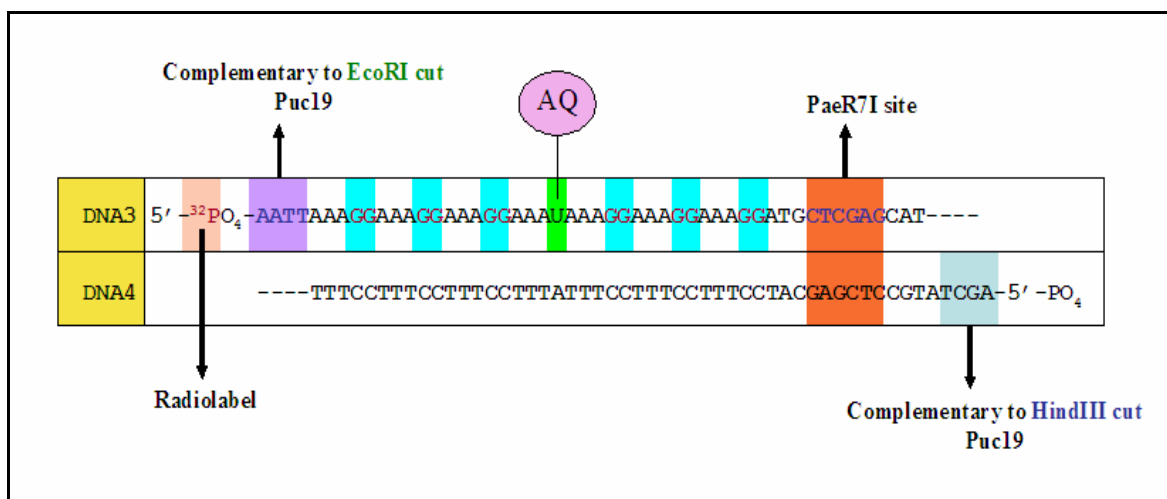


Figure 3.4: Design of Oligomer Sequences DNA3 and DNA4.

3.5 Synthesis of Uridine Anthraquinone (UAQ)

The synthesis of the **UAQ** follows the procedure described by Yamana and co-workers and Broom and coworkers^{20-21, 25}. The N³ position of the pyrimidine ring of Uridine is protected with benzoyl protecting group followed by the coupling of the methyl anthraquinone to the 2' position of the Uridine sugar moiety. The 5'-OH of the sugar is further protected by dimethoxytrityl chloride (DMT-Cl) and then reacted with chlorocynoethyl phosphoramidite to generate the 3' phosphoramidite. As its DMT-protected cyanophosphoramidite, **UAQ** is readily incorporated into oligonucleotides by simple modification of standard automated, solid-phase DNA synthesis methods.

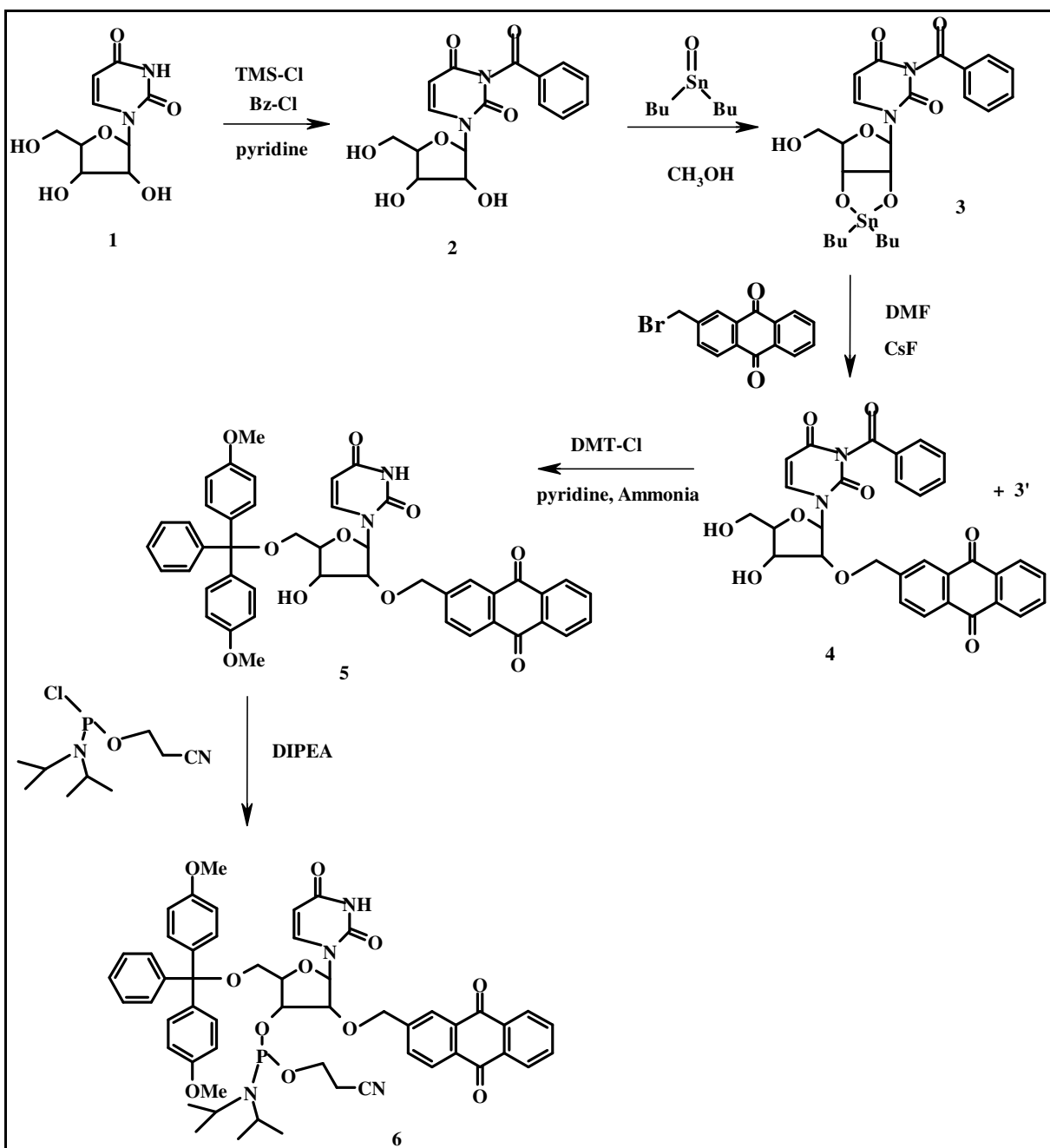


Figure 3.5: Scheme for Synthesis of Uridine Anthraquinone (UAQ)

3.6 Experimental

3.6.1 Materials and methods

All chemicals required for UAQ synthesis were obtained from Sigma-Aldrich and used as received. The pUC19 plasmid, T4 DNA ligase, HindIII, Eco RI, PaeR7 I restriction endonucleases and T4 Polynucleotide Kinase were purchased from New England Biolabs. [γ - 32 P]ATP and non radioactive ATP were purchased from GE Healthcare, formerly Amersham Biosciences. Gel-extraction kits were purchased from Qiagen. Gelase Agarose Gel-Digesting Preparation was obtained from Epicenter Biotechnologies and spermidine hydrochloride was obtained from Aldrich. Phosphorylation of the 5' end of DNA3 was achieved in the DNA synthesizer by using Chemical Phosphorylation Reagent II, obtained from Glen Research (Sterling, VA) along with all other normal nucleoside phosphoramidites. The oligonucleotides were purified by reverse-phase HPLC on a Hitachi (Tokyo) preparative HPLC system by using a Dynamax C18 column. Purified oligomers were desalted with Sep-Pak columns and characterized by mass spectroscopy. UV melting and cooling curves were recorded on a Cary 1E spectrophotometer (Varian) equipped with a multicell block, temperature controller, and sample transport accessory. The extinction coefficients were determined using nearest neighbor method (UAQ replaced with U for calculation purposes) using a biopolymer calculator. The mass of each oligonucleotide was determined by a Micromass Quattro Electrospray Ionization (ESI) mass spectrometer at the mass spectra facility at Georgia Tech. Buffer exchanging spin columns, enzyme removal and other spin columns were obtained from Millipore Corporation (Bedford, MA). Circular Dichroism (CD) measurements were conducted on a Jasco-720 instrument equipped with a

temperature controller. Dynamic light scattering experiments were done using a Dynapro MS_X dynamic light-scattering instrument (Proterion, Piscataway, New Jersey). Transmission Electron Microscopy images were recorded on a JEOL-100 C Transmission Electron Microscope at 100,000 magnification. Autoradiography was performed on a Fuji 2340 BAS-Image system. Kodak films were purchased from Aldrich. Spin columns and centrifugal filters were obtained from Millipore. Carbon coated copper grids for Transmission Electron Microscopy were purchased from Ted Pella Inc., Redding, California.

3.6.2 Uridine Anthraquinone (UAQ) synthesis

*N*³-Benzoyluridine (2)

Uridine (2.44 g, 10.0 mmol) was dissolved in pyridine (40 mL, 500 mmol) at room temperature and chlorotrimethylsilane (6.4 mL, 50.4 mmol) was added and stirred for 20 min. Benzoyl chloride (5.8g, 42 mmol) was added to this solution slowly and stirred for additional 2 h, cooled in an ice bath and then extracted with ethyl acetate (2 x 200 mL). The combined organic fractions were washed with brine and dried over MgSO₄ and purified by column chromatography (silica, CH₂Cl₂/MeOH = 8:1, R_f = 0.25). Yield 3.3 g (95%). ¹H NMR (DMSO-d₆) δ 3.5-3.7 (m, 2H, H_{2'} and H_{3'}), 3.75 (q, 1H, H_{4'}), 4.00-4.12 (m, 2H, H_{5'}), 5.10 (d, 1H, C_{2'}-OH), 5.18 (t, 1H, C_{5'}-OH), 5.50 (d, 1H, C_{3'}-OH), 5.77 (d, 1H, H₁), 5.95 (d, 1H, uracil H₅), 7.63, 7.78 and 7.97 (m, 7H, AQ), 8.18 (d, 1H, uracil H₆).

2', 3'-O-(Dibutylstannylene)-N³-benzoyluridine (3)

A suspension of N³-benzoyluridine (**2**, 2.8 g, 8.1 mmol) and dibutyltin oxide (2.03 g, 8.1 mmol) in methanol were heated to reflux for 30 min, and resulting clear solution was evaporated to dryness and dried *in vacuo* to give the desired crude product (~90% pure). ¹H NMR (DMSO-*d*₆) δ 0.80-1.60 (m, 18H, alkyl chain), 3.45-3.80 (m, 3H, H_{2'}, H_{3'} and H_{4'}), 4.10-4.20 (m, 2H, H_{5'}), 5.10 (t, 1H, C_{5'}-OH), 5.60 (d, 1H, H_{1'}), 5.95 (d, 1H, uracil H₅), 7.50-8.00 (m, 7H, AQ), 8.12 (d, 1H, uracil H₆).

BzU(2'-UAQ) (4)

A solution of **3** (2.8 g, 4.8 mmol) in anhydrous DMF (100 mL) was stirred with bromomethyl anthraquinone (2.7 g, 9.0 mmol) and CsF (1.8g, 11.8 mmol) at room temperature for 48 h and the reaction mixture was extracted with ethyl acetate and organic layer dried over MgSO₄. The solvent was removed *in vacuo* and the compound was purified by silica gel column chromatography using CH₂Cl₂/MeOH (20:1) as the solvent in 50% yield. The desired compound and the 3'-isomer were collected together. ¹H NMR (2'-isomer) (DMSO-*d*₆) δ 3.50-3.80 (m, 2H, H_{2'} and H_{3'}), 4.00, 4.08, 4.15, 4.25 and 4.40 (m, 3H, H_{4'} and H_{5'}), 4.70- 5.00 (m, 2H, CH₂), 5.30 and 5.45 (m, 2H, C_{2'}-OH, C_{3'}-OH and C_{5'}-OH), 5.75-6.00 (m, 2H, uracil H₅ and H_{1'}), 7.50-8.30 (m, 8H, AQ and uracil H₆).

DMT-U(2'-AQ) (5)

4 and the 3'-isomer (1.04 g, 1.8 mmol) and DMT-Cl (0.74g, 2.2 mmol) were dissolved in 20 mL dry pyridine and mixed with 5 mL concentrated ammonia solution and

allowed to stir for 16 h at room temperature. The mixture was concentrated to dryness and applied to silica column. Elution with CH₂Cl₂/MeOH (20:1) gave the desired DMT-U(2'-AQ) in 45% yield (overall 90%, 2' + 3'). ¹H NMR (DMSO-*d*₆) δ 3.30 (m, 2 H, H_{5'}), 3.72 (s, 6 H, CH₃O of DMT), 4.10(m, 2 H, H_{2'} and H_{3'}) 4.28 (ddd, 1 H, H_{3'}), 4.92 (dd, 2 H, ArCH₂), 5.24 (d, 1 H, uracil H₅), 5.47 (d, 1 H, 3-OH), 5.95 (d, 1 H, H₁), 6.87 and 7.27 (m, 13 H, DMT), 7.68 (d, 1 H, uracil H₆), 7.90 and 8.20 (m, 7H, AQ), 12.40 (s, 1 H, amide).

UAQ Phosphoramidite (6)

DMT-U(2'-AQ) (**5**, 234 mg, 0.27 mmol) was dissolved in dry CH₂Cl₂, followed by addition of DIPEA (0.24 mL, 1.37 mmol) and 2-cyanoethylchlorophosphoramidite (0.12 mL, 0.60 mmol) and the reaction mixture was stirred for 30 min and applied directly to silica column. Elution with CH₂Cl₂/EtOAc/Et₃N (48:48:4) gave the desired product as pale yellow oil, which was used directly in the DNA synthesis. ¹H NMR (DMSO-*d*₆) δ 2.4 (m, 12H, methyl of phosphoramidite), 3.2 (m, 4H, 2 x CH₂ of phosphoramidite), 3.30 (m, 2 H, H_{5'}), 3.72 (s, 6 H, CH₃O of DMT), 4.10(m, 3 H, H_{2'}, H_{3'}, CH of isopropyl) 4.3 (m, 1 H, H_{3'}), 4.95 (dd, 2 H, ArCH₂), 5.24 (d, 1 H, uracil H₅), 5.90 (d, 1 H, H₁), 6.92 and 7.32 (m, 13 H, DMT), 7.68 (d, 1 H, uracil H₆), 7.90 and 8.20 (m, 7H, AQ), 12.40 (s, 1 H, amide).

3.6.3 Synthesis of DNA single strands

The DNA oligomers DNA3 and DNA4 were synthesized with standard phosphoramidite chemistry on an ABI expedite DNA synthesizer, using UAQ phosphoramidite and other normal nucleotides with dimethoxy trityl (DMT) and

phosphoramidite protecting groups on the 5' and 3'OH'S of the sugar, respectively. To phosphorylate the 5'end of DNA4, Chemical Phosphorylating Reagent II ([3-(4,4'-Dimethoxytrityloxy)-2,2-dicarboxyethyl]propyl-(2-cyanoethyl)-N,N-diisopropylphosphoramidite) was used. Treatment with 1 M ammonium hydroxide at room temperature for 45 minits, results in the cleavage of the oligomer sequences from the CPG solid support and then incubation of the DNA samples in the same ammonium hydroxide solution at 60⁰C for 18 hours remove the oligomer protecting groups. The samples were dried *in vacuo* and purified by reverse phase HPLC using appropriate ratio of water, Acetonitrile and Triethylammonium acetate buffer. Following isolation of the purified oligomers from the HPLC, the salts in solution were removed by passing the sample through a sep-pak desalting cartridge. The concentration of the DNA oligomers was measured from Absorbance and extinction coefficient values. Approximately 10 µL of the individual samples (concentration >100 µM) were submitted for Electron Spray Ionization Mass Spectra analysis to determine the oligomer purity.

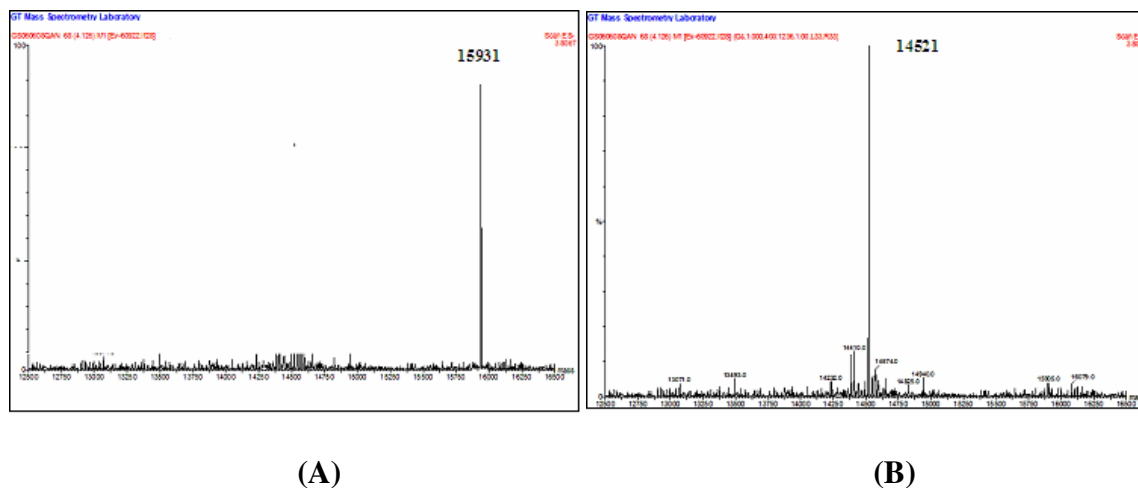


Figure 3.6.A: Mass Spectra of DNA3. **B:** Mass Spectra of DNA.

3.6.4 Characterization of DNA duplex

Thermal Denaturation

The thermal stability of the DNA duplexes DNA3-DNA4 was determined by monitoring the change in absorbance at 260 nm. The DNA samples were prepared by mixing 25 μL of 100 μM of the individual strands and 100 μL of 100 mM sodium Phosphate buffer (pH=7.0) in a total volume of 1000 μL in water to make a 2.5 μM overall concentration of the individual strands in 10 mM sodium phosphate buffer. The measurements were carried out in UV transparent quartz cuvettes with 1 cm pathlength inside a Cary 1E Spectrophotometer. The samples were heated to 90⁰C and then cooled to 20⁰C at a rate of 1⁰C/min, followed by the subsequent heating back to 90⁰C at the same rate. This cycle was repeated four times for each experiment to ensure consistent results.

Circular Dichroism

The secondary structure of DNA duplex DNA3-DNA4 was confirmed by circular Dichroism (CD) experiment at room temperature. The exact samples used for the thermal denaturation experiments previously described were used for the CD experiment, therefore had the same DNA and salt concentration.

3.6.5 Preparation of Radiolabeled DNA

The DNA3 oligomer (Fig. 3.4) was radiolabeled with [γ -³²P] ATP and T4-Polynucleotide Kinase enzyme (PNK). 5 μL of 100 μM solution of DNA3 was made to react with 2 μL of freshly purchased [γ -³²P] ATP in presence of 5 μL of PNK enzyme at 1x PNK buffer concentration for 1 hour at 37⁰C in a total volume of 20 μL . The reaction

mixture was diluted to 50 μ L with water and passed through ProbeQuant G-50 Micro Column (GE healthcare). The column was placed in a 1.5 mL screw cap microcentrifuge tube and spun at 735 x g centrifuge speed for 2 minits. The purified samples, free of unreacted [γ -32P] ATP, enzyme and buffer salts were collected at the bottom of the support tube. The samples thus collected were precipitated by addition of cold ethanol, vortexed, placed at -78⁰C, and then centrifuged. The supernatant was discarded and the DNA sample was washed twice with 80% ethanol and air-dried. The air dried DNA pellets were redissolved in appropriate amount of water to obtain the desired concentration of the DNA.

3.6.6 Restriction Endonuclease Cutting of Plasmid

2 μ g of Puc19 plasmid was treated with 5 μ L HindIII restriction endonuclease in a microcentrifuge tube with a total volume of 50 μ L containing 1 X HindIII buffer and incubated overnight at 37°C. This same procedure was carried out for restriction cutting of Puc19 with EcoRI enzyme. Analytical, non-denaturing, low-melting agarose gels were run in all cases to identify and compare the products from uncut supercoiled and relaxed form of the plasmid. The restriction digests were passed through Micropure-EZ centrifugal filter devices to eliminate the restriction enzyme. The restriction buffer was replaced with nanopure water with buffer exchange spin columns. The linearized Plasmid samples were further precipitated with ethanol and washed with 80% ethanol and checked for plasmid concentration by UV-Vis spectroscopy.

3.6.7 Ligation of Plasmids with Radiolabeled Oligonucleotides

Single Ligation

Equimolar concentrations (3 μM) of radiolabeled DNA3 obtained as described above and complementary sequence DNA4 were mixed in 10 mM sodium phosphate buffer at pH 7.0 and annealed by heating the resulting solution for 10 min at 90°C and then cooling very slowly to room temperature. The oligomer was ligated to the HindIII linearized pUC19 plasmid (10:1 molar ratio) with T4 DNA ligase, 10 mM ATP in 1x T4 ligase buffer at 16°C overnight in a Neslab RTE-7 incubator (Newington, NH). The success of ligation reaction was tested by autoradiography on an analytical, nondenaturing low-melting agarose gel by following standard procedures.

The DNA in the reaction mixture was ethanol washed and mixed with non denaturing dye containing bromophenol blue and xylene cyanol in water and glycerol (4:1). The ligated plasmid DNA band was isolated from a nondenaturing 1% preparative agarose gel in 1X TAE buffer (Tris-acetate- EDTA) containing ethidium bromide for visualization. The gel pieces were collected in centrifuge tubes and heated at 65°C for 10 min followed by addition of 1 μL of 50x reaction buffer of Gelase Agarose Gel-Digesting enzyme, per 50 μL of molten agarose. The solutions were incubated overnight after addition of one unit of Gelase enzyme per 200 mg of molten agarose at 37°C. The Gelase digestion were ethanol washed and then passed through Qiagen Nucleotide removal spin columns for further elimination of last traces of agarose.

Double Ligation

The gel extracted purified single ligated plasmid (SLP) were further subjected to second phase of ligation after measuring the concentration of the SLP with the help of Absorbance measurement. Here, the convention OD = 1.0 means 50 µg/mL of DNA was followed. The ligation was achieved by the addition of equimolar (2.5 µM) ratio of SLP and linearized puc19 plasmid, cut with Eco RI restriction enzyme, in presence of 100 units of T4 DNA Ligase enzyme and 10 mM ATP in 1x T4-Ligase buffer at 16°C. Preparative agarose gel electrophoresis and gel extraction procedures as mentioned in previous chapter were performed to get purified double ligated plasmid (DLP). Autoradiography of agarose gel was done by placing the gel between blotting paper and cellophane and drying the gel *in vacuo* in a gel drying apparatus, followed by exposure of the gel to Kodak film in cascade at -78°C for 10 hours. The films were developed by using developer and fixer solutions and washed with water and air dried.

3.6.8 Dynamic light scattering study

Spermidine solutions were prepared at different concentrations from 50-600 µM at intervals of 50µM. A solution of doubly ligated plasmid containing the sandwiched oligomer duplex-DNA3-DNA4 (25 µg/mL) was added to an equal volume of spermidine solutions separately to different concentration. All experiments were performed in 10mM sodium phosphate buffer (pH 7.2). All solutions were filtered through Amicon UltraFree MC centrifugal filters (diameter, 0.22 µm; Millipore) to make them dust free, before introducing them into light scattering instrument. After 5 min of gentle agitation of the

DNA and spermidine solution mixture, the samples were analyzed by dynamic light scattering using a Dynapro MS_X dynamic light-scattering instrument (Proterion, Piscataway, NJ). Decondensation experiments were performed by addition of 2M NaCl to the solutions containing the DNA and spermidine at appropriate concentrations.

3.6.9 Transmission Electron Microscope study

Condensates were prepared by mixing 7.5 μ L of doubly ligated DNA sample (25 μ g/mL) in sodium phosphate buffer and equal volume of 200 μ M spermidine. After gentle flickering for 5 minits, 10 μ L of the condensate sample was deposited on a carbon-coated copper grid (Ted Pella, Redding, CA) and allowed to settle for 10 min. The grids were stained by the direct addition of 5 μ L of 2% uranyl acetate, rinsed in 95% ethanol and air-dried. Images of the DNA condensates at room temperature were collected on film using a JEOL-100C Transmission Electron Microscope at 100 000 X magnification.

3.6.10 UV Irradiation

DNA solutions of the radiolabeled oligomer duplex, SLP and DLP were irradiated in microcentrifuge tubes (20 μ L, 10 mM sodium phosphate buffer) containing varying concentrations of spermidine at $\approx 30^0$ C in a Rayonet Photoreactor (Southern New England Ultraviolet, Barnsford, CT) equipped with 16 x 350 nm lamps. After irradiation, samples were precipitated with ethanol and washed twice with 80% ethanol, and air dried.

3.6.11 Restriction Endonuclease cutting of Double Ligated plasmid

The irradiated and ethanol washed double ligated plasmids were further treated with PaeR7I restriction endonuclease, which cut the ligated system at only one position (see Figure 3.4). The air dried irradiated DNA samples were dissolved in nanopure water and 5 μ L of PaeR7I was added along with the enzyme buffer to make a total volume of 50 μ L. The sample was incubated at 37⁰C for 6 hours and cold ethanol and 2 μ L glycogen was added to precipitate the DNA. After storing the sample for 1 hour at -78⁰C, the sample was centrifuged for 1 hour and the supernatant discarded. The precipitated DNA were washed twice with 80% ethanol and dried *in vacuo*.

3.6.12 Piperidine treatment and PAGE analysis

100 μ L of 1M piperidine were added to each of the air dried DNA samples and heated at 90⁰C for 30 minutes. The piperidine was evaporated *in vacuo* and 20 μ L of water added to each of the sample centrifuge tubes. The water was evaporated again to ensure complete removal of piperidine.

The DNA samples were suspended in denaturing loading dye (bromophenol blue, zylene cyanol in formamide water mixture). The radioactive counts are adjusted by diluting the samples by addition of appropriate amount of the denaturing loading dye so that the final radioactive counts in each of the samples were ~ 1000 cpm per μ L. The samples were then loaded on the wells of a polyacrylamide gel, with 5000 cpm (5 μ L solution) per lane. After completion of electrophoresis at 70 watts for 2.5 hours, the gels was separated from the glass plates and sandwiched between blotting paper and cellophane

and dried *in vacuo* at 80⁰C for 3 hours on a gel drier. The dried gel was then placed in closed casket and exposed to a Kodak film for 18 hours. Development of the Kodak film with developer and fixer solution give the autoradiograph of the PAGE gel.

The same PAGE gel was further dried at room temperature in the gel drier for 2 hours and kept in FUJI caskets for 6 hours and then removed. To quantify the relative amount of DNA damage at each GG step, the gels was “counted” on a FUJI 2340 BAS-Image system as described in the previous chapter.

3.7 Results

3.7.1 Design, Synthesis and Characterization of UAQ-DNA and its Complementary Sequence.

In previous work on single ligated plasmids with oligonucleotides, the photochemical hole-injector anthraquinone was attached covalently to the 5'-terminus of a linearized plasmid-oligomer construct. The anthraquinone group in such a construct was in an “end-capped” fashion in the DNA duplex. In the present study, the AQ is attached at a central position of the DNA duplex in the form of UAQ, and is thus intercalated inside the DNA.

The oligomer duplex DNA3-DNA4 contains two cohesive ends. The complementary sequence DNA4 contains a 5'-AGCT-3' overhang, which is complementary to the HindIII cut restriction ends of Puc 19. The 3'-end of DNA3 is the recessed cohesive end by four bases, consistent with the HindIII cut plasmid. Ligation of duplex oligomer DNA3-DNA4 with the HindIII enzyme cut Puc19 forms the single ligated

oligomer-plasmid (SLP). The 5'-end of DNA3, which is the GG containing strand, ends with a 5'-AATT-3' base overhang that is compatible with the EcoRI restriction cut ends of Puc19. This 5'-end also contains the ^{32}P radiolabeled phosphate for autoradiography and also serves as the phosphate group required for ligation. Ligation of SLP with EcoRI cut plasmid Puc19 forms the double ligated oligomer-plasmid (DLP). The HindIII compatible end of DNA3-DNA4 also contains an adjacent restriction site 5'-CTCGAG-3'/ 3'-GAGCTC-5', for PaeR7 I restriction endonuclease. This restriction site is absent in Puc19, and allowed selective cutting of the SLP and DLP oligomers for analytical purposes.

3.7.2 Thermal integrity and structural confirmation of DNA oligomer duplex

The thermal stability of the DNA duplex DNA3-DNA4 was determined by monitoring the change in absorbance at 260 nm due to the hyperchromicity of the DNA duplexes. As dsDNA is thermally denatured, i.e. melted into two separate single strands, the intensity of the absorbance at 260 nm is increased. This is due to the increase in rotational freedom of the nucleotides as the transition from dsDNA to ssDNA occurs allowing the ssDNA to adopt more energy levels and absorb more of the UV light. Plotting this change in absorbance with time gives a curve with a change in inflection point, and plotting the first derivative of the curve gives the temperature at which the concentrations of ssDNA and dsDNA are equivalent. The melting temperature for DNA which contains intercalators are generally higher than the normal DNA duplexes. As expected for the AQ containing strand, DNA3-DNA4 melts at ca. 71 $^{\circ}\text{C}$, which is about 2 $^{\circ}\text{C}$ higher than the non-AQ containing strand ($T_m = 69^{\circ}\text{C}$), where the AQ has been replaced by a simple thymine.

The melting temperature of blunt ended DNA3-DNA4 ($T_m = 73^\circ\text{C}$) is only 2 degrees higher than the cohesive end DNA3-DNA4 ($T_m = 71^\circ\text{C}$), showing that presence of cohesive ends does not decrease the stability of the DNA duplex significantly.

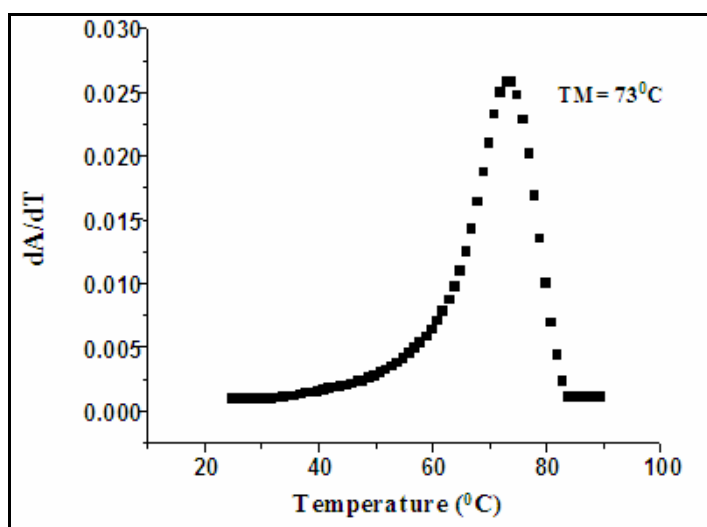


Figure 3.7: Thermal Denaturation Curve for DNA3-DNA4 in 10 mM Sodium Phosphate Solution.

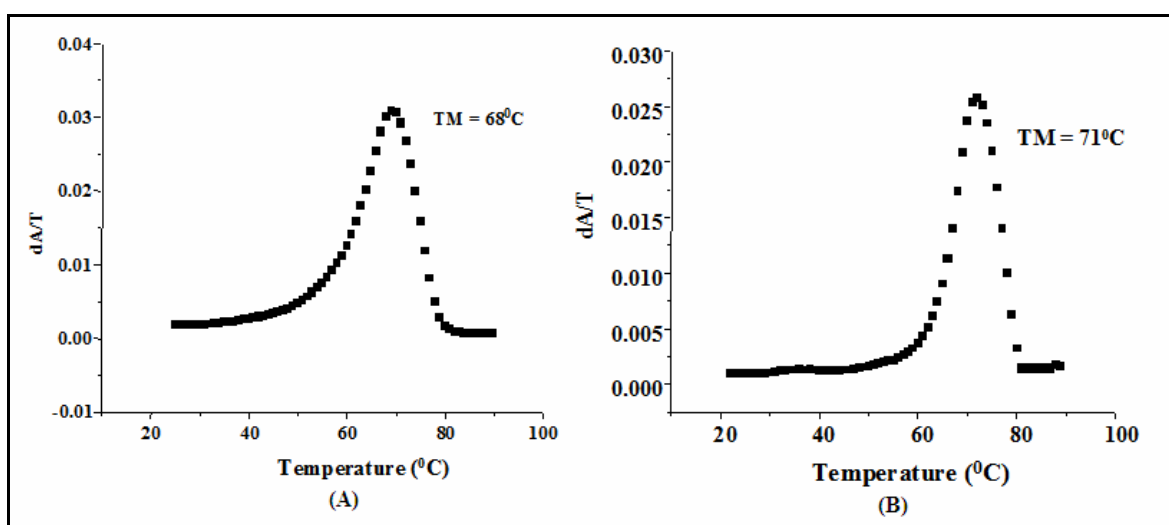


Figure 3.8. A: Thermal Denaturation Curve for Non-AQ Containing DNA3-DNA4
B: Thermal Denaturation Curve for Blunt Ended DNA3-DNA4

Circular Dichroism spectra revealed the secondary structure of DNA3-DNA4, which was essentially B-form DNA. The characteristic positive peak at ~275 nm and negative peak at ~245 nm²⁶ were obtained from the CD spectra, which show formation of stable B-form duplex structure of the oligomer DNA3-DNA4.

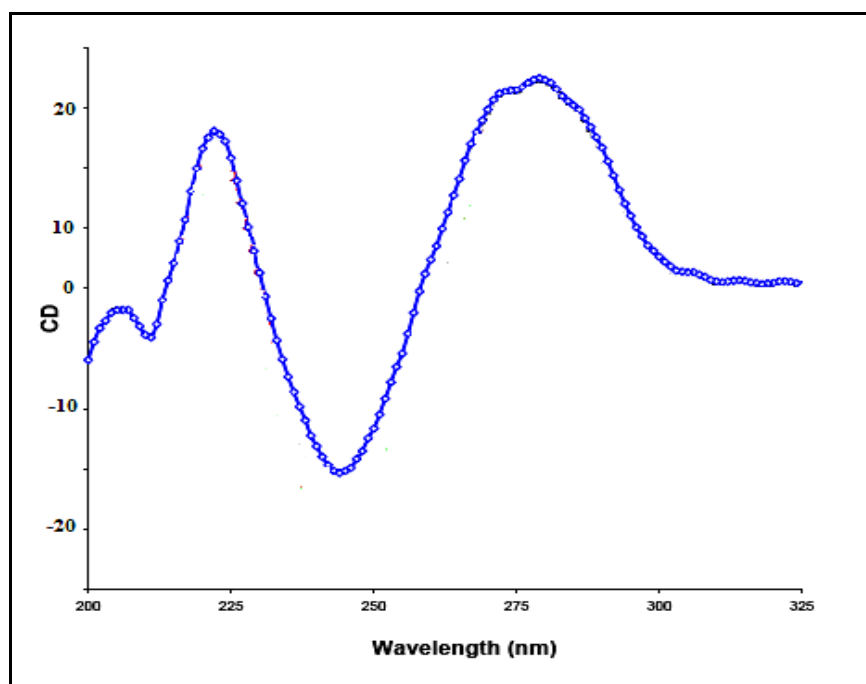


Figure 3.9: Circular Dichroism Spectra of DNA3-DNA4

3.7.3 Ligation of plasmid DNA with oligomer duplex

The reaction of the HindIII cut linearized plasmid with the oligomer duplex DNA3-DNA4 (10 times excess) in presence of T4 DNA ligase linked the duplex oligomer to the plasmid to form the singly ligated linearized plasmid (SLP). Preparative agarose gels were used to separate the unligated and self ligated DNA3-DNA4 from the plasmid band, which contains single ligated plasmid (SLP) and HindIII cut unligated plasmid. The yield of the

ligation reaction was approximately 50% as estimated from the intensity of bands. The gel excised bands were purified by performing standard extraction procedures and made ready for the second phase of ligation. The second ligation was done following similar protocols except that now SLP was used with Eco RI cut Puc19 in equimolar ratio. A nondenaturing agarose gel showed ca. 50% formation of DLP, making the overall yield of DLP approximately 25%. The plasmid bands were separable and they were gel extracted and purified for further analysis. Formations of multiple products in SLP as well as DLP are common. Since the oligomer duplex was used in excess, and the linearized puc19 have two cohesive HindIII compatible ends, the oligomer can be ligated once or twice to the plasmid. The unligated plasmid, the two ligated species (collectively named as SLP) travels in the gel with the same mobility and are inseparable. In the next stage of ligation, the major product formed was the oligomer duplex DNA3-DNA4 sandwiched between HindIII and EcoRI cut linearized puc19. Comparison with 1Kb DNA ladder showed formation of double ligation products. The presence of these self-ligated, non-radiolabeled plasmids does not complicate the analysis because they do not appear in PAGE analysis owing to lack of radioactivity. Similarly, the presence of multiple ligation products containing radiolabeled oligomer duplexes is acceptable, since they will be cut again with restriction enzymes after irradiation.

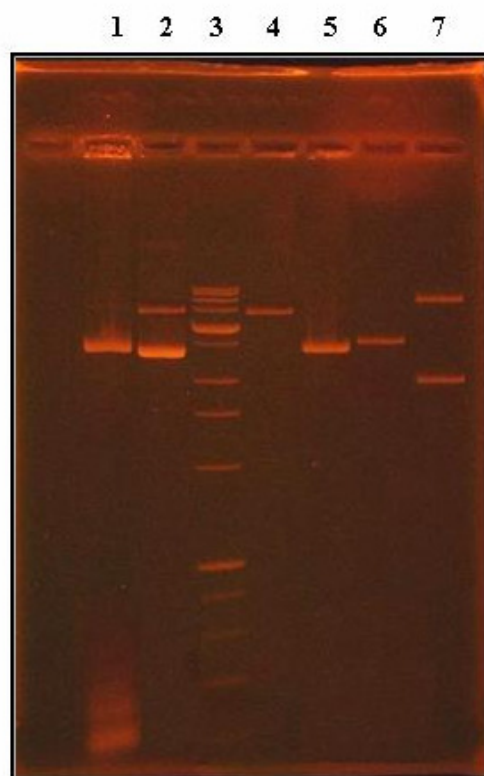


Figure 3.10: Non-Denaturing Low Melting Agarose Gel Showing Mobility of DNA3-DNA4, SLP and DLP

Lane 1: Reaction mixture of ligation of DNA3-DNA4 with HindIII cut plasmid. Lane 2: Reaction mixture of ligation of Gel-extracted SLP and Eco RI cut linearized Puc19. Lane 3: 1 Kb DNA ladder; Lane 4: gel extracted DLP; Lane 5: gel extracted SLP. Lane 6: Puc 19 control, cut with HindIII restriction endonuclease; Lane 7: Circular Puc19 in supercoiled and relaxed form.

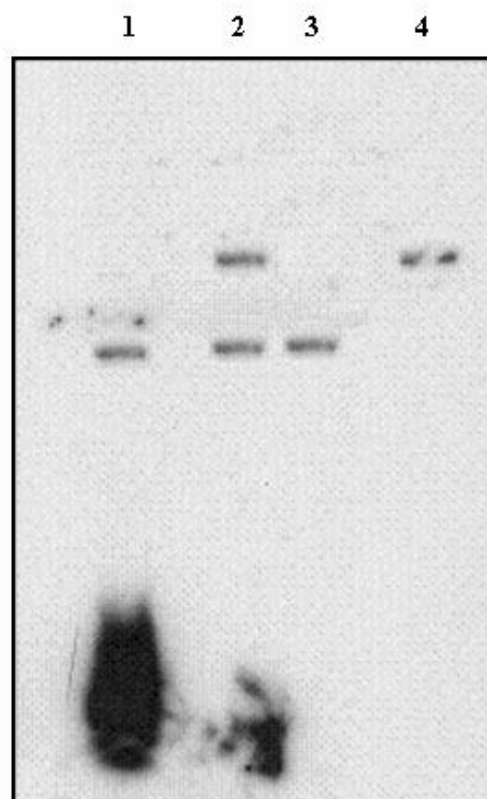


Figure 3.11: Autoradiography of Agarose Gel Showing DNA3-DNA4, SLP and DLP
 Lane 1: DNA3-DNA4 + HindIII cut plasmid + T4 ligase (SLP); Lane 2: SLP + ECORI cut plasmid + T4 ligase; Lane 3: purified SLP; Lane 4: purified DLP.

3.7.4 DNA condensates from SLP and DLP with spermidine

Dynamic light scattering experiments were conducted to assess the effect of spermidine on SLP and DLP. Solutions of purified SLP and DLP oligomers were prepared along with various concentrations of spermidine. The hydrodynamic radii of the condensates were measured by light scattering. In absence of spermidine, SLP and DLP do not form condensates. With the addition of spermidine, the light scattering intensity increased indicating that particles are being formed and that the hydrodynamic radii increased with the spermidine concentration (Figure 3.12). The intensity of scattered light

was low and particle radii range was 40-50 nm at spermidine concentrations between 25 μM and 50 μM . With further increase in spermidine concentration to the range of 75 μM and 125 μM the light scattering intensity values increased and then reached a plateau, which represents formation of stable condensate particles. At higher spermidine concentration (>150 μM), the light scattering experiment indicated the formation of aggregates. The formation of condensates was reversed by the addition of NaCl (2M) as indicated by the increase in noise and lack of consistent autocorrelation curve at that high concentration of NaCl.

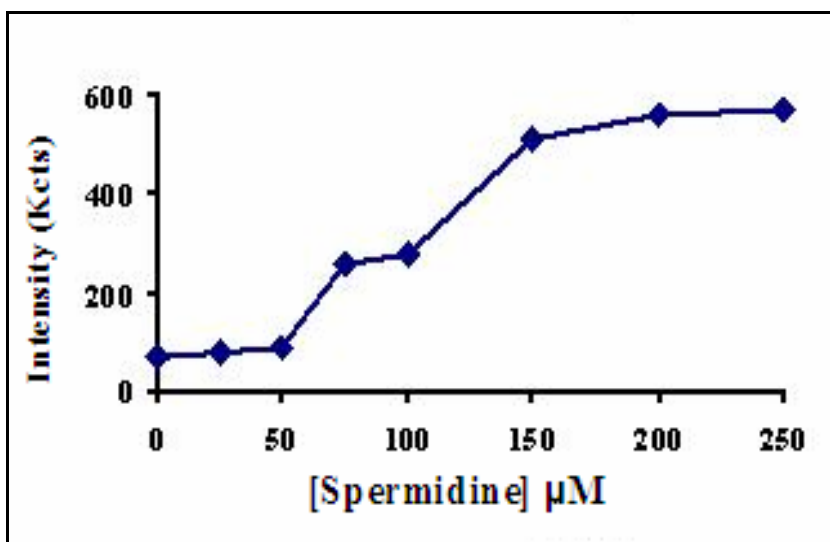


Figure 3.12: Plot of Intensity of Scattered Light vs. Concentrations of Spermidine.

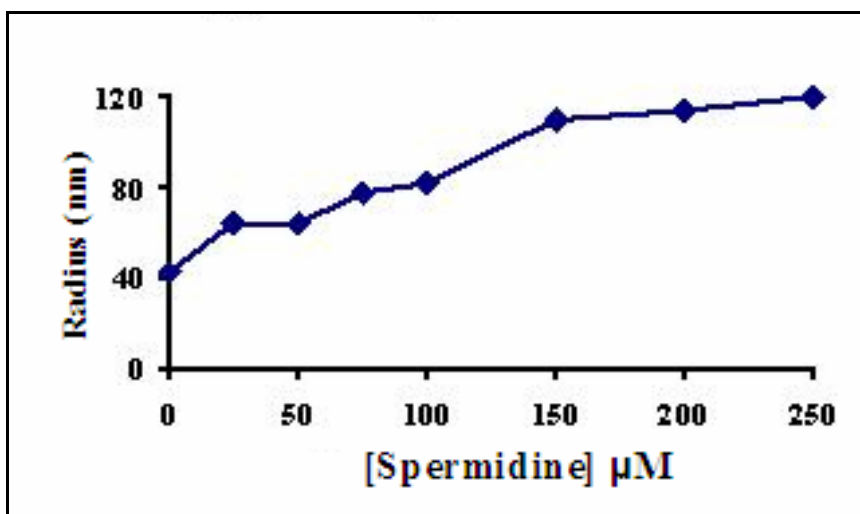


Figure 3.13: Plot of Average Hydrodynamic Radii vs. Spermidine Concentration.

The stability of the condensates was determined by Dynamic Light Scattering by taking data readings over a period of 4 hours of time. Since some of the SLP and DLP samples were irradiated for 4 hours, it was reasonable to check the stability of the condensates over this period of time. Light Scattering data (Figure 3.14) showed that there was no significant increase in light scattering intensity over this time, suggesting that the condensates were stable and not being converted to aggregates. Also the hydrodynamic radii over this period of time remained consistent, confirming the stability of the condensates (Figure 3.15).

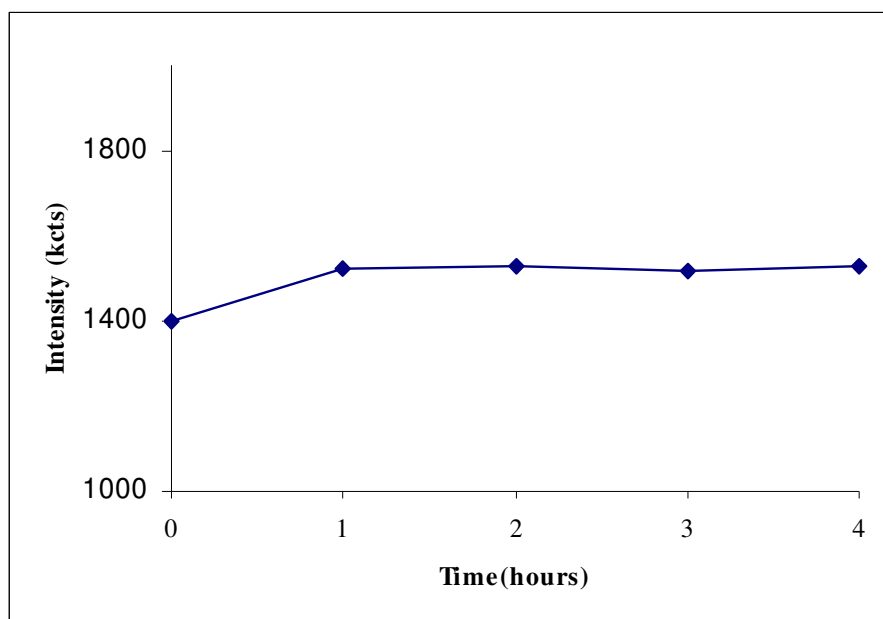


Figure 3.14: Plot of Intensity of Scattered Light vs. Time

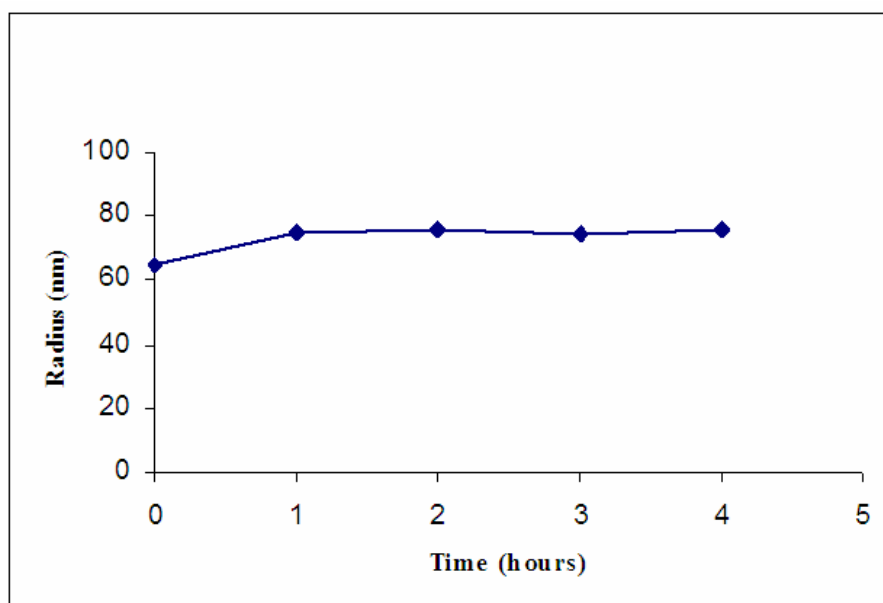


Figure 3.15: Plot of Average Hydrodynamic Radii vs. Time

The structure of condensates was confirmed by Transmission Electron Microscopy, which showed presence of stable toroid like condensates at spermidine concentration around 100 μ M.



Figure 3.16: Transmission Electron Microscopic Image of DNA Condensate Formed from DLP.

3.7.5 Photochemistry of UAQ-DNA3-DNA4, SLP and DLP with spermidine

It is known that UAQ intercalates in duplex DNA and upon UV irradiation injects a radical cation, which is responsible for long range DNA damage. The DNA damage is revealed typically as strand cleavages at remote GG sites²⁷. Figure 3.17 shows the autoradiogram from the PAGE analysis following addition of spermidine and irradiation of the DNA3-DNA4, SLP and DLP at $\sim 30^{\circ}\text{C}$ and pH=7. The DLP was treated with restriction endonuclease PaeR7I before treatment with piperidine, to cut out the oligomer portion from the plasmid-oligomer-plasmid DLP system, making it suitable for PAGE analysis.

The autoradiogram of the PAGE gel shown in Figure 3.17 represents the GG damage pattern where lane 1, 2 and 3 represent the DNA damage pattern of DNA3-DNA4 in presence of 100 μ M of spermidine. Lane 1 is the dark controlled, lane 2 and 3 are irradiated for 22 and 45 minutes respectively. Lane 4, 5 and 6 shows the damage pattern for DNA3-DNA4, in absence of spermidine and irradiated for 0 (dark controlled), 22 and 45 minutes respectively. Lane 7 and 9 shows damage pattern of SLP for 2 and 4 hours of irradiation and lane 8 and 10 represent SLP mixed with 100 μ M of spermidine for 2 and 4 hours of irradiation respectively. Lane 11 represents dark controlled lane for double ligated plasmid (DLP). Lane 12 is DLP, irradiated for 2h and lane 13 is the DLP mixed with 100 μ M spermidine, 2h irradiation. Lane 14 and lane 15 are the DLP and DLP mixed with 100 μ M spermidine and both of them irradiated for 4 hours. The strand cleavage pattern shows that in presence of spermidine, there is an increased distance dependence of GG damage, in the 5'-end of SLP, that is, GG damage decrease sharply with distance from the UAQ towards the 5'-end. This result is consistent with earlier findings as reported in the previous chapter. A close look at the GG damage pattern of the DLP reveals that the GG steps, which are at the 5'-end, are all damaged approximately to the same extent, unlike the case as in SLP. In this respect, the DLP behaves more like the oligomer duplex DNA3-DNA4 than the SLP, which is surprising.

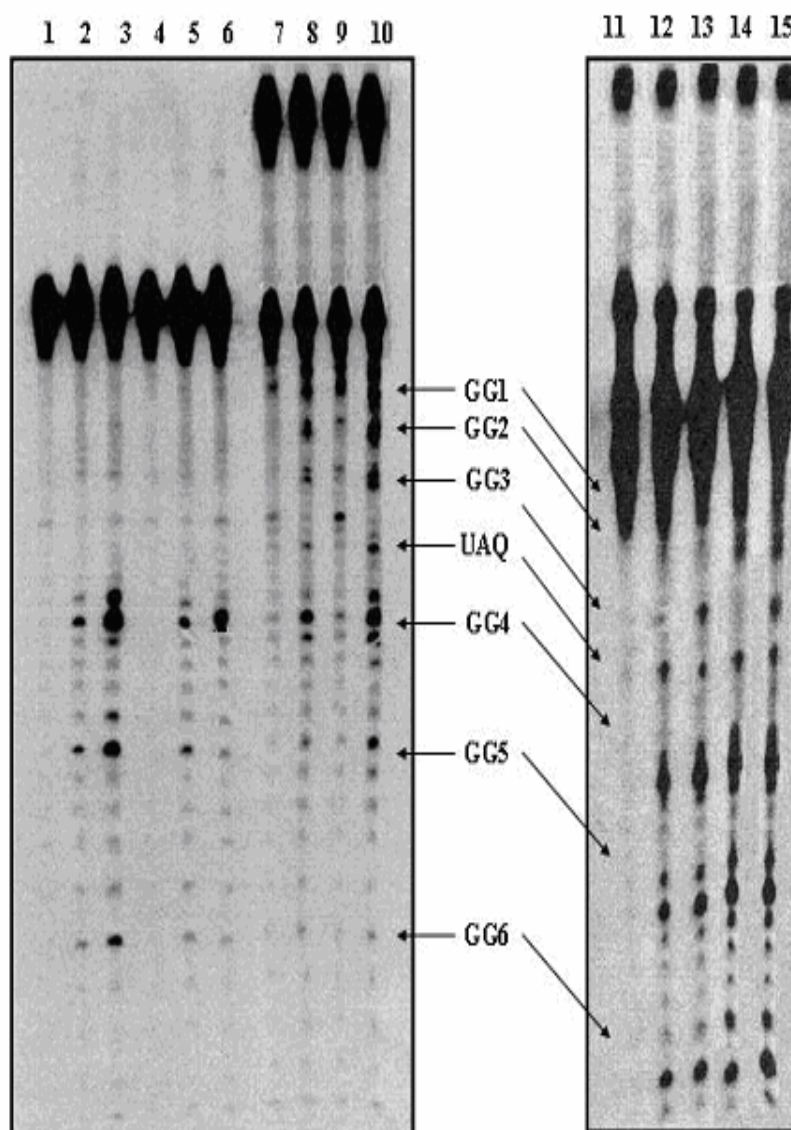


Figure 3.17: Autoradiogram Showing Strand Cleavage of DNA3-DNA4, SLP and DLP in Presence of Spermidine

Lane 1-3: DNA3-DNA4 + 100 μ M spermidine, 0, 22 & 45 min irradiation; Lane 4-6: DNA3-DNA4, 0, 22, 45 min irradiation; Lane 7-8: SLP, 2 & 4 h irradiation; Lane 9-10: SLP + 100 μ M spermidine, 2 & 4 h irradiation; Lane 11-12: DLP, 0 & 2h irradiation; Lane 13: DLP + 100 μ M spermidine, 2h irradiation; Lane 14: DLP, 4h irradiation, Lane 15: DLP + 100 μ M spermidine, 4h irradiation.

In order to find whether spermidine has any effect in the DNA damage pattern of DNA3-DNA4 oligomer duplex, we irradiated the DNA3-DNA4 in presence of different concentration of spermidine (25, 100 and 250 μ M) for 0, 22 and 45 minutes. The PAGE analysis of the DNA samples is shown in Figure 3.18. The damages in the GG steps were similar in presence and absence of spermidine. We found that the DNA duplex was unresponsive to spermidine, indicating that spermidine has no influence on the radical cation transfer in oligomer duplex and whatever changes in damage pattern we observed in ligated plasmid in condensed form was due to the condensate formation. However, a close look at the gel picture reveals one important difference. With increase in spermidine concentration, the UAQ site damage decreased and at spermidine concentration of 250 μ M, it was nearly invisible.

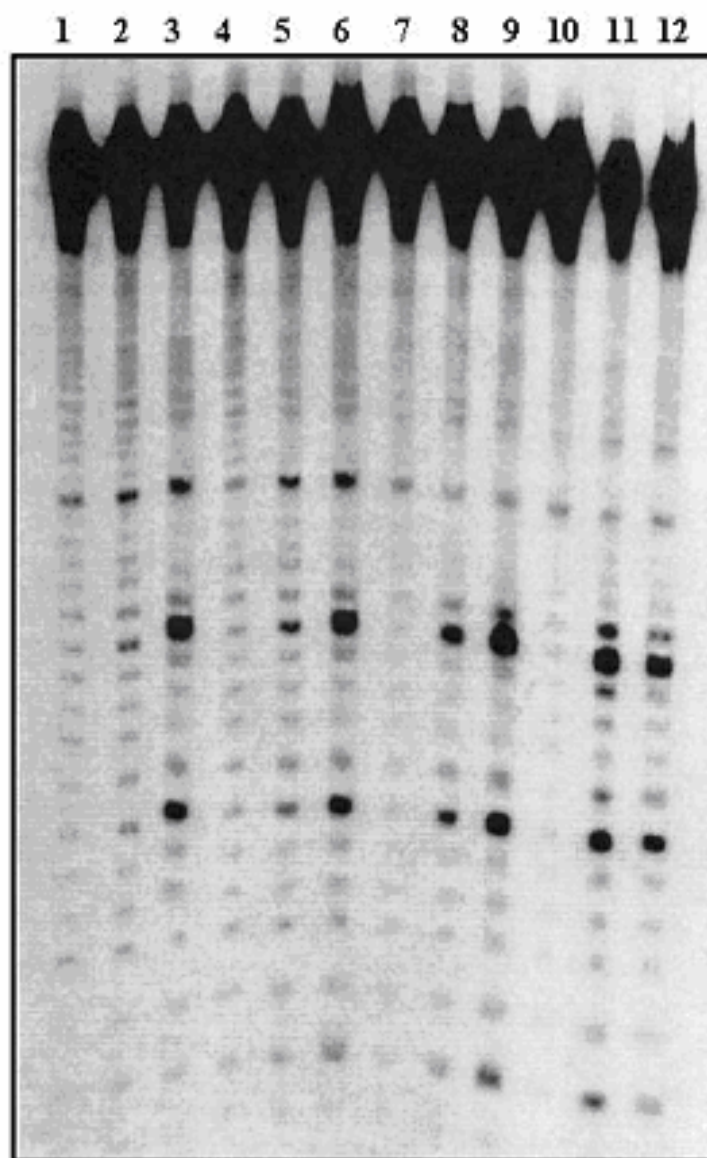


Figure 3.18: Autoradiogram Showing Results of Irradiation of DNA3-DNA4 with Different Concentrations of Spermidine.

Lane 1, 2, 3: DNA3-DNA4, no spermidine, 0, 22, 45 min irradiation. Lane 4, 5, 6: DNA3-DNA4 + 25 uM spermidine, 0, 22, 45 min irradiation. Lane 7, 8, 9: DNA3-DNA4 + 100 uM spermidine, 0, 22, 45 min irradiation. Lane 10, 11, 12: DNA3-DNA4 + 250 uM spermidine, 0, 22, 45 min irradiation.

3.7.6 Phosphoimagery

Results of quantification of the GG damages for the DNA3-DNA4, SLP and DLP are shown in Figure 3.19. The damages at the individual GG steps of the SLP are comparable to earlier results (chapter 2). The distance dependence of the GG damages in SLP was prominent and radical cation migration is significantly less efficient than the oligomer duplex. But the GG damages for the 5' side of the UAQ of the DLP are comparable to that of the oligomer duplex. In this aspect, the DLP behaves more like the oligomer by allowing the charge to migrate through the sequence efficiently. There is slight difference in the charge transfer efficiency between the oligomer duplex and the DLP in the 3' side of the UAQ. Here the radical migrates more efficiently to the 3' end of the UAQ in case of the oligomer duplex than the DLP.

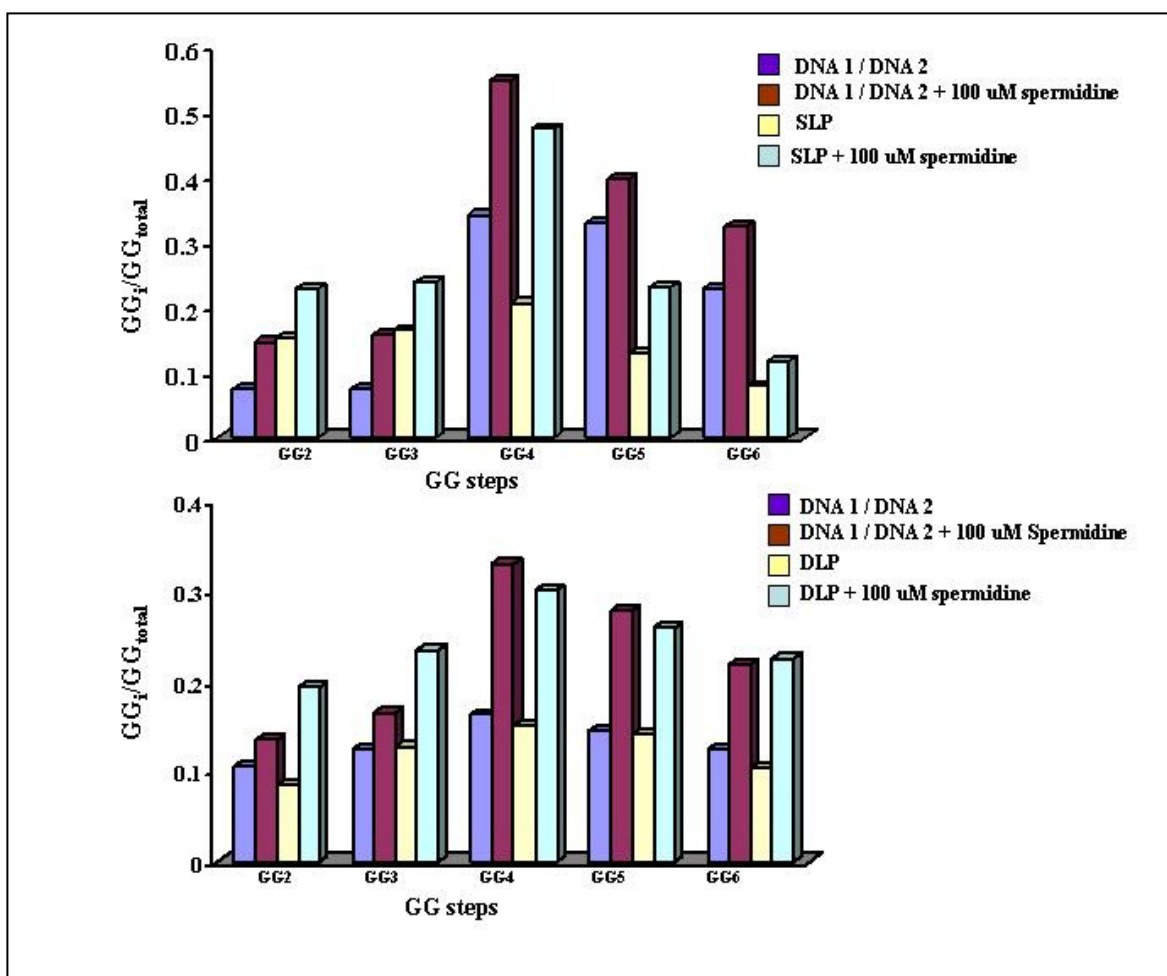


Figure 3.19: Fuji Phosphoimager Experiment Histogram Showing the Relative Damage at the GG steps of DNA3-DNA4, SLP and DLP

3.8 Discussion

Earlier reports about the role of polycations like spermine and spermidine in inhibiting DNA damage have successfully established two facts. It has been shown that reactive oxygen species attack on guanine residues can be prevented in presence of spermidine and absence of polycations encourage plasmid uncoiling from supercoiled state due to singlet oxygen and other reactive oxidative species attack²⁸. But the mechanism by

which spermine and spermidine offers resistance to one electron oxidation and subsequently DNA damage is not known clearly. Through our experiments we tried to explain the mechanistic aspect of inhibition of DNA damage brought about by the presence of spermidine in the light of charge hopping mechanism in DNA. One electron oxidation generates a localized radical cation that migrates or hops by an activated process requiring local structural distortion of DNA along the discrete molecular orbitals. These local structural distortions along with the surrounding water and counterions are responsible for stabilizing the self trapped radical cation. If the rate of hopping of the radical cation is greater than its irreversible trapping at guanine rich regions of the DNA, then the radical cation is supposed to be distributed approximately equally to all equivalent sites denying possibility of finding distance dependence²⁹. However, if the trapping of the radical cation is greater than hopping then chances of reaction at remote sites are slim and most of the damages will be found near site of radical cation generation.

In presence of spermidine, the Anthraquinone is forced to remain inside and internally intercalated within the DNA duplex. This phenomenon enhances the probability of greater charge injection directly inside the DNA molecule, which is apparent from the more reaction at the GG sites of DNA3-DNA4 in presence of spermidine. An important implication of this fact is that the geometry and conformation of the AQ have a significant role to play in radical cation migration. The charge transfer properties are affected considerably by the length of the linker as well as the DNA sequence in the surrounding of the AQ. All these factors contribute towards the charge transfer properties in DNA and decide whether the radical cation will migrate or form cross links or other reactivities³¹⁻³².

Detailed study on quinone intercalation into DNA has shown that the long axis of the anthraquinone of UAQ is parallel to the long axis of the base pairs at the intercalation site³⁰. As a result, the radical cation can be injected either in the 3'- or the 5'-direction on the quinone containing strand and also in its complementary strands, further confirmed by calculations from Rehm-Weller Equation³³. Irradiation times for the oligomer duplexes were different from SLP and DLP, since more photons were necessary to see any effect of charge transfer due to the shielding effect of thousands of bases present in SLP and DLP. While DNA3-DNA4 needs only a maximum of 45 minits of irradiation, SLP and DLP requires at least 2 hours of irradiation with 16 (350 nm) lamps to get the same effects of DNA damage, under single hit condition. For oligomer duplexes, more strand cleavage occurs at the 5'-side of the UAQ strands, while 3'-damages are higher for SLP and DLP containing spermidine. The compaction of SLP and DLP into condensates can bring the 3'-GG steps much closer to the quinone than in the linear form and inviting an equal competition between the 5'-and 3'-strand cleavage.

One electron oxidation of the quinone moiety generates the AQ radical anion and a "hole" or radical cation is injected in the DNA sequence. This radical cation generated in the DNA strands are mobile, with the driving forces for its migration being the columbic attraction to the negative charges as well as the differences in local ionization energies of the bases. Mutual neutralization of the hole and the electron results in electronic excitation that in turn causes backbone cleavage³⁴ which is manifested by DNA strand cleavage at UAQ site. The exothermicity of electron-hole recombination is sufficient to bring about carbon-nitrogen bond breakage. Also, deprotonation and subsequent strand cleavage is a

common result of this hole-electron recombination event. The oligomer duplexes which cannot form any well defined structure in presence of spermidine shows similar trend in UAQ site damage. But UAQ site damage is very negligible for both SLP and DLP that have been treated with spermidine. The structural compaction brought about by spermidine in SLP and DLP at higher concentrations of spermidine induces the hole to ionize the next available polaron before it can combine with the quinone radical anion, preventing possible deprotonation and strand cleavage.

In earlier reports we have shown that charge hopping rate (k_{hop}) decreases significantly in presence of spermidine in long pieces of DNA, when the AQ is terminally located. But surprisingly, we found that the rate of charge migration in DLP containing an internally linked UAQ is different. In spermidine containing DLP, the radical cation migration is very facile and all the GG steps on both sides of the UAQ are nearly equally damaged. This observation shows that the rates of hopping of the radical cation in doubly ligated plasmids are unaffected by formation of DLP condensates. Back-electron transfer in this DLP condensates are unlikely which mediate a very fast radical cation migration along the duplex strand unless can be annihilated by high activation barrier. The only possibility which can explain the radical cation migration behavior in DLP condensates is the decrease in the rate of trapping of the cation (k_{trap}). The trapping rate of the radical cation in DLP condensates is very low, which helps the radical cation to migrate long distances in both directions without being significantly trapped at GG sites. The scheme of radical cation migration in SLP and DLP in presence of spermidine is represented in

DNA. The presence of polycations at strategic positions near the DNA is important to exert the protective effect of this polycation from DNA damage. The oligomer duplexes react differently than long pieces of DNA and apparently show different kind of interaction with spermidine inducing different charge transfer properties. We already know that the introduction of a charge in the DNA distort its structure and the DNA respond quickly to the change¹⁹. One probable response is the reduction of intra base pair distance, which is further intensified by the formation of condensates with spermidine. Increase in pi-overlap also is a common adjustment which is more likely in the DLP thus stabilizing the radical cation⁴⁰. Formation of charge transfer effective states are hindered in case of SLP but DLP behaves altogether differently. The DLP condensates offer strong resistance to trapping reactions by inhibiting contact of the radical cation with trapping agents, hence allowing free migration of the cation in the DLP condensates. From the comparison of charge migration in single ligated plasmid and double ligated plasmid, in presence of spermidine, it is evident that radical cation introduced towards the terminal end of long pieces of DNA intend to drop the charge near the site of its formation, whereas a radical formed deep inside a long DNA sequence travels long distances very fast from its site of generation. In either way, the underlying significance of these two different behaviors by two different types of condensates might be towards achieving the same goal of DNA damage protection.

3.10 References

1. Casero, R. A. Jr.; Celano, P.; Ervin S. J.; Applegren, N. B.; Wiest L.; Pegg A. E. *J. Biol. Chem.* **1991**, 266, 810–814.
2. Jacob T. A.; Jaruga P.; Nath, R. G.; Dizdaroglu, M.; Brooks, P. J. *Nucleic Acids Res.* **2005**, 33, 3513–3520.
3. Kawakita, M.; Hiramatsu, K. *J. Biochem.* **2006**, 139, 315-322;
4. R Nicoletti, I Venza, G Ceci, M Visalli, D Teti and A Reibaldi, *Br. J. Ophthalmol.* **2003**, 87, 1038-1042.
5. Higuchi, C. M.; Wang, W. *J. Cell. Biochem.* **1995**, 57, 256-261.
6. Alhonen L.; Parkkinen, J. J.; Keinanen T. *Proc. Natl. Acad. Sci. U.S.A.* **2000**, 97, 8290-8295.
7. Brune, B.; Hartzell, P.; Nicotera, P.; Orrenius, S. *Exp. Cell. Res.* **1991**, 195 323–329.
8. Snyder, R. D. *Biochem. J.* **1989**, 260, 697–704.
9. Khan, A. U.; Mei, Y.-H.; Wilson, T. *Proc. Natl. Acad. Sci. U.S.A.* **1992**, 89, 11426–11427.
10. Khan, A. U.; Di Mascio, P.; Medeiros, M. H. G.; Wilson, T. *Proc. Natl. Acad. Sci. U.S.A.* **1992**, 89, 11428–11430.
11. Tadolini, B. *Biochem. J.* **1998**, 249, 33–36.
12. Basu, H. S.; Schwietert, H. C. A.; Feuerstein, B. G.; Marton, L. J. *Biochem. J.* **1990**, 269, 329–334.
13. Demple, B.; Harrison, L. *Annu. Rev. Biochem.* **1994**, 63, 915–948.

14. Gasper, S. M.; Schuster, G. B. *J. Am. Chem. Soc.* **1997**, 119, 12762–12771.
15. Nunez, M.; Hall, D. B.; Barton, J. K. *Chem. Biol.* **1999**, 6, 85–97.
16. Schuster, G. B.; Landman, U. *Topics. Curr. Chem.* **2004**, 236, 139–162.
17. Liu, C.S.; Hernandez, R.; Schuster, G. B. *J. Am. Chem. Soc.* **2004**, 126, 2877-2884.
18. Das, P.; Schuster, G. B. *Proc. Natl. Acad. Sci. U.S.A.* **2005**, 102, 14227-14231.
19. Schuster, G. B. *Acc. Chem. Res.* **2000**, 33, 253-260.
20. Ly, D.; Sanii, L.; Schuster, G. B. *J. Am. Chem. Soc.* **1999**, 121, 9400-9410.
21. Deshmukh, H.; Joglekar, S. P.; Broom, A. D. *Bioconjugate Chem.* **1995**, 6, 578-586.
22. Moore, J. N.; Phillips, D.; Nakashima, N.; Yoshihara, K. *J. Chem. Soc., Faraday Trans. 2* **1987**, 83, 1487-1508.
23. Gasper, S. M.; Schuster, G. B. *J. Am. Chem. Soc.* **1997**, 119, 12762- 12771.
24. Guckian, K. M.; Schweitzer, B. A.; Ren, R., X.-F.; Sheils, C. J.; Paris, P. L.; Tahmassebi, D. C.; Kool, E. T. *J. Am. Chem. Soc.* **1996**, 118, 8182-8183.
25. Yamana, K.; Nishijima, Y.; Ikeda, T.; Gokota, T.; Ozaki, H.; Nakano, H.; Sangen, O.; Shimidzu, T. *Bioconjugate Chem.* **1990**, 1, 319- 324.
26. Baase, W. A.; Johnson, W. C. Jr. *Nucl. Acids. Res.* **1979**, 6, 797-814.
27. Ly, D.; Kan, Y.; Armitage.; Schuster, G. B. *J. Am. Chem. Soc* **1996**, 118, 8747-8748.
28. Dypbuk, J. M.; Ankarcrona, M.; Burkitt, M.; Sjöholm, A.; Strom, K.; Orrenius, S.; Nicotera, P. *J. Biol. Chem.* **1994**, 269, 30553–30560.
29. Giese, B. *Acc. Chem. Res.* **2000**, 33, 631–636.

30. Gasper, S. M.; Armitage, B.; Hu, G. G.; Shui, X.; Yu, C.; Williams, L. D.; Schuster, G. B. *J. Am. Chem. Soc.* **1998**, *120*, 12402-12409.
31. Bergeron, F., Nair, V. & Wagner J. R. *J. Am. Chem. Soc.* **2006**, *128*, 14798-14799.
32. Bergaron, F.; Houde, D.; Hunting, D. J.; Wagner J. R. *Nucl. Acids. Res.* **2004**, *32*, 6154-6163.
33. Rehm, D.; Weller, A. *Isr. J. Chem.* **1970**, *8*, 259-271.
34. Bogdan, B. A.; Haselmann, K. F.; Zubarev, R. A. *Chem. Phys. Lett.* **2001**, *342*, 299-302.
35. Bloomfield, V. A. *Curr. Opinion Struct. Biol.* **1996**, *6*, 334-341.
36. Bloomfield, V. A. *Biopolymers* **1997**, *44*, 269-282.
37. Chatteraj, D. K.; Gosule, L. C.; Schellman, J. A. *J. Mol. Biol.* **1978**, *121*, 327-337.
38. Koltover, I.; Wager, K.; Safinya, C. R. *Proc. Natl. Acad. Sci. USA* **2000**, *97*, 14046-14051.
39. Gosule, L. C.; Schellman, J. A. *Nature* **1976**, *259*, 333-335.
40. Breslin, D. T.; Yu, C.; Ly, D.; Schuster, G. B. *Biochemistry* **1997**, *36*, 10463-10471.

PART II

DNA DIRECTED SELF ASSEMBLY OF CONDUCTING POLYMERS

CHAPTER 4

INTRODUCTION TO DNA-DIRECTED ASSEMBLY OF CONDUCTING POLYMERS

Ever since the discovery of the structure of DNA by Watson and Crick in 1953, DNA has been motivating scientists to study its immense physical and chemical properties. The function of DNA is greatly dependant on its fascinating structure. Throughout these years, scientists have been trying to explore the unique structural features of DNA and take advantage of the DNA design and apply them to solve other complex problems. Today, apart from being the genetic material of any living organism, DNA has been employed to a variety of applications. Breaker and coworkers found that DNA can work as a catalyst (DNA-enzymes)¹; Recently, Seeman has exploited the highly selective nucleobase recognition properties to create nanoscale DNA walking robot²⁻³. Hao Yan and coworkers at Duke University has devised X-shaped DNA tiles that link up into a switchable grid to be used as a nanofilter or in biological sensors⁴⁻⁵. Coating the grid with silver creates a lattice of nano-wires, which could be used in ultra-miniature electronic circuits. Liu and coworkers have worked on DNA templated organic reactions and functional group transformations⁶⁻⁷. Moreover, the development of DNA as a “smart glue” to guide the self assembly of nanostructures into functional circuits have rendered the usefulness of DNA beyond their typical biological function⁸. Recently, there is a rapidly growing awareness that the self-recognizing and self-organizing properties of DNA can be used to fabricate the formation of nanometer sized wires (nanowires). DNA templated metallization have become a popular method towards achieving this goal⁹.

Ongoing investigations have revealed that nanowires may also be created from conducting organic polymers such as polyaniline (PANI) by using surfactants or DNA as “soft” templates that control formation and structure of the polymer¹⁰. In this approach, the monomers of the polymers self assemble on the surface of the surfactant or the DNA and thus allow the formation of the para-directed or head to tail polymerization of the organic monomer units. This process allows creation of regular controlled length conducting polymers, which may be used as nanowires in miniature electronic devices.

Here we report the synthesis and characterization of some organic monomer units as part of a long conducting polymer. The process of attaching such monomer units with DNA templates for a self assembly process of polymerization is also outlined.

4.1 The Concept of Nanowire

A nanowire is a wire of diameter of the order of a nanometer (10^{-9} meters). Alternatively, nanowires can be defined as structures that have a lateral size constrained to tens of nanometers or less and an unconstrained longitudinal size. Typical nanowires exhibit length-to-width ratio of 1000 or more. For this reason they are often referred to as 1-Dimensional materials. Nanowires have many interesting properties that are not seen in bulk or 3-D materials. This is because electrons in nanowires are quantum confined laterally and thus occupy energy levels that are different from the traditional continuum of energy levels or bands found in bulk materials. Hence nanowires are also known as quantum wires. Nanowires are not observed spontaneously in nature and must be produced in a laboratory. Different techniques have been developed to produce nanowires ranging

from Vapor-Liquid-Solid (VLS) method¹¹⁻¹², deposition method, chemical etching to bombardment of bigger wire with high energy particle.

The conductivity of a nanowire is expected to be much less than that of the corresponding bulk material. This is due to the scattering from the wire boundaries, when the wire width is below the free electron mean free path of the bulk material. However, the conductivity of nanowires can be increased by chemical doping¹³⁻¹⁴. The nanowires can show peculiar shapes but mostly exhibit noncrystalline order. The lack of crystalline order is due to the fact that a nanowire is periodic only in one dimension (along its axis). Hence it can assume any order in the other directions (in plane) if this is energetically favorable.

Nanowires still belong to the experimental world of laboratories. It's possible that nanowire crossings will be important to the future of miniature circuits. Though there are other uses for nanowires beyond these, the only ones that actually take advantage of physics in the nanometer regime are electronics.

4.2 Conducting polymers for nanowire

A conductive polymer is an organic polymer semiconductor. Conductive organic polymers often have extended delocalized bonds (often composed of aromatic units). At least locally, these create a band structure similar to silicon, but with localized states. When charge carriers (from the addition or removal of electrons) are introduced into the conduction or valence bands (see below) the electrical conductivity increases dramatically. Some well known conducting polymers are polyacetylene, polypyrrole, polyaniline, polythiophene, polyfluorene, polytetrathiafulvalenes, polynaphthalenes, poly(p-phenylene

sulfide), and poly(para-phenylene vinylene) and their derivatives. The biggest advantage of these conductive polymers is their processibility. Conductive organic polymers are mostly plastics combined with the mechanical properties of having high electrical conductivities of a doped conjugated polymer. Structures of some conducting polymers are shown in Figure 4.1.

Considerable success have been achieved in the production of conducting polymer nanowires of controlled dimension with site-specific positioning, alignment and chemical compositions following nanolithography technique¹⁵, coaxial electrospinning technique¹⁶ and others. This has enabled patterning conducting polymer nanostructures on semiconducting and insulating surfaces which could help facilitate the fabrication of polymer nanodevices.

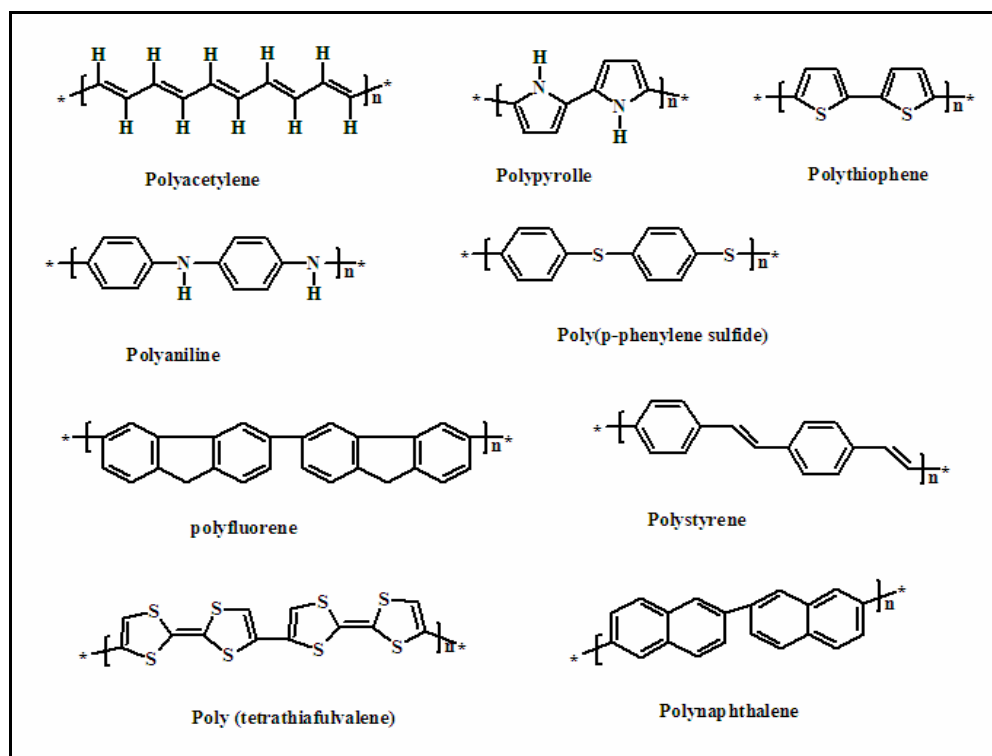


Figure 4.1: Structures of Common Organic Conducting Polymers.

4.3 Conducting polymers from Polyaniline

Polyaniline (PANI) is a conducting polymer of the semi-flexible rod polymer family, which can be converted to conductive polymers by appropriate oxidations or doping. Polymerized from the aniline monomer, polyaniline can be found in one of three distinct oxidation states.

- Leucoemeraldine
- Emeraldine
- Pernigraniline

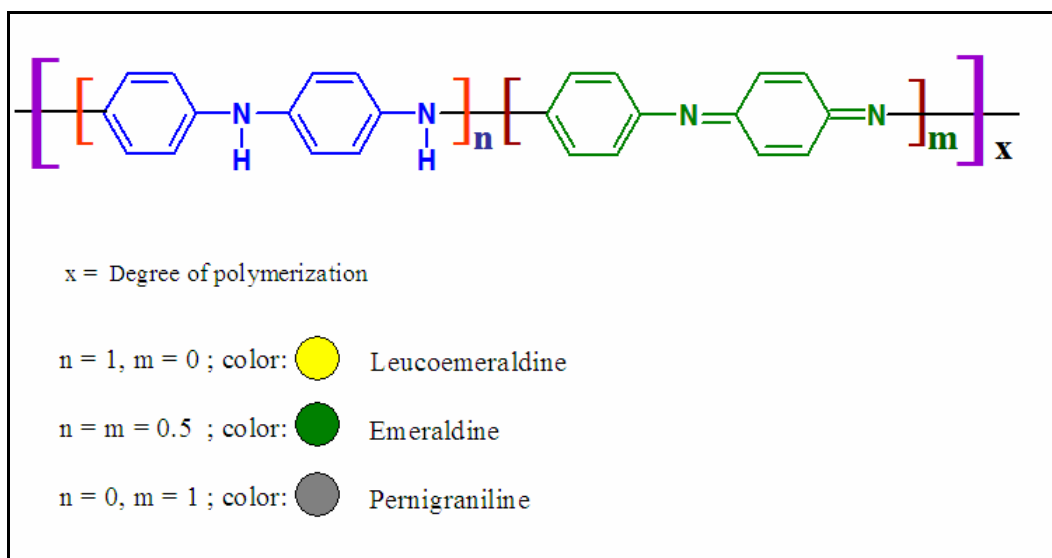


Figure 4.2: Structure of Polyaniline in Three Oxidation States.

There are also two other less common forms of aniline, namely Protoemeraldine and Nigraniline.

Polyanilines have attracted enormous interest as components of nanometer scale devices because of their wide range of conductivity, their stability and the ease of

synthesis. Synthesis of PANI can be achieved chemically by using oxidizing agent like ammonium peroxydisulfate in protic acid solution¹⁷⁻¹⁸. Electrochemically, the synthesis is achieved by anodic polymerization either in potentiostatic or potentiodynamic way¹⁹⁻²⁰. In particular, PANI can be prepared enzymatically under mild conditions using the enzyme horse radish peroxidase and hydrogen peroxide²¹⁻²².

Different copolymers involving PANI have been synthesized to achieve various goals. For example PANI have been associated with polyfluorene²³, polyvinyl chloride²⁴, polyacrylonitrile²⁵ and others which has been either copolymerized for increasing the solubility or tuning the conductivity or any other reasons.

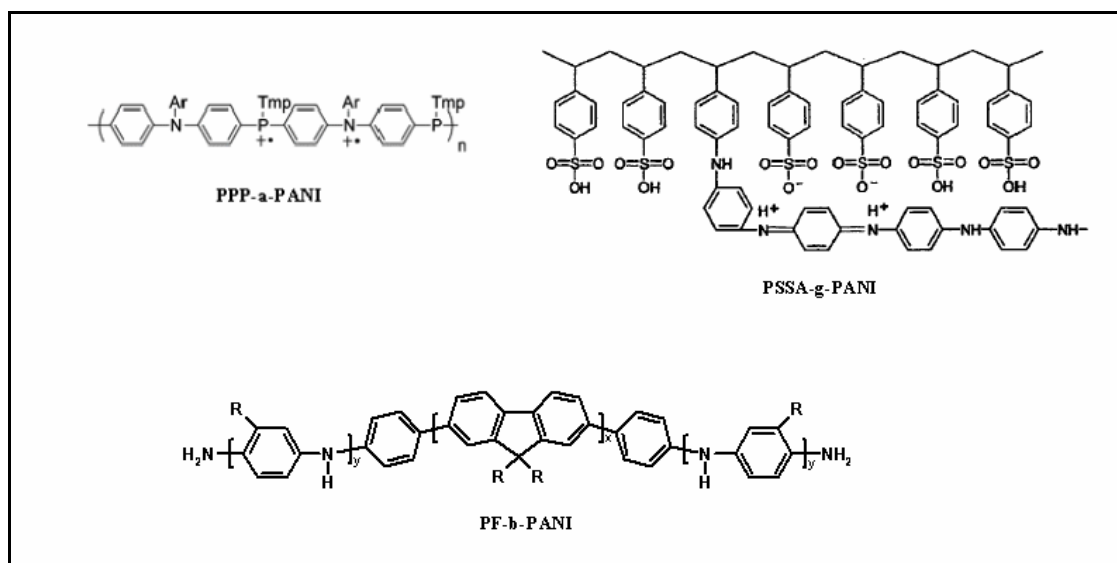


Figure 4.3: Structures of Different types of Copolymers of PANI.

B. 1.4 Self assembly of conducting polymers

Self-assembly (SA) in the classic sense can be defined as the spontaneous and reversible organization of molecular units into ordered structures by non-covalent

interactions. The most important property of a self-assembled system is the spontaneity of the self-assembly process: the interactions responsible for the formation of the self-assembled system act on a strictly local level. Another characteristic common to self-assembled systems is their thermodynamic stability: in order for SA to take place without the intervention of external forces, the process must lead to a lower Gibbs free energy, thus self-assembled structures are thermodynamically more stable than the single, unassembled components. A direct consequence is the general tendency of self-assembled structures to be relatively free of defects.

The success of self assembly in a molecular system is characterized by five characteristics of a system²⁶.

- a. **Components:** The molecules or molecular segments of a self assembly may be the same or different, but they should interact with each other. Their interaction leads from some less ordered state (a solution, disordered aggregate or random coil) to a final state (a crystal or folded macromolecule) that is more ordered.
- b. **Interactions:** Self-assembly occurs when molecules interact with one another through a balance of attractive and repulsive interactions. These interactions are generally weak (comparable to thermal energies) and noncovalent (van der Waals and Coulomb interactions, hydrophobic interactions, and hydrogen bonds) but relatively weak covalent bonds (coordination bonds) are recognized increasingly as appropriate for self-assembly²⁶⁻²⁷. Complementarity in shapes among the self-assembling components is also crucial.

- c. **Reversibility:** For self-assembly to generate ordered structures, the association either must be reversible or must allow the components to adjust their positions within an aggregate once it has formed. The strength of the bonds between the components, therefore, must be comparable to the forces (e.g. Thermal motion) tending to disrupt them.
- d. **Environment:** The self-assembly of molecules normally is carried out in solution or at an interface to allow the required motion of the components. The interaction of the components with their environment can strongly influence the course of the process.
- e. **Mass Transport and Agitation:** For self-assembly to occur, the molecules must be mobile. In solution, thermal motion provides the major part of the motion required to bring the molecules into contact.

The use of self assembly of polymer and block-copolymers as architectural units in the design of complex structures, and the control, manipulation, and functionalization of polymer surfaces have gained immense importance in recent years.

4.5 Templated polymer synthesis

Electrically conductive polymers are relatively insoluble in water. Therefore, these polymers are typically formed in an organic solvent. Attempts to increase the water solubility of these polymers have included derivatization of the monomer before polymerization or the resulting polymer formed. However, derivatization of monomers typically slows polymerization, and has been reported to cause some degradation. To

overcome these issues, developments have been made towards using templates for the synthesis of the conducting polymers.

A template binds to and aligns the monomers so as to maximize conjugation and minimize branching of the polymers formed according to the new methods. The template can be a polyelectrolyte. The template can also be a micelle, an oligomer, or a polymer. Examples of suitable templates include azo-polymer, substituted polystyrene, substituted vinyl polymer (e.g., polyvinyl phosphonate, polyvinyl phosphate, or polyvinyl benzoic acid), sulfonated polymer (e.g., lignin sulfonate, sulfonated polystyrene, or polystyrene sulfonic acid), polynucleotides (e.g., deoxyribonucleotide or ribonucleotide), polypeptides, zeolites, caged compounds, or sulfonated micelles (e.g., micelle containing dodecyl benzene sulfonic acid). The template can be positively charged, such as a polycation (e.g., poly(diallyl dimethyl ammonium chloride)) or negatively charged, such as a polyanion (e.g., sulfonated polystyrene). It is important that the charged groups of a template are indeed in their charged form under the required reaction conditions.

In 2003, Samuelson and coworkers reported a highly sophisticated method for polyelectrolyte templated polyaniline synthesis²⁸. They claim that the templated polymer synthesis serves at least three important functions. First, it serves as a charged scaffold upon which the monomers preferentially align themselves to form a complex, thereby promoting extended conjugation of the resulting polymer chains (limiting parasitic branching). This preferential alignment provides improved electrical and optical properties of the polymer. Secondly, the template can serve as long molecular dopant species that is complexed and essentially locked in the polymeric products. The polyelectrolyte template

virtually locks the dopants into the polymer which ensures that the electrical nature of the polymer's backbone is maintained and the desired electrical and optical properties are stabilized. Thirdly, the polyelectrolyte template provides water solubility of the final polymer-template complex for further processing.

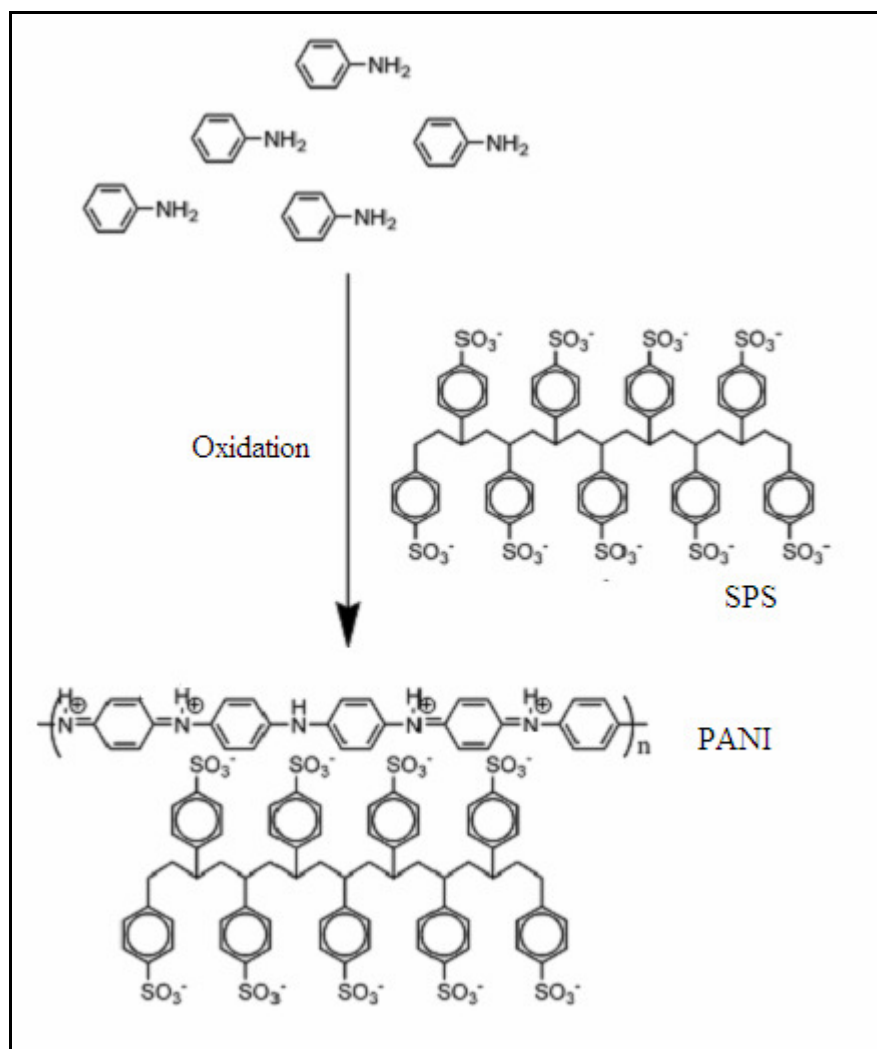


Figure 4.4: Polyaniline Formation on Sulphonated Polystyrene Template.

4.7 DNA templated polymerization of conducting polymers

DNA has a unique secondary structure where the base pairs create a stack of π electrons and a flurry of negative charge on the backbone associated with the phosphate groups attached to the sugar moiety. This makes DNA a natural polyelectrolyte with surface negative charge, which can be used for the assembly of materials with specific electronic properties²⁹⁻³¹. Samuelson and coworkers has reported a strategy that exploits the inherent molecular order as well as the polyelectrolyte behavior of DNA to synthesize and assemble polyaniline from its precursor monomer²². Discovery of mild oxidation procedure like the enzymatic polymerization at neutral pH have significantly improved the templated behavior of DNA because the DNA helix remains chemically and structurally unaltered in absence of strong acids and other oxidizing reagents³². The phosphate-based template provided the requisite local environment to facilitate the para-directed coupling of the polymer. Ma and coworkers have successfully fabricated polyaniline nanowire arrays on silicon substrates by using fully stretched DNA as growing template. First, they immobilized the DNA on silicon surface and then used the DNA for templating the polymerization of aniline³³.

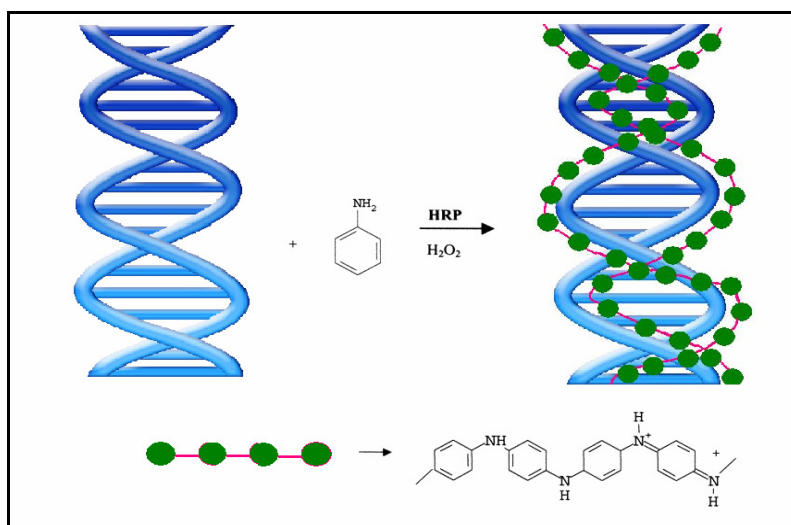


Figure 4.5: Schematic Representation of DNA Templated Polymerization of PANI in Solution²².

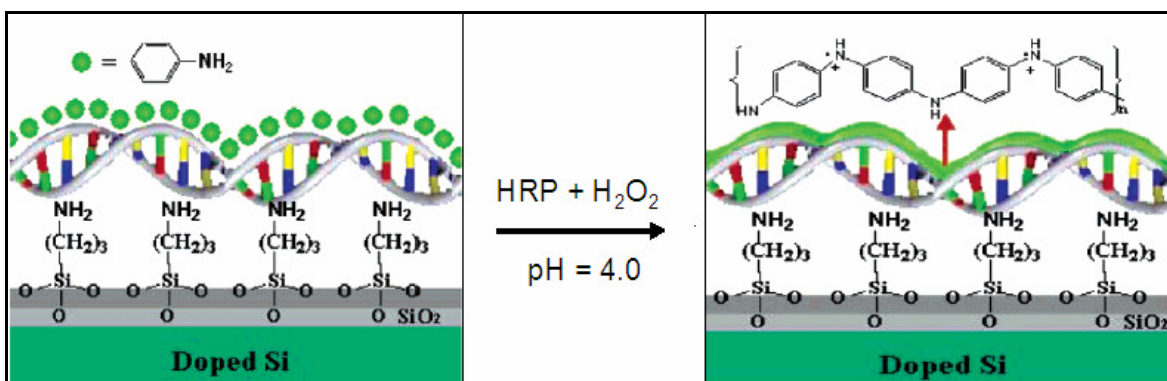


Figure 4.6: Schematic Representation of Polymerization of PANI on DNA Template Immobilized on Silica Surface³³.

After immobilization of the DNA-Polyaniline complex on mica or silicon surface, agglomeration of the DNA-Polyaniline strands have been observed due to reduction in electrostatic repulsion caused by the concomitant shielding of the DNA negative charges. Though the aniline groups arrange themselves on the negative charges of the phosphate backbone and held together by electrostatic interactions, they still enjoy some flexibility in

their movement due to the weakness of the nature of the interaction between the monomer units and the DNA. Thus, the possibility of branching in PANI oligomer formation cannot be precluded. Also, for other conducting polymers containing aromatic rings in excess to one provides additional positions for reactions and branching.

All the DNA templated polymer synthesis methods have resulted in creation of homopolymer that cannot take advantage of the sequence information intrinsic to DNA. Recently, Schuster and Datta have reported the synthesis of a PANI oligomer having the properties of a conducting polymer by the enzyme-initiated reaction of oriented aniline monomers covalently linked to nucleobases of duplex DNA³⁴. These findings provide a method to use DNA as a template as well as apply the sequence programmability of DNA to the preparation of unique nanoscale materials with tailored electronic properties. This work is an approach towards the synthesis and characterization of monomer units of conducting polymer covalently attached to DNA, which has the potential to use both the templating and scaffolding roles of DNA in synthesis of conducting polymer units of controlled length.

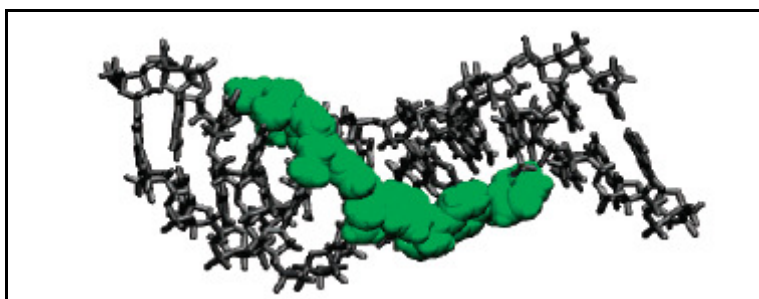


Figure 4.7: Computer Generated Structural Model Showing Six Aniline Groups Bonded head-to-tail Conjoined to a DNA Oligomer³⁴.

4.8 References

1. Breaker, R. R.; Joyce, G. F. *Chem. Biol.* **1994**, 1, 223-229.
2. Sherman, W. B.; Seeman, N. C. *Nanoletters* **2004**, 4, 1203-1207.
3. Ding, B.; Seeman, N. C. *Science* **2006**, 314, 1583-1585.
4. Feng, L.; Park, S. H.; Reif, J. H.; Yan, H. A *Angew. Chem. Int. Ed.*, **2003**, 42, 4342- 4346.
5. Yan, H.; Park S. H., Finkelstein, G.; Reif, J. H.; LaBean, T. H. *Science*, **2003**, 301, 1882-1884.
6. Gartner, Z. J.; Grubina, R.; Calderone, C. T.; Liu. D. R. *Angew. Chem. Int. Ed. Eng.* **2003**, 42, 1370-1375.
7. Gartner, Z. J., M. W. Kanan & D. R. Liu. *J. Am. Chem. Soc.* **2002**, 124, 10304-10306.
8. Williams, K. A.; Veenhuizen, P. T. M.; Torre, B. G.; Eritja R.; Dekker, C. *Nature* **2002**, 420, 761.
9. Braun, E; Eichen, Y.; Sivan, U.; Ben-Yoseph, G. *Nature* **1998**, 391, 775-778.
10. Zhang, G.; Wang, Y. *Mater. Sci. Eng. B* **2006**, 134, 9-14.
11. Wagner, R. S.; Ellis, W. C. *Appl. Phys. Lett.* **1964**, 4, 89-90.
12. Wagner, R. S.; Ellis, W. C.; Jackson, K. A.; Arnold, S. M. *J. Appl. Phys.* **1964**, 35, 2993-3000.
13. Von Klitzing, K.; Dorda, G.; Pepper, M. *Phys. Rev. Lett.* **1980**, 45, 494-497.
14. Landauer, R. *J. Phys. Cond. Matter.* **1989**, 1, 8099-8106.

15. Maynor, B. W.; Filocamo, S. F.; Grinstaff, M. W.; Liu, J. *J. Am. Chem. Soc.* **2002**, 124, 522-523.
16. Sun, B.; Duan, B.; Yuan, X. *J. App. Polym. Sci.* **2006**, 102, 139–145.
17. Guo, Q.; Yi, C.; Zhu, L.; Yang, Q.; Xie, Y. *Polymer* **2005**, 46, 3185-3189.
18. Xia, H.; Cheng, D.; Xiao, C.; Chan, H. S. *J. Mater. Chem.* **2005**, 15, 4161 – 4166.
19. Hoang H. V.; Holze, R. *Chem. Mater.* **2006**, 18, 1976 -1980.
20. Mondal, S. K.; Barai, K.; Munichandraiah N. *Electrochimica Acta* **2007**, 52, 3258-3264.
21. Shan, J.; Han, L.; Bai, F.; Cao, S. *Pol. adv. Technol.* **2003**, 14, 330-336.
22. Nagarajan, R.; Liu, W.; Kumar, J.; Tripathy, S. K.; Bruno, F. F.; Samuelson, L. A. *Macromolecules* **2001**, 34, 3921-3927.
23. Asawapirom, U.; Güntner, R.; Forster M.; Scherf, U. T. *Solid Films* **2005**, 477, 48-52.
24. Cho, H. S.; Park, Y. H. *Synthetic metals* **2004**, 145, 141-146.
25. Hosseini, S. H.; Dabiri, M. ; Ashrafi M. *Polym. Int.* **2006**, 55, 1081-1089.
26. Sirringhaus, H.; Kawase, T.; Friend, R. H.; Shimoda, T.; Inbasekaran, M.; Wu, W.; Woo, E. P. *Science*. **2000**, 290, 2123–2126.
27. Olenyuk, B.; Whiteford, J. A.; Fechtenkotter, A.; Stang, P. J. *Nature* **1999**, 398, 796-799.
28. Samuelson, L. A.; Tripathy, S. K.; Bruno, F.; Nagarajan, R.; Kumar, J.; Liu, W. *U.S. Patent No. 6,569,651 B1*, **2003**.
29. Eichen, Y.; Braun, E.; Sivan, U.; Ben-Yoseph, G. *Acta Polym.* **1998**, 49, 663-670.

30. Uemura, S.; Shimakawa, T.; Kusabuka, K.; Nakahira, T.; Kobayashi, N. *J. Mater. Chem.* **2001**, 11, 267-268.
31. Kobayashi, N.; Uemura, S.; Kusabuka, K.; Nakahira, T.; Takahashi, H. *J. Mater. Chem.* **2001**, 11 1766-1768.
32. Nickels, P.; Dittmer, W. U.; Beyer, S.; Kotthaus, J. P.; Simmel, F. C. *Nanotechnology* **2004**, 15, 1524-1529.
33. Ma, Y. F.; Zhang, J. M.; Zhang, G. J.; He, H. X. *J. Am. Chem. Soc.* **2004**, 126, 7097-7101.
34. Datta, B.; Schuster, G. B.; McCook, A.; Harvey, S. C.; Zakrzewska, K. *J. Am. Chem. Soc.* **2006**, 128, 14428-14429.

CHAPTER 5

SYNTHESIS AND CHARACTERIZATION OF MONOMER UNITS OF CONDUCTING POLYMER ATTACHED TO DNA TEMPLATE

5.1 Introduction

The most challenging aspect of creating functional nanoscale materials is the development of general techniques for the construction of designed molecular assemblies having nonrecurring, irregular structures. Recent investigation have showed that the self-recognition and self assembly properties of DNA offer unique advantages for the preparation of such materials.¹ However, several experiments have now proved the fact that DNA itself may be unsuitable for electronic devices,²⁻³ and innovative approaches are being developed to create suitably modified DNA-based materials.⁴ In particular, synthetic methods which use the advantage of the sequence programmability of DNA could enable production of the complex, non-periodic structures⁵ that are required for molecular electronic applications.⁶

Development of organic conducting polymers like polyaniline (PANI) and several copolymers of polyaniline have attracted enormous interest because of their relative ease of synthesis and their unique electrical and optical properties.⁷⁻⁸ The discovery that aniline can be polymerized enzymatically under mild conditions using DNA as a template,⁹ have ushered in considerable interest to develop functional nanoelectronic devices out of them. However, this method yields a homopolymer that cannot take advantage of the sequence information intrinsic to DNA. Recently Schuster and coworkers have synthesized a PANI

oligomer having the properties of a conducting polymer by the enzyme-initiated reaction of oriented aniline monomers covalently linked to nucleobases of duplex DNA¹⁰. Based on this concept, here we report the synthesis of some monomer units and the process of their covalent linking with DNA, which can use the sequence information of the DNA to align themselves for production of controlled length conducting polymer. These findings could provide a method to apply the sequence programmability of DNA to the preparation of unique nanoscale materials with tailored electronic properties.

5.2 DNA sequence programmability applied to formation of PANI

One of the striking features of Watson and Crick DNA double helix model is the base pairing and complementarity of the nucleobases. Under normal conditions, Adenine always pairs with Thymine by virtue of two hydrogen bonds and Guanine pairs with Cytosine with three hydrogen bonds. This unique base pairing property of DNA suggests that a particular DNA sequence will always find its complement and interact with it, even in presence of numerous other DNA sequences. This property has been advantageously used to align or self assemble monomer units of conducting polymer on DNA.

Covalent attachment of the monomer units with DNA helps to accomplish several purposes.

- The DNA sequence acts as a template for the self assembly of the monomer units in the polymerization process.
- The polymerization process can be programmed and controlled in any direction by utilizing the sequence specificity, intrinsic to DNA.

- The parasitic branching of the growing polymer chain can be completely eliminated, resulting in formation of well defined linear polymer.
- The length of the polymer chain can be controlled with very high precision using the exact number of desired DNA linked monomer units.
- DNA linked monomer units are water soluble, which makes them easier to process.

Figure 5.1 shows the schematic of the polymerization scheme of DNA conjoined PANI and 4-aminobiphenyl as reported by Schuster and Datta¹⁰. It has been found that the PANI oligomers that are formed by this process indicate their close similarity to conventional conducting polymers. Detailed molecular modeling has suggested that the region of the DNA duplex bearing the PANI oligomer is distorted with reduced inter-base hydrogen bonding, which can be improved by incorporating longer flanking duplex DNA regions (“leads”). The role of the DNA is to constrain the covalently-linked monomers and to provide a template for formation of a PANI oligomer, once this is completed, the properties of the conducting nanowires should be largely independent of the structural fate of the conjoined DNA.

Figure 5.2 shows the scheme for attaching two different monomer units of a conducting polymer conjoined to two different DNA strands. One monomer unit has terminal amino functional groups (compound number **12**), while the other monomer end in simple aryl groups (compound number **2**). Once, aligned properly in bonding distances with the help of the DNA complementary sequence (template), they can be coupled following standard enzymatic oxidation method. This approach could give us a method to link different kinds of monomer units intermolecularly over an array of DNA sequences. The synthesis of the monomer units (**2** and **12**) and their attachment with the DNA strands (PSA 1 and PSA 2 in Figure 5.10) are outlined in this work.

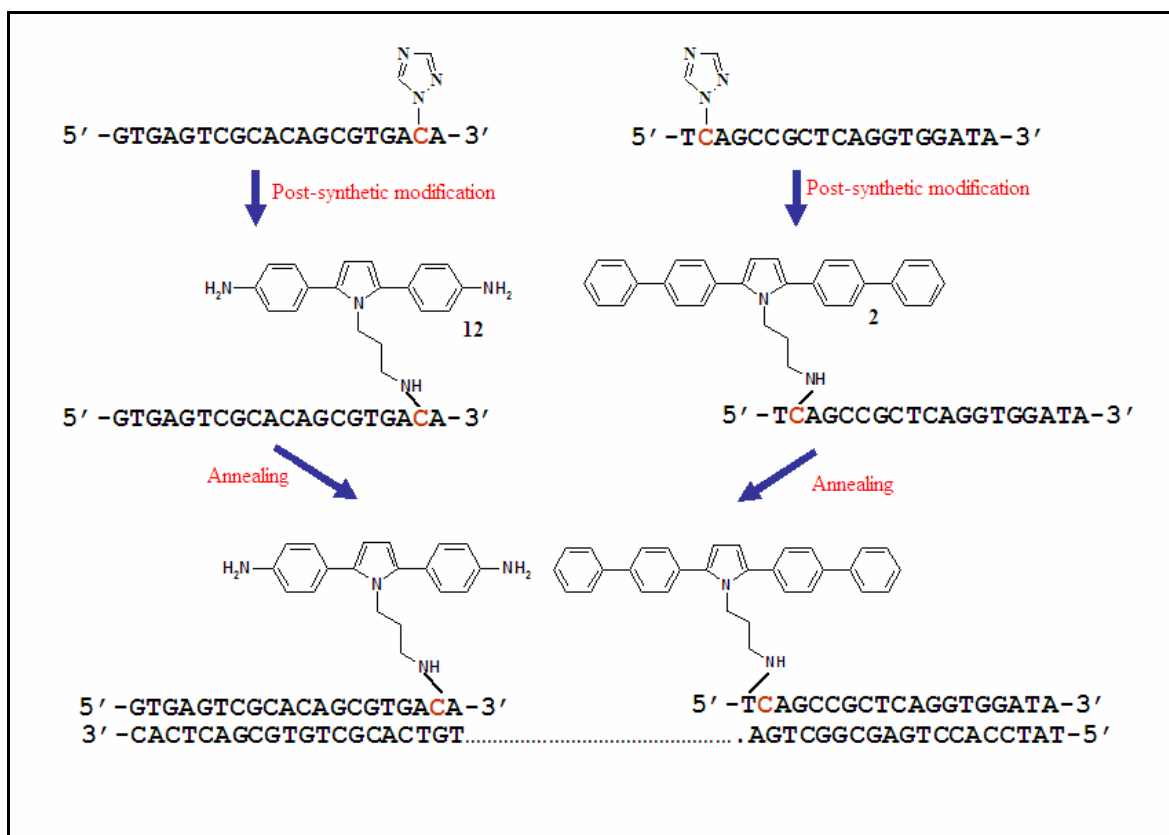


Figure 5.2: Scheme for Intermolecular Attachment of DNA-Conjoined Monomer units.

The intramolecular orientation of the monomer units over a single DNA strand can be achieved by synthesizing the DMT-protected phosphoramidite of deoxyuridine containing one particular monomer derivative (compound number **6** of Figure 5.7) and incorporating the same at any internal positions of the DNA sequence. The other monomer units (**12**) can be attached by replacing the triazole group of convertible nucleobases of the DNA strands (Figure 5.3) following a post synthetic modification process outlined in the experimental section. To test the success of internal linking of the monomer unit, compound **6** was synthesized.

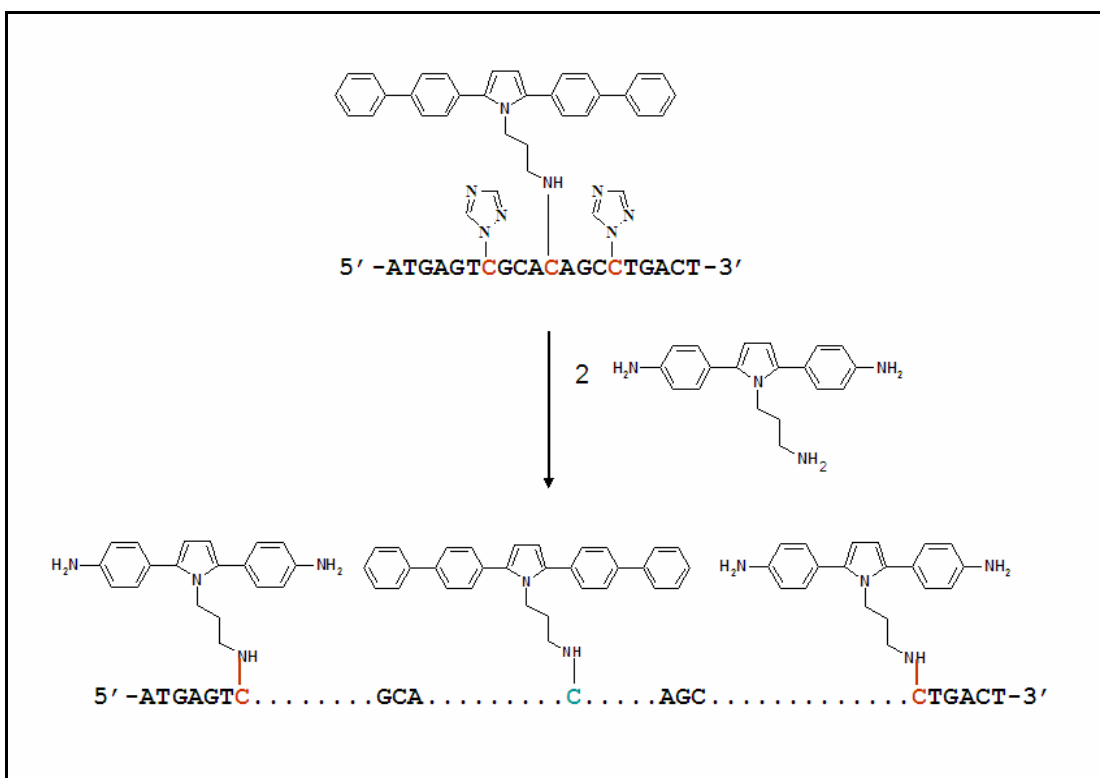


Figure 5.3: Scheme for Intramolecular Attachment of DNA-Conjoined Monomer units.

Figure 5.4 shows the structure of an internally linked monomer unit of a conducting polymer (compound number **16**), where 2 and 5 position of the pyrrole is occupied by biphenyl-aniline moiety. This is an example of a horizontally extended monomer unit of a PANI like polymer to DNA by a single linker. Figure 5.5 shows the Hyperchem generated model of a monomer unit conjoined with a DNA sequence. Calculations showed that this monomer unit spans a DNA of 8 base-sequences. The short single strand DNA containing the covalently linked monomer unit can be coannealed with a sufficiently long complementary DNA sequence, along with other small DNA sequences, also containing conjoined monomer units in a self assembly pattern. For practical achievement of this goal, monomer units of appreciable horizontal length with a single linker are required to minimize the distortion of the DNA of interest. Synthesis and characterization of such monomer unit (**16**) of conducting polymers are attempted and envisioned through this work.

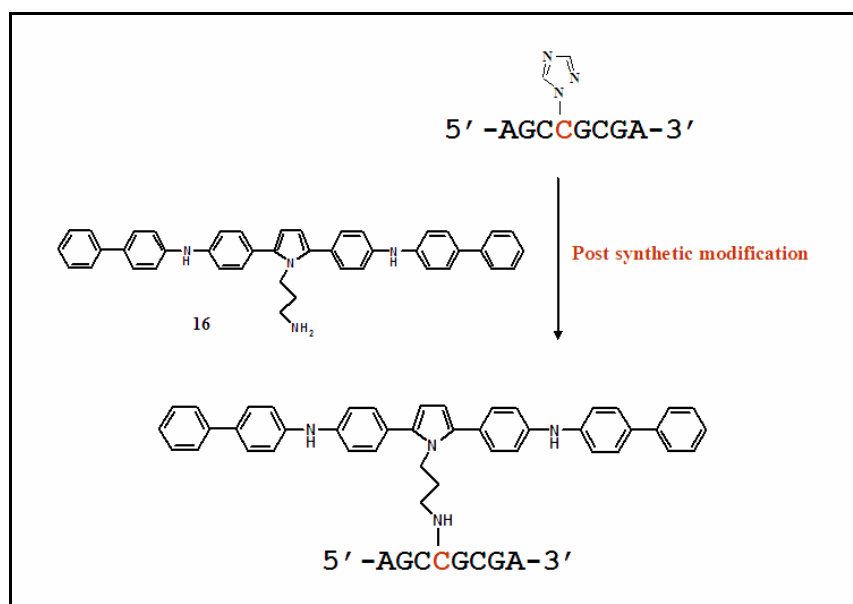


Figure 5.4: Scheme for Attachment of Horizontally Extended Monomer unit.



Figure 5.5: Hyperchem Model of PANI like Monomer Linked Covalently to DNA.

The individual steps involved in the scheme for the synthesis of the key compounds **2**, **6**, **12** and **16** are outlined in Figure 5.6 – Figure 5.9.

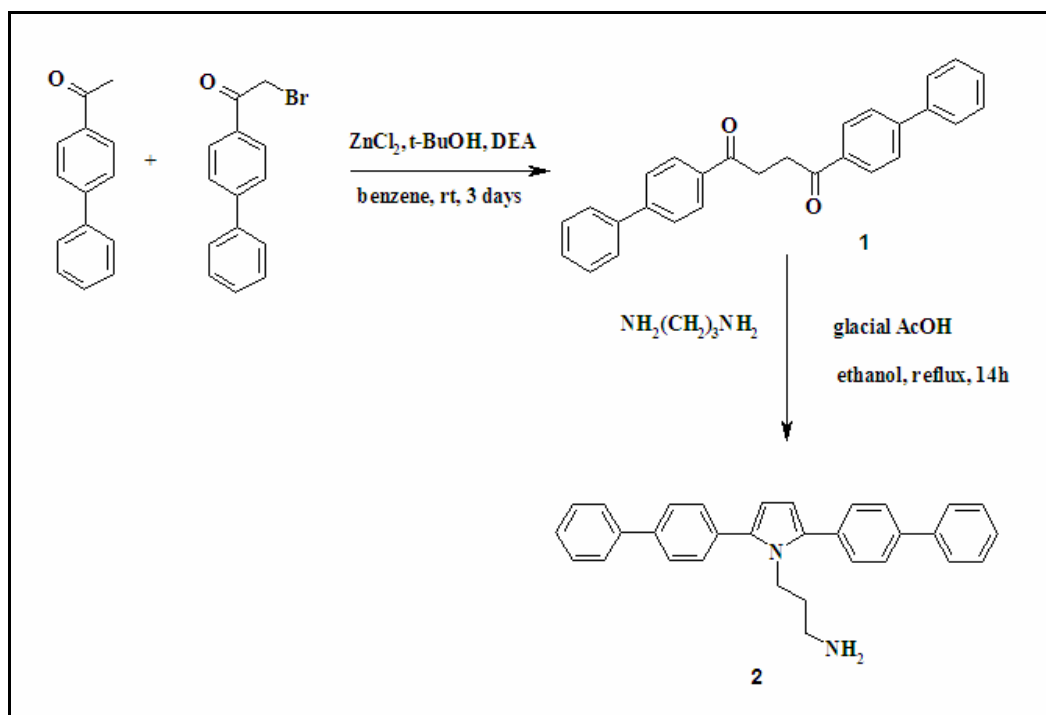


Figure 5.6: Scheme for the Synthesis of **2**.

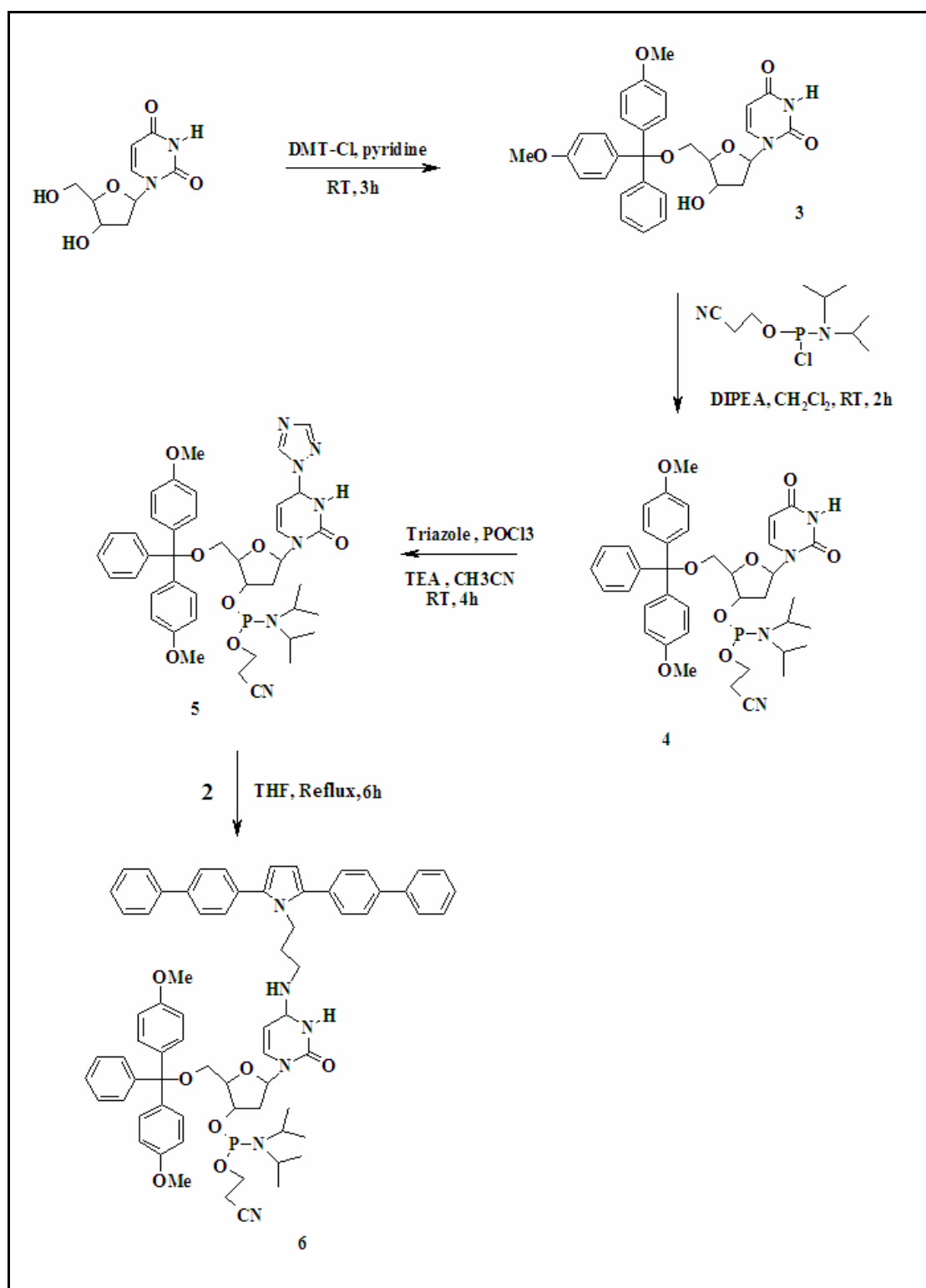


Figure 5.7: Scheme for the Synthesis of **6**.

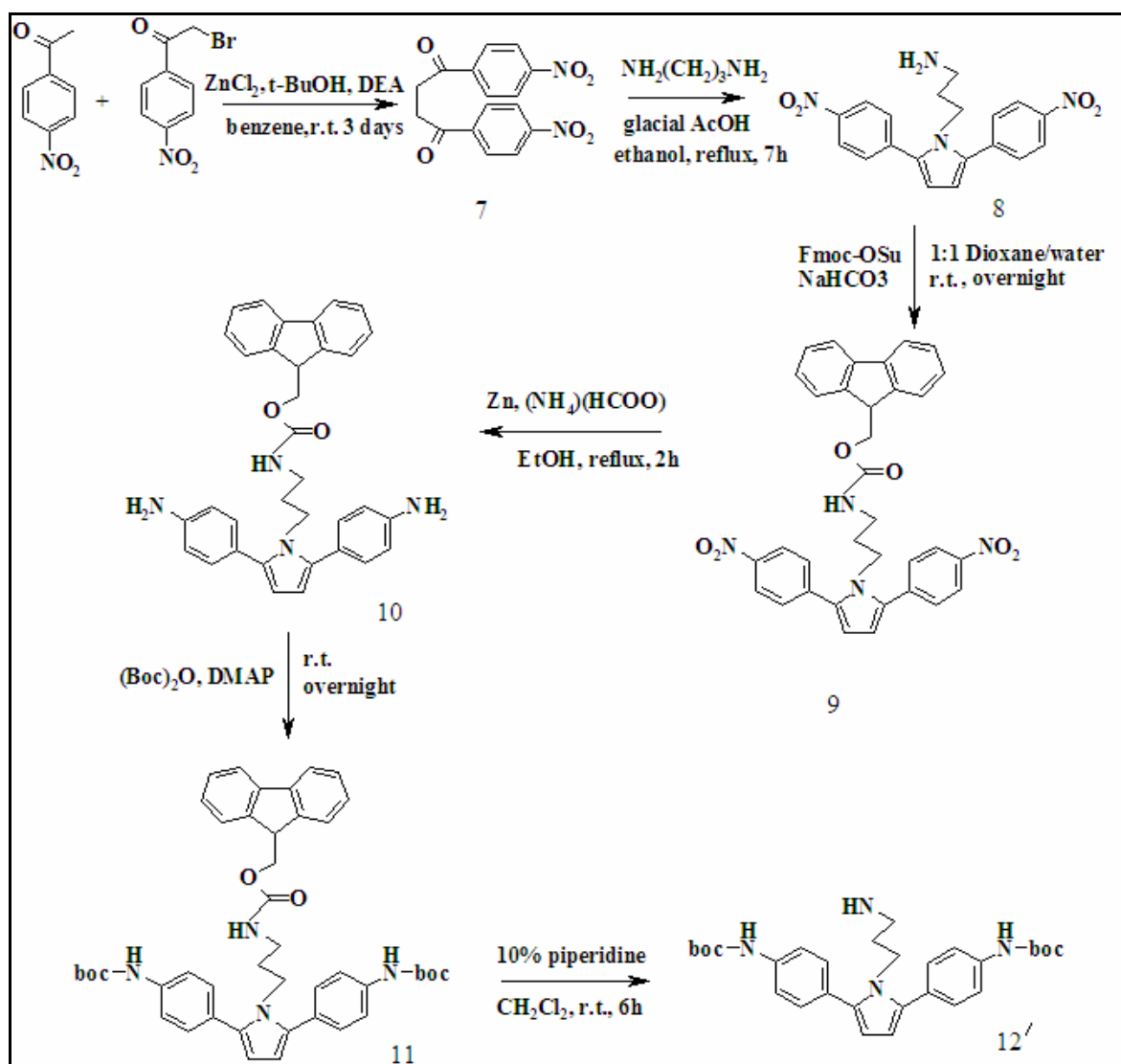


Figure 5.8: Scheme for the Synthesis of Boc-Protected **12**.

5.4 Experimental

5.4.1 Materials and methods

4-acetylbiphenyl, α -Bromo-4'-phenylacetophenone, Zinc chloride, diethylamine, 1,3-diaminopropane, DMT-chloride, diisopropyl chlorocynoethyl phosphoramidite, triazole, α -Bromo-4'-nitroacetophenone, Fmoc-OSu, (BOC)₂, Pd(OAc)₂, S-BINAP, Na-O^tBu and DMAP were obtained from Sigma-Aldrich and were used as received without further purification. 4-Nitroacetophenone was obtained from TCI Chemicals (Tokyo, Japan) and was used as received. POCl₃ was obtained from Sigma Aldrich and was distilled under vacuum before use. Deoxyuridine obtained from Sigma Aldrich was dried *in vacuo* by suspending with dry pyridine two times before use. 4-Aminobiphenyl was obtained from Sigma-Aldrich and was crystallized from hot ethanol and stored under argon. O4-triazolyl-deoxyuridine phosphoramidite was purchased from Glen Research along with other normal nucleoside phosphoramidite. DNA oligomers were synthesized on an Applied Biosystems Inc. Expedite DNA synthesizer. The DNA samples were treated with ammonia at room temperature overnight to detach the DNA from the solid support and also to remove the protecting groups. The modified synthetic DNA oligonucleotides were purified by reverse phase HPLC on a Hitachi 7000 HPLC system equipped with Varian Dynamax C-18 column using appropriate ratio of Acetonitrile, Triethylammonium Acetate buffer (pH=7.0) and water and their concentrations calculated by using biopolymer calculator and calculating their absorbance at 260 nm in a Hewlett-Packard spectrophotometer. The mass of the oligonucleotides were determined by Electrospray Ionization (ESI) mass spectrometer at the mass spectra facility at Georgia Tech.

5.4.2 Synthesis of 3-(2,5-di(biphenyl-4-yl)-1H-pyrrol-1-yl)propan-1-amine (2)

1,4-di(biphenyl-4-yl)butane-1,4-dione (1)

Commercial anhydrous ZnCl_2 (5.44g, 40mmol) was placed into a one-neck, 50-mL round bottomed flask and dried to melting under vacuum at 250°C for 15 min. After cooling under vacuum to r.t., benzene (25 mL), diethylamine (3.3 mL, 30 mmol), and $t\text{-BuOH}$ (2.8 mL, 30 mmol) were successively added. The mixture was stirred until zinc chloride was fully dissolved (approx 2h). 4-acetylbiphenyl (5.9 g, 30 mmol) and α -bromo-4'-phenylacetophenone (6.87 g, 25 mmol) were successively added to the reaction mixture and stirred at r.t. for 3 days. The benzene was evaporated and the reaction mixture was quenched with 5% aqueous H_2SO_4 and filtered in a Buchner funnel. The crystalline precipitate was washed successively with benzene, H_2O and MeOH and dried *in vacuo* to get the product in 75% yield. TLC of reaction mixture showed disappearance of both the 4-acetylbiphenyl ($R_f=0.5$) and α -bromo-4'-phenylacetophenone ($R_f=0.4$) and appearance of the product spot ($R_f=0.2$). ^1H NMR (300 MHz, benzene- d_6) δ 3.25 (s, 4H, 2 CH_2), 7.42 (t, 2H, $\text{H}_{4'}$), 7.50-7.52 (m, 8H, 4 H_2 , 4 H_3), 7.75 (d, 4H, H_3), 8.05 (d, 4H, H_2).

3-(2,5-di(biphenyl-4-yl)-1H-pyrrol-1-yl)propan-1-amine (2)

In a 500 mL three neck round bottomed flask, 1 (3.9 g, 10 mmol) and 25 mL glacial acetic acid were successively added to 250 mL dry ethanol. The mixture was stirred for 15 min at r.t. and 1,3-diaminopropane (5 mL, 54 mmol) was added slowly under nitrogen. The reaction mixture was heated to reflux for 14 hours until a clear solution was obtained. Formation of the product ($R_f = 0.5$) was confirmed by monitoring with TLC

(1:19: MeOH: CH₂Cl₂). After completion of the reaction, the reaction mixture was made into slurry by evaporating the ethanol and poured slowly into ice cold saturated solution of sodium bicarbonate with continuous stirring. The resultant precipitate was filtered under suction and washed with water. The precipitate was further dissolved in CH₂Cl₂, washed with brine, dried over MgSO₄ and purified by column chromatography (neutral alumina, MeOH/CH₂Cl₂ =1:19) to get the product as a pale yellow powder. Yield 82%; ¹H NMR (300 MHz, CDCl₃) δ 1.90 (m, 2H, CH₂), 2.32 (t, 2H, CH₂), 4.24 (t, 2H, CH₂), 5.31 (br s, 2H, NH₂), 6.38 (s, 2H, CH pyrrole), 7.39 (t, 2H, H_{4'}), 7.49 (t, 4H, 4H_{3'}), 7.53 (d, 4H, 4H_{2'}), 7.69 (d, 4H, H₃), 7.75 (d, 4H, H₂).

5.4.3 Synthesis of 2,5-Bis(biphenyl)-pyrrole linked deoxycytidine-DMT-phosphoramidite (6)

1-(5-((bis(4-methoxyphenyl)(phenyl)methoxy)methyl)-4-hydroxytetrahydrofuran-2-yl)pyrimidine-2,4(1H,3H)-dione(3)

Deoxyuridine (3.5 g, 15.33 mmol) was dissolved in 70 mL of pyridine and the suspension was treated with DMT-Cl (6.23 g, 18.4 mmol) at 0°C for 30 min with constant stirring. The reaction mixture was brought to r.t. and stirred for additional 2.5 h. Formation of product was confirmed by TLC (MeOH/CH₂Cl₂ =1:19, R_f = 0.4) and the reaction was quenched by adding 10 mL MeOH. The solvent was evaporated *in vacuo* and the product was purified by column chromatography (silica, 0-5% MeOH in CH₂Cl₂, 0.2% TEA). Yield 62%; ¹H NMR (300 MHz, CDCl₃) δ 2.24 (m, 1H, H_{2'}), 2.40 (m, 1H, H_{2'}), 3.45-3.49 (m, 3H, 2H_{5'}, C_{3'}-OH), 3.77 (s, 6H, OCH₃), 3.99 (m, 1H, H_{3'}), 4.52(m, 1H, H_{4'}), 5.39 (d,

1H, H₅), 6.28 (t, 1H, H_{1'}), 6.84 (d, 4H, aromatic H₃), 7.25 (d, 4H, aromatic H₂), 7.27-7.37 (m, 5H, phenyl), 7.74 (d, 1H, H₆).

2-((bis(4-methoxyphenyl)(phenyl)methoxy)methyl)-5-(2,4-dioxo-3,4-dihydropyrimidin-1(2H)-yl)tetrahydrofuran-3-yl 2-cyanoethyl diisopropylphosphoramidite (4)

To a solution of 3 (3.5 g, 6.6 mmol) in anhydrous CH₂Cl₂ (50 mL), DIPEA (3 mL, 26.4 mmol) and 2-cyanoethyldiisopropyl chlorophosphoramidite (2.55 mL, 8 mmol) was successively added under argon atmosphere. The reaction mixture was stirred at r.t. for 2 h, the solvent was evaporated *in vacuo* and the residue was purified by column chromatography (silica; 8.7:1:0.3, EtOAc: Hexane: TEA; R_f = 0.7 and 0.8 for two 3'-diastereomers) to obtain the product as a thick yellowish oil in 58% yield. ¹H NMR (400MHz, CDCl₃) δ 1.18 (d, 12H, CH₃-phosphoramidite), 2.30 (m, 1H, H_{2'}), 2.42 (m, 1H, H_{2'}), 2.61 (t, 2H, CH₂-CN), 3.40 (m, 2H, H_{5'}), 3.58 (m, 1H, H_{3'}), 3.61 (m, 2H, CH-phosphoramidite), 3.78 (s, 6H, OCH₃), 4.08 (t, 2H, CH₂-O-P phosphoramidite), 4.7 (m, 1H, H_{4'}), 5.39 (d, 1H, H₅), 6.26 (m, 1H, H_{1'}), 6.80 (d, 4H, aromatic H₃), 7.23-7.35 (m, 5H, phenyl), 7.41 (d, 4H, aromatic H₂), 7.8 (d, 1H, H₆), 8.40 (s, 1H, N-H).

2-((bis(4-methoxyphenyl)(phenyl)methoxy)methyl)-5-(2-oxo-4-(1H-1,2,4-triazol-1-yl)-3,4-dihydropyrimidin-1(2H)-yl)tetrahydrofuran-3-yl 2-cyanoethyldiisopropyl phosphoramidite (5)

Triazole (1.3g, 18.7 mmol) was dissolved in anhydrous CH₃CN (20 mL) and the suspension was cooled to 0°C and POCl₃ (0.38 mL, 4.2 mmol) was added dropwise. The

mixture was stirred for 10 min, followed by dropwise addition of TEA (2.6 mL, 18.6 mmol). To this reaction mixture was added a solution of **4** (1g, 1.37 mmol) in CH₃CN (10 mL) and stirred at 0°C for 30 min and then allowed to warm to r.t. The stirring was continued for 4h until the solution turns yellow and TLC (5: 4.7: 0.3, EtOAc: Hexane: TEA) showed formation of product (R_f = 0.4 & 0.45, for two 3'-diastereomers). The reaction mixture was diluted with EtOAc (200 mL), TEA (25 mL) and washed with 5% aqueous NaHCO₃ solution (2x 200 mL). The organic layer was dried over MgSO₄ and evaporated *in vacuo*. The residue was purified by flash column chromatography (5: 4.7: 0.3, EtOAc: Hexane: TEA) and both the diastereomers were collected together in 80% overall yield. ¹H NMR (300 MHz, CDCl₃) δ 1.20 (d, 12H, CH₃-phosphoramidite), 2.41 (m, 3H, H₂', CH₂-CN), 2.61 (m, 1H, H₂'), 2.80 (m, 2H, CH-phosphoramidite), 3.52-3.61 (m, 5H, 2H₅', H₃', CH₂-O phosphoramidite), 3.8 (s, 6H, OCH₃-DMT), 4.22 (m, 1H, H₄'), 4.75 (d, 1H, H₅), 6.21 (m, 1H, H₁'), 6.60 (d, 1H, H₄), 6.84 (d, 4H, aromatic H₃), 7.2-7.29 (m, 6H, aromatic H₂, phenyl), 7.40 (m, 3H, aromatic), 8.07 (s, 1H, H₃-triazole), 9.21 (s, 1H, H₅-triazole).

2-((bis(4-methoxyphenyl)(phenyl)methoxy)methyl)-5-(4-(3-(2,5-di(biphenyl-4-yl)-1H-pyrrol-1-yl)propylamino)-2-oxo-3,4-dihydropyrimidin-1(2H)-yl)tetrahydrofuran-3-yl 2-cyanoethyl diisopropylphosphoramidite (6)

A solution of **5** (640 mg, 0.82 mmol) in 10 mL anhydrous THF was added to a solution of **2** (1.75g, 4.1 mmol) in 15 mL anhydrous THF under argon and the resulting solution was heated under reflux for 6 h. The residual THF was evaporated and the product was purified by neutral alumina plate TLC (6: 3.7: 0.3, EtOAc: Hexane: TEA; R_f = 0.7). Yield = 42%; ¹H NMR (300 MHz, CDCl₃) δ 1.15 (d, 12H, CH₃-phosphoramidite), 1.45

(m, 2H, CH₂ (C₂)-pyrrole linker), 2.15 (m, 2H, CH₂ (C₃)-pyrrole linker), 2.40 (t, 2H, CH₂-CN), 2.58 (m, 2H, H_{2'}), 2.76 (m, 2H, CH-phosphoramidite), 3.54 (m, 3H, 2H_{5'}, H_{3'}), 3.76 (s, 6H, OCH₃-DMT), 4.10 (m, 2H, CH₂-O-phosphoramidite), 4.30 (t, 2H, CH₂(C₁)-pyrrole linker), 4.62 (m, 2H, H_{4'}, H₄), 4.95 (d, 1H, H₅), 6.36 (m, 3H, 2CH-pyrrole, H_{2'}), 6.82 (t, 4H, aromatic H₃), 7.25-7.71 (m, 27H, aromatic: phenyl, biphenyl)

5.4.4 Synthesis of tert-butyl 4,4'-(1-(3-aminopropyl)-1H-pyrrole-2,5-diyl)bis(4,1-phenylene)dicarbamate (12')

1,4-Bis(4-nitrophenyl)-butane-1,4-dione (7)

Commercial anhydrous ZnCl₂ (2.72g, 20 mmol) was heated *in vacuo* to melting and mixed with DEA (1.6 mL, 15 mmol) and *t*-BuOH (1.4 mL, 15 mmol) in benzene (20 mL) with continuous stirring until the ZnCl₂ was fully dissolved (approx 2h). 4-nitroacetophenone (2.48 g, 15 mmol) and α-bromo-4'-nitroacetophenone (2.44g, 10 mmol) were successively added to the solution and stirring was continued at r.t. for 3 days. The reaction was quenched with cold 5% aqueous H₂SO₄ and filtered under suction. The precipitate was washed with benzene, water and MeOH and recrystallized from CHCl₃. Quenched mixture or combined filtrates were diluted with ethyl acetate, the organic layer was separated, dried over MgSO₄ and crystallized to afford an additional amount of the diketone. The overall yield of the reaction was 75%. ¹H NMR (300 MHz, CDCl₃) δ 3.56 (s, 4H, CH₂-C=O), 8.10 (d, 4H, aromatic C₂), 8.38 (d, 4H, aromatic C₃).

3-(2,5-bis(4-nitrophenyl)-1H-pyrrol-1-yl)propan-1-amine (8)

To a suspension of **7** (2.5g, 7.6 mmol) in anhydrous ethanol (250 mL), 1,3-diaminopropane (3.5 mL, 38 mmol) and acetic acid (10 mL) were added and the resulting mixture was heated to reflux for 7 h. The reaction mixture was made into slurry by evaporating the ethanol and added slowly to cold NaOH solution (2N, 200 mL). The resulting precipitate was filtered under suction, air dried and purified by column chromatography (silica, 1: 9; MeOH/CH₂Cl₂) to obtain the compound as bright yellowish orange solid in 84% yield. ¹H NMR (300 MHz, CDCl₃) δ 2.28 (m, 2H, CH₂ (C₂- propyl)), 2.70 (t, 2H, CH₂ (C₃-propyl)), 4.42 (t, 2H, CH₂ (C₁-propyl)), 6.54 (s, 2H, CH-pyrrole), 7.82 (d, 4H, aromatic C₂), 8.36 (d, 4H, aromatic C₃).

(9H-fluoren-9-yl)methyl 3-(2,5-bis(4-nitrophenyl)-1H-pyrrol-1-yl)propylcarbamate (9)

Fmoc-OSu (2.07g, 6.3 mmol) was dissolved in 1,4-dioxane (15 mL) and added dropwise to a suspension of **8** (1.5g, 4.2 mmol) in dioxane (15 mL) and water (15 mL) containing NaHCO₃ (0.7 g, 8.4 mmol). The reaction mixture was stirred at 0°C for 4h and stirring was continued at r.t. overnight. The reaction was quenched by addition of aqueous 10% HCl (200 mL), extracted with EtOAc (2 x 200 mL), and washed successively with 5% NaHCO₃ and brine, dried over MgSO₄. The organic layer was evaporated and the residue was purified by column chromatography (silica, CH₂Cl₂, R_f = 0.3) to give **9** as a yellow solid in >90% yield. ¹H NMR (300 MHz, CDCl₃) δ 1.55 (m, 2H, CH₂ (C₂- propyl)), 2.84 (t, 2H, CH₂ (C₃-propyl)), 4.15 (t, 1H, CH-fluorene), 4.41(t, 2H, CH₂ (C₁-propyl)), 4.57 (d, 2H, CH₂-fluorene), 6.62 (s, 2H, CH-pyrrole), 7.45 (m, 4H, C₂-fluorene), 7.60 (m, 2H, C₃-

fluorene), 7.70 (d, 2H, C₁- fluorine), 7.78 (d, 2H, C₄- fluorine), 7.98(d, 4H, aromatic,C₂), 8.50 (d, 4H, aromatic C₃).

(9H-fluoren-9-yl)methyl3-(2,5-bis(4-aminophenyl)-1H-pyrrol-1-yl)propylcarbamate)(10)

A mixture of **9** (1.56g, 2.65 mmol), Zinc (1.033g, 15.8 mmol) and HCOONH₄ (1.32g, 21 mmol) in 300 mL ethanol were heated under reflux until a clear colorless solution was obtained (2 h approx). The ethanol was evaporated and the residue was extracted with CH₂Cl₂ (300 mL) and washed with brine. The organic layer was dried over MgSO₄, evaporated *in vacuo* and purified by column chromatography (silica, 1: 8.9: 0.1, MeOH/CH₂Cl₂/TEA, R_f= 0.6) to obtain **10** as a yellow solid (>90% yield). ¹H NMR (400 MHz, CDCl₃) δ 1.39 (m, 2H, CH₂ (C₂- propyl)), 2.60 (t, 2H, CH₂ (C₃-propyl)), 3.32 (s, 4H, NH₂), 4.06 (t, 2H, CH₂ (C₁-propyl), 4.14 (t, 1H, CH-fluorene) 4.57 (d, 2H, CH₂-fluorene), 6.00 (s, 2H, CH-pyrrole), 6.75 (d, 4H, aromatic C₃), 7.14 (d, 4H, aromatic C₂), 7.30 (t, 2H, C₂-fluorene), 7.38 (t, 2H, C₃-fluorene), 7.60 (d, 2H, C₁- fluorine), 7.81 (d, 2H, C₄-fluorene), 7.96 (br s, 1H, NH).

(9H-fluoren-9-yl)methyl3-(2,5-bis(4-(tert-butylcarbonyl)aminophenyl)-1H-pyrrol-1-yl)propylcarbamate) (11)

To a solution of **10** (1.4 g, 2.4 mmol) in THF (20 mL) in a 50 mL round bottom flask, (BOC)₂O (1.3 mL, 5.7 mmol) and iodine (10 mole %, 60 mg, 0.476 mmol) was added. The reaction mixture was allowed to stir at r.t. overnight. The reaction was quenched with 200 mL 5% Na-thiosulphate solution and extracted with 200 mL EtOAc.

The organic layer was washed twice with 10% NaHCO₃ solution, dried over MgSO₄ and evaporated *in vacuo*. Purification by column chromatography (neutral alumina, 2.5: 7.5, EtOAc: Hexane, R_f=0.7) gave **11** as a brown solid in 85% yield. ¹H NMR (400 MHz, CDCl₃) δ 1.50 (s, 18H, CH₃-boc), 2.70 (m, 2H, CH₂ (C₂- propyl)), 2.60 (t, 2H, CH₂ (C₃-propyl)), 3.89 (t, 1H, CH-fluorene), 4.05(t, 2H, CH₂ (C₃-propyl)), 4.11 (t, 2H, CH₂ (C₁-propyl)), 4.29 (d, 2H, CH₂-fluorene), 6.20 (s, 2H, CH-pyrrole), 6.46 (br s, 2H, NH-boc), 7.31 (d, 4H, aromatic C₃), 7.34-7.41 (m, 6H, aromatic C₂, C₂-fluorene), 7.52 (t, 2H, C₃-fluorene), 7.60 (d, 2H, C₁- fluorene), 7.78 (d, 2H, C₄- fluorene).

Tert-butyl4,4'-(1-(3-aminopropyl)-1H-pyrrole-2,5-diyl)bis(4,1phenylene)dicarbamate (12')

Piperidine (3 mL) was added dropwise to a solution of **11** (1.25g, 2.5 mmol) in CH₂Cl₂ (27 mL) so that the resulting solution was 10% in piperidine and stirred at r.t. overnight. The reaction mixture was taken up in CH₂Cl₂ (200 mL), washed with brine (100 mL), dried over MgSO₄ and concentrated *in vacuo*. The residue was purified by column chromatography (neutral alumina, 2.5: 7.5, MeOH: CH₂Cl₂, R_f= 0.3). Yield 72%; ¹H NMR (300 MHz, CDCl₃) δ 1.44 (s, 18H, CH₃-boc), 2.15 (br m, 2H, CH₂ (C₂- propyl)), 3.60 (t, 2H, CH₂ (C₃-propyl)), 3.96(m, 4H, CH₂ (C₁, C₃-propyl)), 6.04 (s, 2H, CH-pyrrole), 6.81 (br s, 2H, NH₂), 7.30-7.38 (m, 4H, aromatic C₂, C₃), 7.64 (br s, 2H, NH-boc).

5.4.5 Synthesis of Tert-butyl3-(2,5-bis(4-(biphenyl-4-yl(tert-butoxycarbamate)-aminophenyl)-1H-pyrrol-1-yl)propylcarbamate (16)

1,4-bis(4-bromophenyl)butane-1,4-dione (13)

An oven dried 100 mL round bottom flask was charged with α -bromo-4'-bromoacetophenone (5.56 g, 20 mmol), zinc (1.4g, 20 mmol) and iodine (5% mole, 250mg, 1 mmol) in 50 mL THF. The reaction mixture was heated to reflux for 48 h and the formation of the product was monitored by TLC (1: 12, EtOAc: Hexane, R_f = 0.3). The reaction mixture was diluted by addition of 200 mL EtOAc and washed with brine. The organic layer was dried over $MgSO_4$, concentrated and purified by column chromatography (silica, 1: 9, EtOAc: Hexane) to give **13** as a yellow solid in 68% yield. 1H NMR (300 MHz, $CDCl_3$) δ 3.60 (s, 4H, $CH_2-C=O$), 7.80 (d, 4H, aromatic C_3), 8.05 (d, 4H, aromatic C_2).

3-(2,5-Bis(4-bromophenyl)-1H-pyrrol-1-yl)propan-1-amine(14)

The procedure here was identical to that used for synthesis of 3-(2,5-bis(4-nitrophenyl)-1H-pyrrol-1-yl)propan-1-amine (**8**) using **13** (1.6g , 4mmol) and 1,3-diaminopropane in ethanol (100mL) as reactants. The resultant product was purified by column chromatography (silica, 1: 9, MeOH: CH_2Cl_2 , R_f = 0.4) and the product was obtained as a yellow solid. Yield 83%; 1H NMR (300 MHz, $CDCl_3$) δ 1.88 (m, 2H, CH_2 (C_2 -propyl)), 2.20 (m, 2H, CH_2 (C_3 -propyl)), 4.05 (t, 2H, CH_2 (C_1 -propyl)), 6.22 (s, 2H, CH-pyrrole), 7.31 (d, 4H, aromatic C_3), 7.54 (d, 4H, aromatic C_2).

Tert-butyl 3-(2,5-bis(4-bromophenyl)-1H-pyrrol-1-yl)propylcarbamate (15)

To a suspension of **14** (2g, 4.6 mmol) in THF (25 mL), BOC₂O (1.14g, 5.52 mmol) and DMAP (20 mg) was added and the mixture was stirred at r.t. overnight. The reaction mixture was extracted with EtOAc and washed with brine, dried over MgSO₄, concentrated and purified by column chromatography (neutral alumina, 3: 17 EtOAc: Hexane). Yield 85%; ¹H NMR (300 MHz, CDCl₃) δ 1.30 (s, 9H, CH₃ boc), 1.52 (m, 2H, CH₂ (C₂-propyl)), 2.58 (m, 2H, CH₂ (C₃-propyl)), 3.80 (br s, 1H, NH boc), 4.05 (t, 2H, CH₂ (C₁-propyl)), 6.20 (s, 2H, CH-pyrrole), 7.25 (d, 4H, aromatic C₃), 7.50 (d, 4H, aromatic C₂).

Tert-butyl 3-(2,5-bis(4-(biphenyl-4-yl(tert-butoxycarbamate-amino)phenyl)-1H-pyrrol-1-yl)propylcarbamate (16)

An oven dried 100 mL three neck round bottomed flask was charged with Pd(OAc)₂ (5 mole% , 45mg, 0.25 mmol) and S-BINAP (7.5 mole%, 233 mg, 0.375 mmol) in anhydrous THF (20 mL) under argon. After stirring the mixture for 15 min, a solution of **15** (1.25g, 2.34 mmol) in anhydrous THF (20 mL) was added dropwise and stirring was continued for additional 15 min. 4-aminobiphenyl (0.87g, 5.15 mmol) was added to this suspension as a solution in anhydrous THF (20 mL) while stirring at r.t. After additional 15 min of stirring, anhydrous NaO^tBu (0.96 g, 10 mmol) was added under argon balloon. The reaction mixture was heated to reflux under argon for 16 hours.

BOC₂O (1.06 mL, 5.15 mmol) and DMAP (20 mg) was added and the above reaction mixture along with anhydrous THF (40 mL) under argon and the refluxing was continued for additional 6 h. The reaction was quenched with water and extracted with

CH₂Cl₂, dried over MgSO₄, and concentrated. The residue was purified by flash column chromatography (neutral, alumina, 1: 9, EtOAc: Hexane, R_f = 0.7) to give the compound as a brown solid in 38% yield. ¹H NMR (300 MHz, CDCl₃) δ 1.35 (s, 18H, CH₃ aryl boc), 1.44 (s, 9H, CH₃ boc-aliphatic amine), 1.78 (br m, 2H, CH₂ (C₂-propyl)), 3.05 (br s, 2H, CH₂ (C₃-propyl)), 3.80 (br s, 1H, NH boc), 4.07 (br m, 2H, CH₂ (C₁-propyl)), 6.20 (br s, 2H, CH-pyrrole), 7.05-7.60 (m, 26H, aromatic: phenyl and biphenyl).

5.4.6 Preparation of DNA conjoined monomer units

DNA oligonucleotides modified by monomers **2**, **12** and **16** were synthesized by the convertible nucleotide approach¹¹ for coupling the desired monomer. The DNA oligonucleotides was synthesized in an expedite DNA synthesizer using O⁴-triazoyl-deoxyuridine phosphoramidite at required positions of the oligonucleotides. The resin-bound oligonucleotides containing the convertible nucleotide were treated with 1 mL of 1 M (in anhydrous THF) solution of the appropriate amines for 36 h at 60°C under constant stirring. The solutions along with the DNA bound resins were taken in 4 microcentrifuge tubes (1.5 mL) and centrifuged at 13000 RPM for 30 min. The supernatant containing the monomer amine was carefully collected with eppendorf pipettes keeping the resin undisturbed at the bottom of the centrifuge tubes. The resin in each of the centrifuge tubes was suspended in 1 mL of THF by vortexing and the supernatant discarded after centrifugation. This process is repeated for 5 times for each of the tubes to make sure the unreacted amine is completely eliminated. The amine treated DNA oligonucleotides were cleaved from the resin by treating them with 1 mL (per centrifuge tube) concentrated

aqueous ammonium hydroxide at 37°C for 24 hours. The ammonium hydroxide solution was dried on a Speed Vac and the samples reconstituted with water. The combined DNA solutions were collected and passed through a 0.45 μ M filter for purification of the DNA strands by HPLC. The modified oligomers were purified by reverse phase HPLC on a Hitachi preparative HPLC system using a Dynamax C18 column using appropriate ratio of acetonitrile, water and triethylammonium acetate buffer (pH = 7.0). The purified DNA oligonucleotides were introduced to sep-pak columns for desalting. The absorption spectra of the DNA oligomers were measured at 260 nm in a Hewlett-Packard spectrophotometer and their concentration determined with the help of biopolymer calculator (nearest neighbor method). 10 μ L of the DNA oligomers (concentration above 100 μ M) were submitted to the mass spectra facility at Georgia Tech to evaluate the success and purity of the DNA modification. This method was used to modify DNA sequences PSA 1, PSA 2 and PSA 3 (Figure 5.10)

5.5 Results

5.5.1 Synthesis of monomer units 2, 6, 12 and 16

Synthesis of biphenyl linked pyrrole with linker chain (2)¹²⁻¹⁴

Substituted 1,4-Diketones are useful synthetic intermediates for the preparation of five membered heterocyclic compounds. The reaction of 4-acetyl-biphenyl and α -Bromo-4'-phenylacetophenone with zinc chloride, tertiary butanol and diethylamine gave the bis-biphenyl substituted 1,4-Butadione. Treatment of this substituted 1,4-Butadione with

diaminopropane in presence of acetic acid in ethanol gave the 3-(2,5-di(biphenyl-4-yl)-1H-pyrrol-1-yl)propan-1-amine as a highly fluorescent compound in good yields.

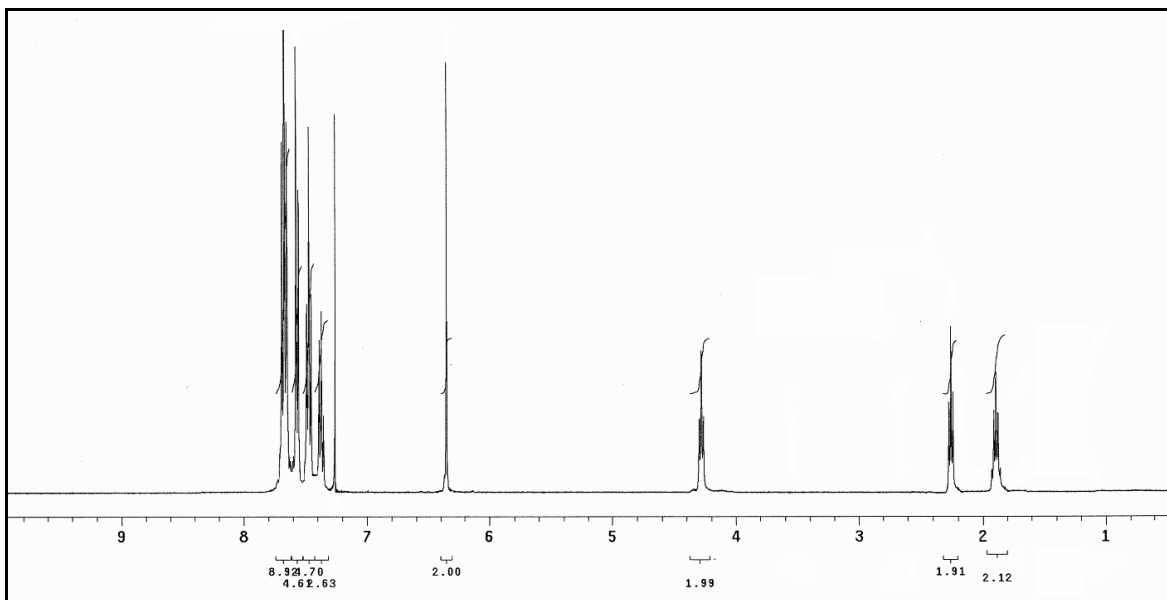


Figure 5.10: ^1H NMR Spectra of Compound **2**

Synthesis of 2,5-Bis(biphenyl)-pyrrole linked deoxycytidine-DMT-phosphoramidite (**6**)¹⁵⁻¹⁶

The DMT protected deoxyuridine was reacted with 2-cyanoethyl-di-isopropyl chlorophosphoramidite, to give the 5'-DMT, 3'-phosphoramidite derivative of deoxyuridine. This product when reacted with triazole, replaces the keto group of the uridine base at the 4 position to give the triazole derivative of the 5'-DMT, 3'-phosphoramidite deoxyuridine. The triazole group is further replaced by the free aliphatic amine group of **2** to give the final product **6**, which is ready to go into the DNA synthesizer for DNA oligomer synthesis with this modified nucleobase. This synthetic strategy helps to

introduce the horizontally extended monomer units at any internal position in the DNA sequence by covalent bonds.

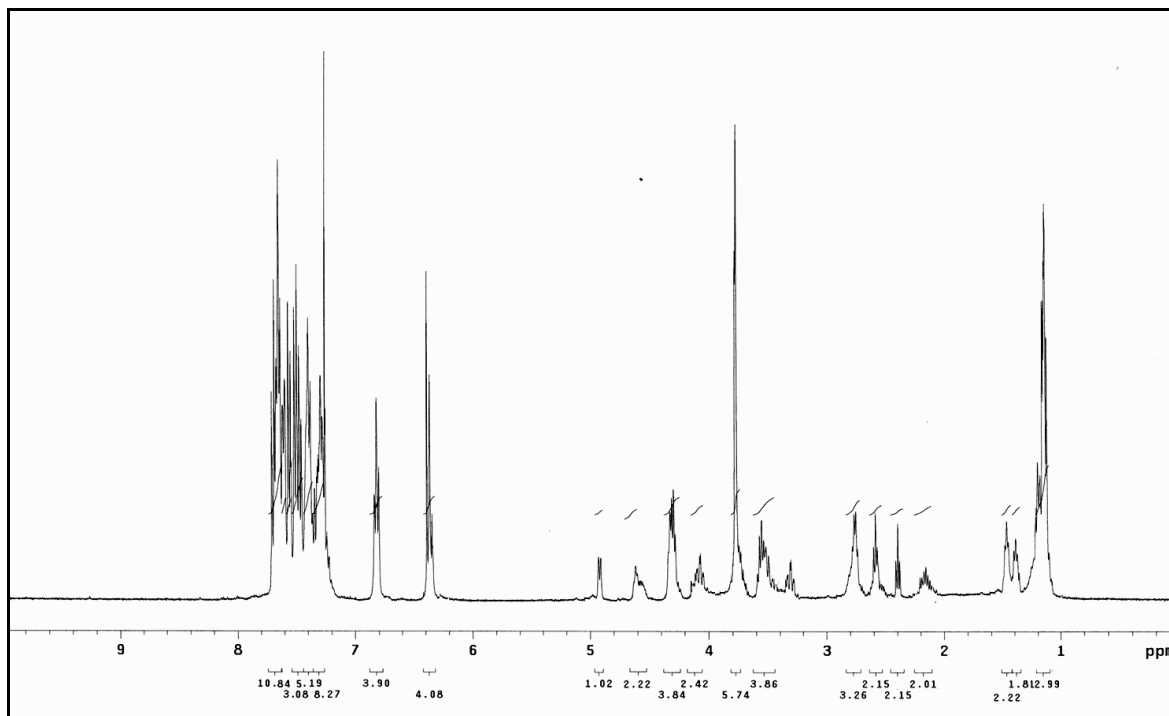


Figure 5.11: ¹H NMR Spectra of Compound 6

Synthesis of aminophenyl linked pyrrole derivative (12', diboc-12)^{14, 17-18}

The reaction of p-Nitroacetophenone and α-Bromo-p-nitroacetophenone under conditions similar as mentioned above gave the bis-p-nitrophenyl substituted 1,4-butadione in high yield. Subsequent reaction of the substituted 1,4-butadione with 1,3-diaminopropane yielded 2,5-bis(p-nitrophenyl)pyrrole with the pyrrole nitrogen being attached with the aminopropyl group. Protection of the aliphatic terminal amino group with Fmoc-OSu gave the corresponding Fmoc protected amine. Reduction of the nitro groups to

amino groups were achieved either with tin chloride dehydrate in ethanol or metallic zinc and ammonium formate under mild condition. The amino groups of the aryl moiety can be protected by tertiary butyl carbamate (boc) protecting groups. Thus, these synthetic steps generate a pyrrole moiety linked with two aminophenyl groups and an amine group attached to a three carbon linker, which is orthogonally protected. The fmoc and boc protected 2,5-Bis(p-aminophenyl)pyrrole-N-propyl amine can be deprotected from the fmoc group with piperidine, while the boc protecting groups on the aryl amines remain intact. Attachment of this monomer unit with DNA is achieved at this point through reaction with triazole containing modified nucleobase with the free amine. The boc protecting groups can be cleaved after attaching the monomer with the DNA using phenol and trimethylsilyl chloride (TMS-Cl)¹⁹.

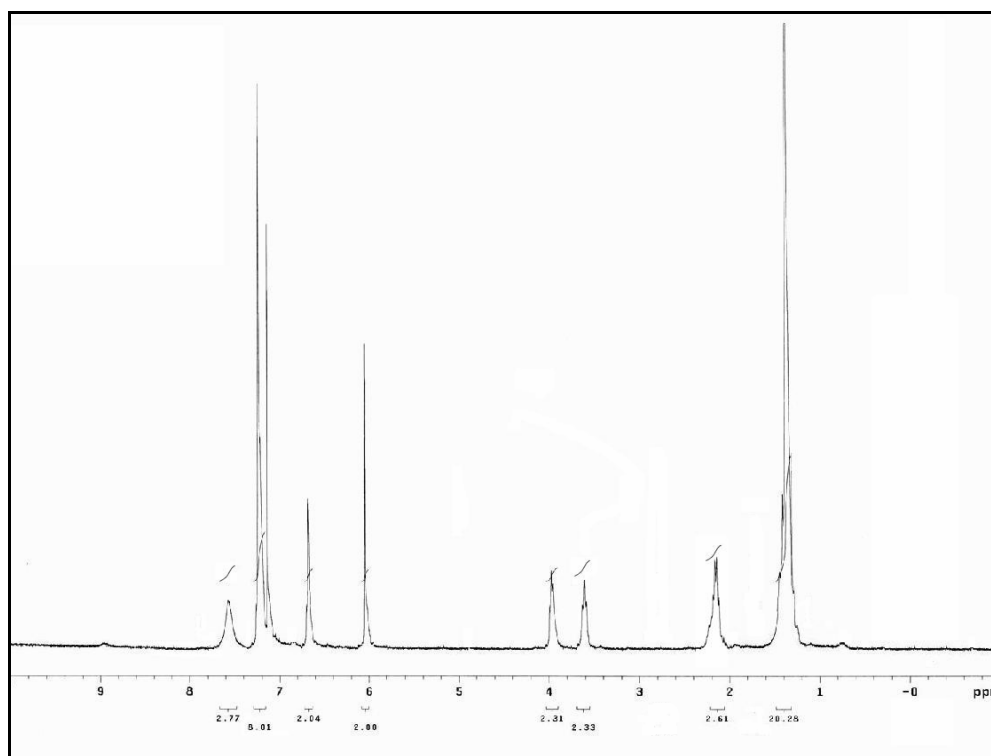


Figure 5.11: ¹H NMR Spectra of Compound **12**

Coupling of biphenylamine with bromophenyl substituted pyrrole (16)²⁰⁻²¹

2,5 Bis(p-Bromophenyl)pyrrole-N-propyl amine was synthesized in two steps. First, α -Bromo-4'-bromoacetophenone was coupled with zinc and catalytic amount of iodine to form the bis-p-bromophenyl 1,4-diketone. This diketone is converted to the corresponding pyrrole by following similar procedure as mentioned above. The aliphatic free amino group of the N-propyl group was protected with boc group. The aryl bromides on both sides of the pyrrole were coupled with aniline and biphenylamine following Buchwald-Hartwig Palladium catalyzed reaction. The resulting product is not so stable under normal experimental conditions. To increase the stability, the reaction product was protected with boc, in situ. The boc protection helps to stabilize the product during the subsequent purification and characterization steps, and finally taken off with phenol and TMS-Cl before reacting it with modified DNA sequences.

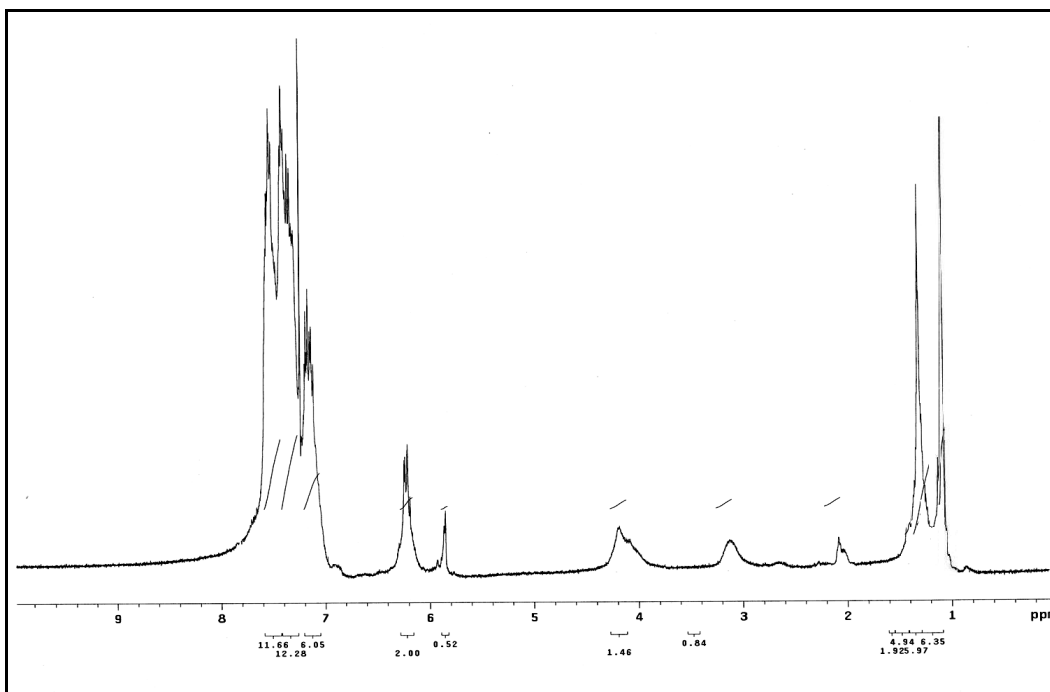


Figure 5.12: ¹H NMR Spectra of Compound 16

5.5.2 DNA conjoined monomer units

A series of DNA oligonucleotides, composed of cytosines bearing covalently linked monomer groups were prepared to assess the possibility of forming conducting polymers that maintain the sequence programmability inherent to DNA. The cytosines were modified by replacement of the 4-amino group by the aliphatic amino groups of the monomers (**2**, **12** and **16**).

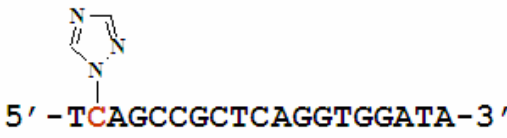
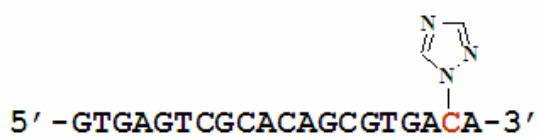
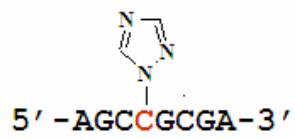
PSA 1	
PSA2	
PSA 3	

Figure 5.13: DNA Sequences Prepared for Attachment of Monomer 2, 12 and 16.

DNA sequences which have been modified by covalent attachment of the monomer units showed much lower mobility than the unmodified sequence in the HPLC column (reverse phase) and required higher percentage of acetonitrile in the eluent as compared to the unmodified DNA.

The presence of the monomer unit in the DNA sequence after the post synthetic modification was confirmed by ESI mass spectra. Figure 5.14 shows one of the representative mass spectra, where PSA 1 has been modified by covalent attachment of the

monomer **2**. The mass spectrum shows an additional mass of 412 compared to the unmodified DNA corresponding to the mass of the monomer moiety which is attached to it.

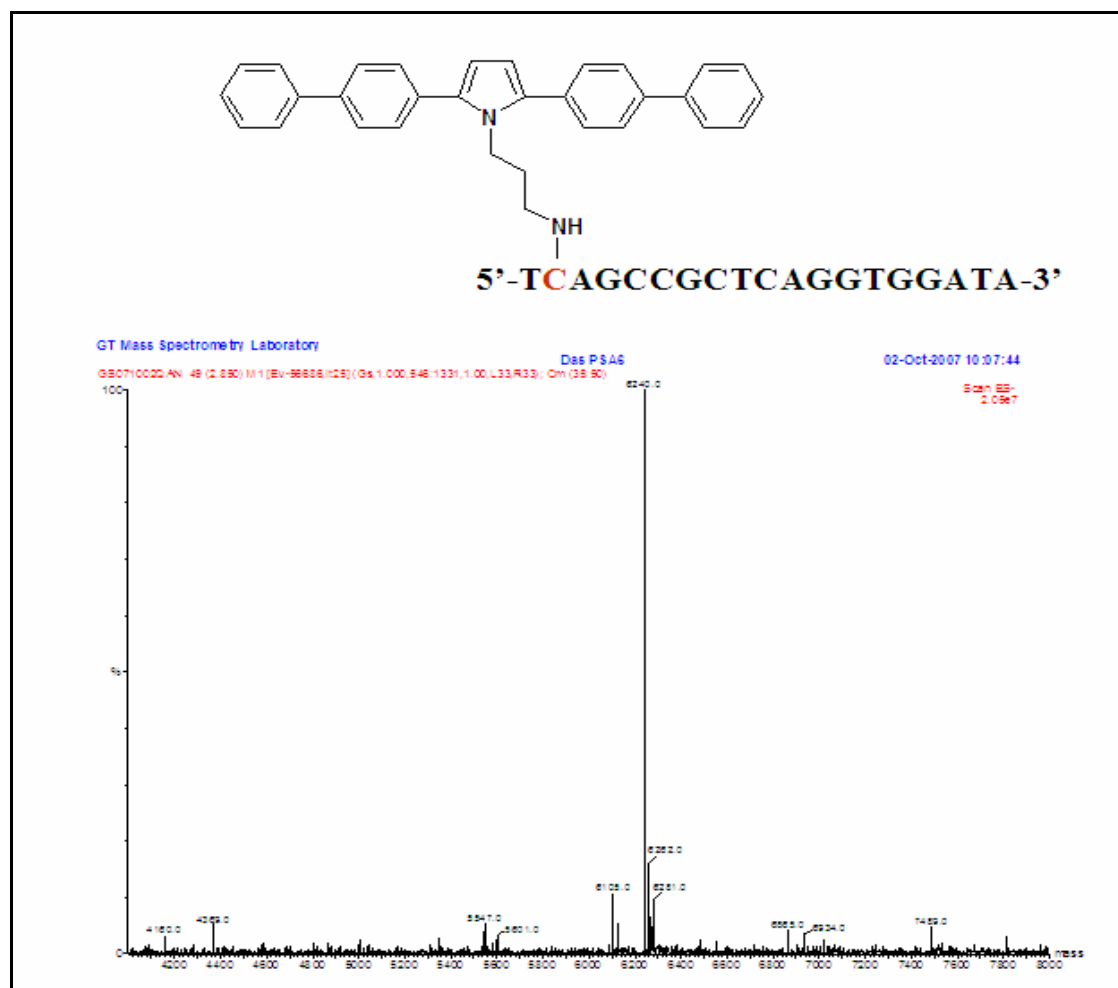


Figure 5.14: ESI Mass Spectra of PSA 1 Attached Covalently to Monomer 2.

5.6 Discussion

PSA 1 and PSA 2 represent two DNA sequences which can be easily modified by covalent attachment of monomer units of conducting polymers. Once attached to the DNA, the monomers (e.g. 2 and **12** in Figure 5.2) can be brought in bonding distances by using the concept of DNA base pairing. A common complementary sequence, acting as a template can co-anneal the modified PSA 1 and PSA 2, and engage the sequences in a self assembly pattern. This provides a method to create an oligomer of a conducting polymer using two distinct DNA-conjoined monomers by chemical ligation of the monomer ends. Methods outlined here also showed the possibility of connecting different monomer units in the same DNA sequence (Figure 5.3). The combination of these two methods effectively demonstrates the power of this technique to use the sequence programmability of DNA to generate conducting polymers having wide range of possible, non-regular structures. In addition to that, single modification leading to the formation of horizontally extended monomer units (e.g. 16) conjoined to the DNA (PSA 3) gives the flexibility of using any monomer unit for the creation of conducting polymers with non-recurring and complex structures.

There is growing awareness that the unique properties of DNA may be exploited to fabricate nanowires and other electrical objects of this length scale^{5, 22}. This work report a novel approach applicable to the fabrication of such devices – the synthesis of building units of conducting polymers conjoined to DNA. Specifically designed DNA sequences with aromatic ring containing monomers covalently linked to the nucleobase can be used as a self-assembly that takes advantage of the sequence programmability properties of

DNA to exercise precise control on polymer formation. Also, the length of the conducting polymer formed in this manner can be precisely controlled.

In contrast to the DNA templated polymerization of free monomers of conducting polymers in solution, the covalent attachment of the same monomers to DNA enforces a particular structural orientation and restricts certain interaction between moieties on different DNA molecules. This can determine the nature of the polymers that can be formed. The DNA templated enzymatic polymerization of aniline has been known to promote a preference for para-directed head-tail-polymerization²³ thereby improving the electrical properties of the resulting polymers. Due to the flexibility of the alkyl tethers linking the DNA, there is still some room for flexibility for the monomers in DNA templated polymerization, which may pave way for polymer branching. This effect is more pronounced for monomers containing multiple aromatic rings (e.g. biphenyl), where a second aromatic ring provides additional positions for reactions and branching. With the strategy of covalently joining the monomer units with DNA sequences and allowing the DNA sequences to align themselves to a common complementary sequence, the parasitic branching of the polymers can be completely eliminated, which can facilitate the formation of well directed head-to-tail polymerization of the monomer units. One advantage of using the strategy of DNA conjoined polymer fabrication is the freedom of using any monomer units with tailored electrical and optical properties to form copolymers of desired design.

The findings reported here provide a method to exploit the self recognition, self-assembly, and sequence programmability of DNA in the formation of conducting

polymers. It is clear that by utilizing variously modified nucleotides this method may be used to generate materials having nonrecurring, irregular structures.

5.7 Conclusions and future scopes

The base pairing ability of DNA can be used to program the synthesis of well defined controlled length conducting polymers. This work reports the synthesis of different monomer units as part of conducting polymer, which can be covalently attached to DNA sequences. Distinctly different DNA sequences containing covalently linked appropriate monomer units can be aligned in a self assembly with a common complementary sequence such that the monomers are in bonding distance, and can be polymerized using standard protocols.

The methodology outlined here can be explored to create conducting polymers of defined length and structure. The ability of DNA sequences to align distinct monomer units in bonding distances and also modification of multiple nucleobases in the same DNA sequence is expected to further expand the range and complexity of polymers that can be formed by this technique. Experiments are currently underway to expand this discovery.

5.8 References

1. Simmel, F. C.; Dittmer, W. U. *Small* **2005**, *1*, 284-299.
2. Storm, A. J.; van Noort, J.; de Vries, S.; Dekker, C. *Appl. Phys. Lett.* **2001**, *79*, 3881-3883.
3. Nogues, C.; Cohen, S. R.; Daube, S.; Apter, N.; Naaman, R. *J. Phys.Chem. B* **2006**, *110*, 8910-8913.
4. Burley, G. A.; Gierlich, J.; Mofid, M. R.; Nir, H.; Tal, S.; Eichen, Y.; Carell, T. *J. Am. Chem. Soc.* **2006**, *128*, 1398-1399.
5. Nickels, P.; Dittmer, W. U.; Beyer, S.; Jorg, K. P.; Simmel, F. C. *Nanotechnology* **2004**, *15*, 1524-1529.
6. Beckman, R.; Beverly, K.; Boukai, A.; Bunimovich, Y.; Choi, J. W.; Delonno, E.; Green, J.; Johnston-Halperin, E.; Luo, Y.; Sheriff, B.; Stoddart, J. F.; Heath, J. R. *Faraday Discuss.* **2006**, *131*, 9-22.
7. MacDiarmid, A. G.; Epstein, A. J. *Faraday Discuss.* **1989**, *88*, 317-332.
8. Genies, E. M.; Boyle, A.; Lapkowski, M.; Tsintavis, C. *Synth. Met.* **1990**, *36*, 139-182.
9. Nagarajan, R.; Liu, W.; Kumar, J.; Tripathy, S. K.; Bruno, F. F.; Samuelson, L. A. *Macromolecules* **2001**, *34*, 3921-3927.
10. Datta, B.; Schuster, G. B.; McCook, A.; Harvey, S. C.; Zakrzewska, K. *J. Am. Chem. Soc.* **2006**, *128*, 14428-14429.
11. Min, C.; Verdine, G. L. *Nucleic Acids Res.* **1996**, *24*, 3806-3810.
12. Nevar, N. M.; Kel'in, A.V.; Kulinkovich, O. G. *Synthesis* **2000**, *9*, 1259-1262.

13. Arafa, R. K.; Brun, R.; Werbovetz, K. A.; Tanious, F. A.; Wilson, W. D.; Boykin, D. W. *Heterocycl. Commun.* **2004**, 10, 423-428.
14. Ling, C.; Lahti, P. M. *J. Am. Chem. Soc.* **1994**, 116, 8784-8792.
15. Noll, D. M.; Noronha, A. M.; Miller, P. S. *J. Am. Chem. Soc.* **2001**, 123, 3403-3411.
16. Xu, Y. Z.; Zheng, Q.; Swann, P. F. *J. Org. Chem.* **1992**, 57, 3839-3845.
17. Varala, R.; Nuvula, S.; Adapa, S. R. *J. Org. Chem.* **2006**, 71, 8283-8286.
18. Cooke, G.; Garety, J. F.; Jordan, B.; Kryvokhyzha, N.; Parkin, A.; Rabani, G.; Rotello, M. V. *Org. Lett.* **2006**, 8, 2297-2300.
19. Kaiser, E.; Tam, J. P.; Kubiak, T. K.; Merrifield R. B. *Tetrahedron Lett.* **1988**, 29, 303-306.
20. Ceylan, M.; Gurdere, M. B.; Budak, Y.; Kazaz, C.; Secen, H. *Synthesis* **2004**, 11, 1750-1754.
21. Sadighi, J. P.; Singer, R. A.; Buchwald, S. L. *J. Am. Chem. Soc.* **1998**, 120, 4960-4976.
22. Ma, Y. F.; Zhang, J. M.; Zhang, G. J.; He, H. X. *J. Am. Chem. Soc.* **2004**, 126, 7097-7101.
23. Samuelson, L. A.; Anagnostopoulos, A.; Alva, K. S.; Kumar, J.; Tripathy, S. K. *Macromolecules* **1997**, 30, 4024-4030.